FACULDADE DE CIÊNCIAS E TECNOLOGIA

UNIVERSIDADE DE COIMBRA

DEVELOPMENT OF AN OPTICAL CONFOCAL MODULE FOR A SLIT LAMP MICROSCOPE

Master's Degree in Biomedical Engineering

Susana Figueiredo e Silva

Coimbra, September 2011

FACULDADE DE CIÊNCIAS E TECNOLOGIA

UNIVERSIDADE DE COIMBRA

DEVELOPMENT OF AN OPTICAL CONFOCAL MODULE FOR A SLIT LAMP MICROSCOPE

Thesis submitted for the degree of Master in Biomedical Engineering.

Supervisor: Professor Doutor António Miguel Morgado

Susana Figueiredo e Silva

Coimbra, September 2011

This work is funded by FEDER, through the Programa Operacional Factores de Competitividade-COMPETE and by National funds through FCT- Fundação para a Ciência e Tecnologia in the frame of project PTDC/SAU-BEB/104183/2008, F-COMP-01-0124-FEDER-010941

Este trabalho é financiado pelo FEDER, através do Programa Operacional Factores de Competitividade-COMPETE e fundos nacionais através da FCT- Fundação para a Ciência e Tecnologia no âmbito do projeto PTDC/SAU-BEB/104183/2008, F-COMP-01-0124-FEDER-010941

Aos meus pais e avós

ACKNOWLEDGEMENTS

Quero começar por agradecer ao meu orientador, Professor Miguel Morgado, por todo o apoio, acompanhamento e tempo dedicado ao longo de todo ano para que a realização deste projecto fosse possível.

Um grande agradecimento vai também para todos os membros da equipa do projecto neuroCornea pelos conselhos e ideias essenciais no decurso deste trabalho.

Aos meus pais, o meu muitíssimo obrigada por todo o esforço, dedicação e confiança depositados em mim durante toda a minha vida e principalmente no percurso universitário. Ao meu pai também agradeço toda a ajuda dada para que os desenhos em 3D fossem concluídos.

Aos meus avós, um grande obrigado por tudo, especialmente à minha avó São por acreditar sempre em mim e ser um constante apoio. A toda a restante família fica também uma palavra de agradecimento.

Às minhas amigas e companheiras de casa, Susana Silva e Rute Cardoso, fica o meu muito obrigada por me "aturarem" durante estes anos e pelos momentos em que tornaram esta vida universitária tão espectacular.

Aos amigos que Coimbra me deu a conhecer, o meu muito obrigada por todos os momentos de diversão, amizade e até estudo que vivemos juntos durante estes 5 anos. Sem vocês, a passagem por Coimbra e pela Universidade não teria metade do sentido.

A todos, o meu sincero Obrigada.

ABSTRACT

Diabetes affects an increasingly large part of the world population. Therefore, a substantial increase in the prevalence of chronic complications associated with diabetes is being observed. One of them is diabetic neuropathy, the major cause of chronic disability in diabetic patients.

There is increasing evidence that diabetic neuropathies can be diagnosed through morphometric analysis of corneal nerves. Corneal confocal microscopy is the technique used to acquire *in vivo* corneal nerve images. However, this technology is expensive and it is only available in large hospitals and clinics. On the contrary, the slit lamp microscope is largely distributed, being frequently used to observe the anterior segment of the eye. Therefore, to develop a confocal module to apply on a slit lamp microscope would have an huge impact on the dissemination of corneal nerves assessment for diabetic neuropathy diagnosis and follow-up.

To fulfill this purpose, it was necessary to project and develop the optical design of the confocal module and of the whole system (confocal module coupled to slit lamp microscope) in order to evaluate and understand the performance. The first step was to characterize the slit lamp optical path and simulate it, using an optical CAD software. Then, the confocal module, comprising microscope objective and other lenses, was added, without modifying the optical path of the slit lamp microscope.

A prototype version of the confocal module was built and installed on a slit-lamp microscope for testing. Field of view, distortion, lateral resolution, contrast and Modular Transfer Function were measured and compared against the simulation results.

The results obtained are close to the expected and are similar to the values measured for a commercial corneal confocal microscope used to image corneal nerves. The laboratory tests also revealed technical difficulties concerning corneal illumination, focus positioning and image stabilization that will have to be addressed in future work.

Keywords: confocal microscopy, slit-lamp microscope, cornea, diabetic neuropathy, optical module.

RESUMO

A diabetes é uma doença crónica que afecta uma parte, cada vez maior, da população mundial. A esta doença estão associadas complicações crónicas, como por exemplo a neuropatia diabética – maior causa de incapacidade em diabéticos.

A análise morfométrica dos nervos da córnea é um método de diagnóstico em crescimento. A microscopia confocal da córnea é a técnica usada para adquirir imagens dos nervos da córnea *in vivo.* No entanto, esta tecnologia é cara e só está disponível em hospitais centrais e clínicas privadas. Por outro lado, o microscópio de lâmpada de fenda está largamente disseminado e é frequentemente usado para observar o segmento anterior do olho humano. Assim, o desenvolvimento de um módulo confocal para aplicação num microscópio de lâmpada de fenda teria um enorme impacto na disseminação da avaliação dos nervos da córnea para o diagnóstico e acompanhamento da neuropatia diabética.

Para cumprir este objectivo, foi necessário projectar e desenvolver um desenho óptico do módulo confocal e do sistema completo. (módulo confocal acoplado ao microscópio de lâmpada de fenda) para avaliar e entender o desempenho do sistema. O primeiro passo foi caracterizar o caminho óptico da lâmpada de fenda e simulá-lo. Para tal foi usado um software de CAD óptico. Seguidamente, um módulo confocal, composto por uma objectiva e outras lentes, foi adicionado sem alterar o caminho óptico da lâmpada de fenda.

Um protótipo do módulo confocal foi construído e instalado num microscópio de lâmpada de fenda para testes. Campo de visão, distorção, resolução lateral, contraste e Função de Transferência Modular foram os parâmetros medidos e comparados com os resultados obtidos na simulação.

Os resultados obtidos estão próximos do esperado e são semelhantes aos valores medidos num microscópio confocal da córnea comercial em imagens de nervos da córnea. Os testes de laboratório também revelaram algumas dificuldades técnicas, entre as quais a iluminação da córnea, posição do foco e estabilização da imagem. Estes problemas terão de ser solucionados no futuro.

Palavras-Chave: microscopia confocal, microscópio de lâmpada de fenda, neuropatia diabética, módulo óptico.

INDEX

FIGURES INDEX

TABLES INDEX

INTRODUCTION

Diabetes Mellitus affects a large part of the world population. This disease is characterized by the uncontrolled rising of the glucose levels in the blood stream as a result of incapacity of the insulin hormone in transforming the glucose. The onset of this disease can induce the onset of other pathologies on several organs of the human body. It is very often associated with neuropathies known as diabetic neuropathies.

Since there are different types of methodologies available to diagnose and define this disease, diabetic neuropathies do not have an established epidemiology. There are cases reported on both dependent and non-dependent insulin patients [1].

Human cornea is a highly enervated tissue where the peripheral nervous system is easily imaged by non-invasive optical techniques. Due to this, once techniques for *in vivo* imaging of corneal nerves were available, diagnostic methods for diabetic neuropathy resting on the observation of corneal nerves were immediately proposed. Corneal confocal microscopy is standard technique to assess corneal nerves in vivo.

Different studies proved that images acquired by this technique can be used to diagnosis and follow up peripheral diabetic neuropathy. Rosenberg et al demonstrated that patients suffering severally from this disease had a loss in their corneal sensitivity and reduction in sub-basal nerve density. Kallinikos et al demonstrated that corneal nerves morphometric parameters are related to the severity of diabetic neuropathy [2, 3, 4].

Although corneal confocal microscopy can produce high quality images of corneal nerves, this type of instrument is expensive and it is only available in central hospitals and large clinics [5].

On the other hand, the slit lamp microscope is an instrument vastly used to observe the anterior segment of the eye and available in a far greater diversity of places. Therefore, the incorporation of the confocal technique in a slit lamp microscope would result in a much higher availability and dissemination of any diabetic neuropathy assessment method based on corneal nerve imaging [5].

This project had as goal to design an optical confocal add-on module for a conventional slit-lamp.

The preliminary specifications of this optical module are based on the characteristics of a commercial corneal confocal microscope, Tomey Confoscan Model P4, used on our laboratory and on clinical practice to acquire images of all corneal layers, including the sub-basal nerve plexus. From the measurements done in the past [6] in our laboratory, it was specified that the optical module should have a field of view around 500 μm x 480 μm, lateral resolution better than 5 μm and distortion should be less than 5%.

CHAPTER 1 – CONFOCAL MICROSCOPY

1.1 -THE PHYSIOLOGY OF THE CORNEA

Corneal tissue is placed at the front of the eye. It consists of a special type of connective tissue with no presence of blood vessels. Nutrients are delivered to the cornea through tear fluid and the aqueous humour that fills the anterior chamber [7, 8].

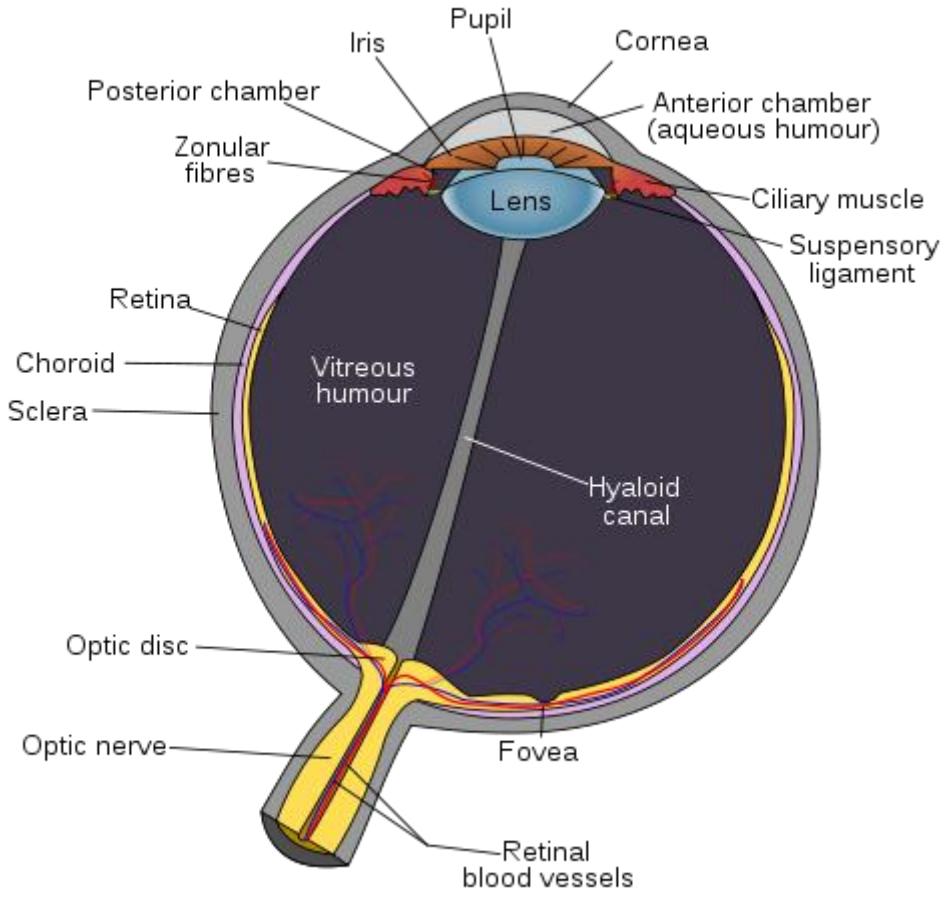

Figure 1- The structure of the eye [9].

The cornea is responsible for two main tasks in the eye: apart from acting like a shield against germs, dust and other harmful matter, it also acts as a lens, contributing with 65

to 75% of the eye's total focusing power. The cornea also protects the retina against UV-B and UV-C radiation, acting like a filter [8].

Light entering the cornea is refracted onto the eye's lens, which is responsible for refocusing that light onto the retina, where the image formed will be transformed into impulses to be sent to the brain [8].

Corneal tissue is divided into five basic layers: the epithelium, the Bowman's layer, the stroma, the Descemet's membrane and the endothelium. Each of these layers has a specific function in cornea [8].

The epithelium is responsible for blocking the passage of foreign material and provides a smooth surface to absorb nutrients and oxygen from tears. Here, thousands of tiny nerve endings can be found which make the cornea so sensitive to touching or scratching. This layer comprises 10% of the total thickness of the cornea and it contains epithelial cells (superficial and basal) and wing cells. The latter are placed between the superficial cells and the basal epithelial cells. The basal cells are seen as near to round cells and smaller than intermediate cells [8, 10].

The Bownman's layer is a transparent sheet of tissue consisting of collagen. It lies right below the epithelium. Large injuries in this layer can cause large scars that could lead to some vision loss. It separates the epithelium from the stroma and it is in this layer that the basal lamina of the epithelium is found. Some nerves can be found in this layer, perforating it and branching to form a basal epithelial nerve plexus in the region just anterior to the basal lamina. Some of these nerves penetrate the basal epithelial cells to terminate in free nerve endings positioned just below, at the superficial epithelial cells. The nerves present in the nerve plexus are very easily detected by confocal microscopy [8, 10, 11].

The stroma is located below the Bowman's layer, and is the largest corneal layer. It is composed by water and collagen fibers. The latter gives the cornea its strength, elasticity and form: Its spatial arrangement is essential to achieve light-conducting transparency. It also contains large nerves and fibroblasts commonly designated as stromal keratocytes [8, 10].

Composed of collagen fibers and endothelial cells, the Descemet's membrane is a barrier against infection and injuries. Below this layer, lies the endothelium [8; 10].

Finally, the most intern single layer of cells composes the corneal endothelium. These cells are very important to maintain the cornea clear. They have the function of maintaining the tight regulation of corneal hydration since they contain in their structure an ion transport system that regulates the fluid flux. Endothelial cells do not have the capacity to regenerate, this resulting in a declined density associated with ageing. Human adults have a normal density of 3500 cells/mm^2. A great loss in density (below 500-700 cells/mm^2) can lead to a lack of hydration regulation, edema and, consequently, transparency loss. However, in healthy people, the corneal density never drops below the limit value, since its decreasing rate is too low for that happen during the human life expectancy [8, 12].

Nerves present in the cornea have some particular features. At the corneal limbal area, nerves from the ophthalmic and maxillary branch of the trigeminal nerve lose the myelin sheath and perineurium, branching into smaller nerves. These smaller branches will enter the cornea and constitute the corneal nerves [11].

The anterior third of the stroma is the area where the majority of stromal nerve fibres are located. These nerves can continue to the corneal epithelium. In this case, they start at the stroma, turning abruptly by 90º and penetrate Bowman's layer through the peripheral and central cornea. Here, the large nerves subdivide in smaller branches which turn again 90º and follow parallel to the corneal surface, forming epithelial leashes between the basal epithelial and the Bowman's layer – subbasal nerve plexus [11].

The epithelial leashes present at subbasal plexus contain both straight and beaded fibres. The beaded fibres are the only ones that can separate from the bundles, branch and course into the superficial epithelial cell layer. The wide distribution of cells in this layer guarantees the pain perception of injuries occurred there [11].

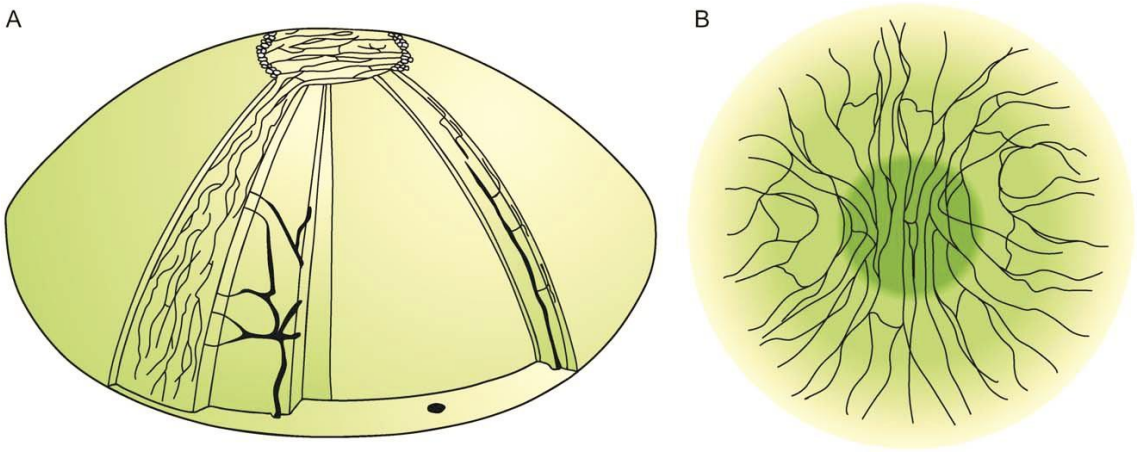

Figure 2 – (A) Schematic distribution of nerves in the stroma and subbasal plexus in human corneas. (B) Scheme of the organization of the subbasal plexus [11].

At the human subbasal plexus the number of nerve bundles is estimated to be between 5400-7200 [1].

1.2 - PRINCIPLES OF CONFOCAL MICROSCOPY

"A confocal microscope is a type of microscope in which a thick object such as the cornea is illuminated with a focused spot of light." The definition is simple, but to accomplish this idea some techniques must be understood [10].

In confocal microscopy as in the epi-microscopy, the same objective plays two different roles in the process of collecting a corneal image. The objective illuminates a point P1 in the object and it also collects the scattered and reflected light from the same point P1. To better illustrate this concept, the scheme described in Figure 3 shows two separate objectives on each side of the thick object. The objective is represented by lenses L1 and L2. Apart from those, the figure also shows two apertures, S1 and S2, and the thick object [10].

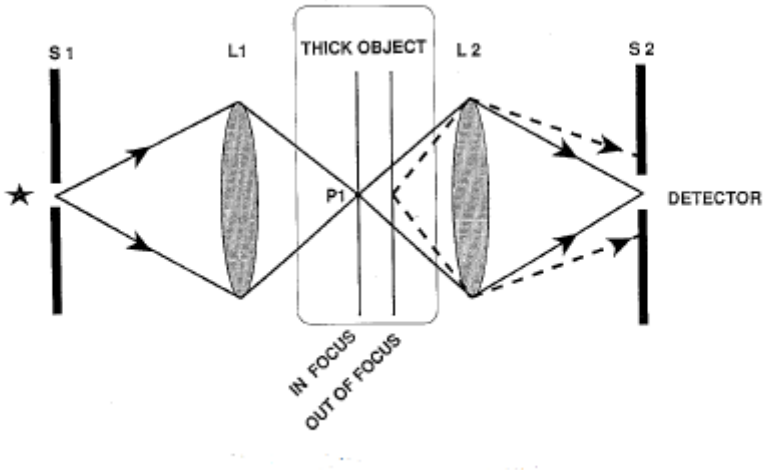

Figure 3 - Schematic representation of the principle of confocal microscopy [10].

The objective on the left side of the object is responsible for the illumination, while the one on the right side is responsible for collecting the scattered light and forming the image. The process is simple: a point source of light originated in the aperture S1 enters L1 which will focus this light onto a small spot in object, at the lens focal plane. On the other hand, L2 will be positioned in a way that its focus is placed in the same focal plane as L1. L2 will a form an image of the small spot at the aperture S2 and all the light collected by L2 is detected at S2 [10].

Out of focus points also reaches the detector. The phenomenon is again very well illustrated in Figure 3. To minimize this problem, the instrument uses a small aperture at the detector which will block the detection of out of focus light. In the real instrument the two apertures are located in conjugate planes – confocal apertures [10].

The goal of confocal microscopy is to acquire two dimensional images. For that, several systems were developed to acquire the image. One of the patents described to solve the problem was fielded by Minsky. He described two methods: stage scanning and beam scanning. In the stage scanning method the object is scanned across a stationary beam of light. Therefore, it cannot be used for *in vivo* ocular observation. In the beam scanning method it is the illumination beam of light that moves and scans the eye. This is the method used in clinical confocal microscopy [10, 13].

The spatial resolution is very important when acquiring images. It is defined as the minimal distance between two points that can be separated and can be quantified using the Rayleigh Criterion. Higher resolution has a lower value of Rayleigh Criterion. In microscopy, two types of resolution are often evaluated: transverse and axial resolution. Transverse resolution is related on the x and y coordinates in the plane of the thick object. On the other hand, axial resolution is related on the z coordinate, orthogonal to the plane of the object. A good value of axial resolution in confocal microscopy allows an improvement on the quality of image by about 40% when compared to conventional techniques [10, 14].

Numerical aperture (NA) is an optical parameter with high influence in the Rayleigh Criterion and, therefore, in the resolution of the microscope. NA is a relation between the refractive index (n) and the half-angle subtended by the object at the microscope's focal plane (a): [15]

$$NA = n \times \sin(a) \quad (1)$$

The transverse resolution, d_{tr} is estimated by the following equation:

$$d_{tr} = a \times \frac{\lambda}{NA} \quad (2)$$

where a is the proportionality constant, λ the wavelength and NA the numerical aperture.

On the other hand, the axial resolution is more sensitive to the NA, with the relation between NA and d_{ax} being:

$$d_{ax} = b \times \frac{n \times \lambda}{NA^2} \quad (3)$$

where b is the proportionality constant, n the refractive index value, λ the wavelength, NA the numerical aperture and d_{ax} the axial resolution [14].

Therefore, to maximise the value of lateral and axial resolution, the objectives used in confocal microscopy should have a high value of NA [14].

Axial resolution is the feature associated with depth of field, the thickness region of the specimen that appears in focus in the final image at a particular focal setting of the

image. Depth of field can be estimated through the value of axial Rayleigh criteria, being half of this value [14].

1.3 - TYPES OF CONFOCAL MICROSCOPES

Since its first appearance, confocal microscopy has suffered developments resulting in several different types of microscopy techniques and microscopes. The most relevant will be described in the following paragraphs. All of these techniques have pros and cons and not all of them are used for *in vivo* corneal confocal microscopy.

1.3.1 - TANDEM SCANNING NIPKOW DISK BASED CONFOCAL MICROSCOPE

The inventors of this instrument were Petran and Hadravsky. (10) They developed an instrument based on the Nipkow disk, a device invented by Paul Gottlieb Nipkow in 1884 [10].

Nipkow aimed to convert a two-dimensional optical image into an electrical signal to be transmitted over a single cable. He achieved his purpose using a spinning opaque disk perforated by a series of rectangular holes. Their arrangement was similar to an Archimedes spiral, with each of the pinholes having a conjugate on the other side of the disk [10, 16].

The disk used in this type of microscope, developed by Petrans and his team, was very similar to the one Nipkow had invented years before. However, this new device had multiple sets of pinholes placed spirally in a circular disk – Figure 4 [10; 16].

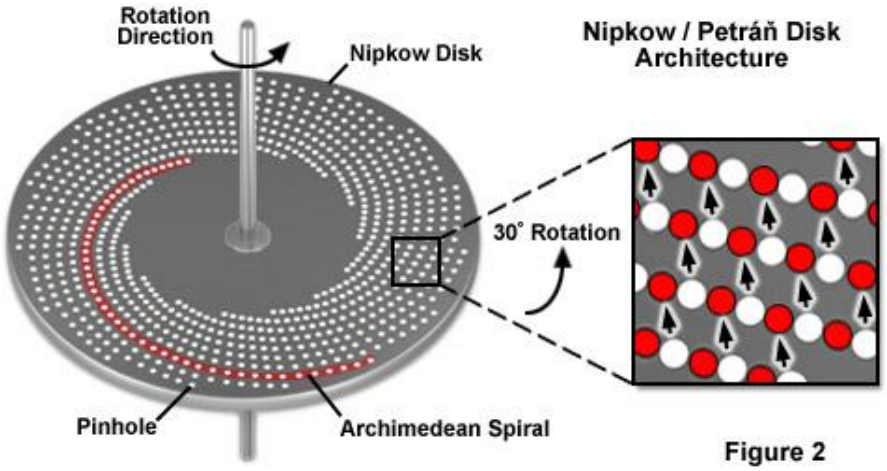

Figure 4 - The Nipkow Disk Architecture [17].

On one side a pinhole allows the illumination beam to pass through it. The microscope objective conveys the illuminations beams to the specimen producing a diffraction limited spot on it. On the other side, the conjugate pinhole allows the passage of the reflected light coming from the specimen. The two-dimensional image of the focal plane is obtained by scanning at the same time the illumination and the reflected light. This is done by spinning the Nipkow disk [10, 16].

This type of microscope had one important disadvantage. As the ratio of the holes to the disk area is very small (about 1-2%), only a small fraction of the illumination reaches the sample. The same problem was observed as far as reflected light is concerned. The fraction of light that passes through the disk and reaches the detector is reduced, resulting in a low image quality or longer acquisition times for a given signal-to-noise ratio. Tandem scanning Nipkow disk microscope (TSM) also represents a bad choice when the specimens to be imaged are weakly reflecting (cornea for example). However it has its advantages like allowing real-time operation at high image acquisition rates [10, 16].

1.3.2 - ONE-SIDED NIPKOW DISK CONFOCAL MICROSCOPE

An evolution to the microscope invented by Petran was proposed by Xiao, Corle and Kino in 1990, the one-sided and real-time Nipkow disk based confocal microscope They developed a system in which the rays of light that illuminate the specimen passed the same pinhole that those reflecting from the surface. The device used a tilted disk in order to direct into a beam stop the light reflected from the surface of the disk. The light was polarized by a polarizer placed between the light source and the disk (illuminating the disk with polarized light). A quarter wave plate was placed between the disk and the specimen, and an analyser was placed between the disk and the detector. This arrangement allowed the perfect separation between the light from the specimen and the light reflecting from the surface of the disk – Figure 5.[10, 16].

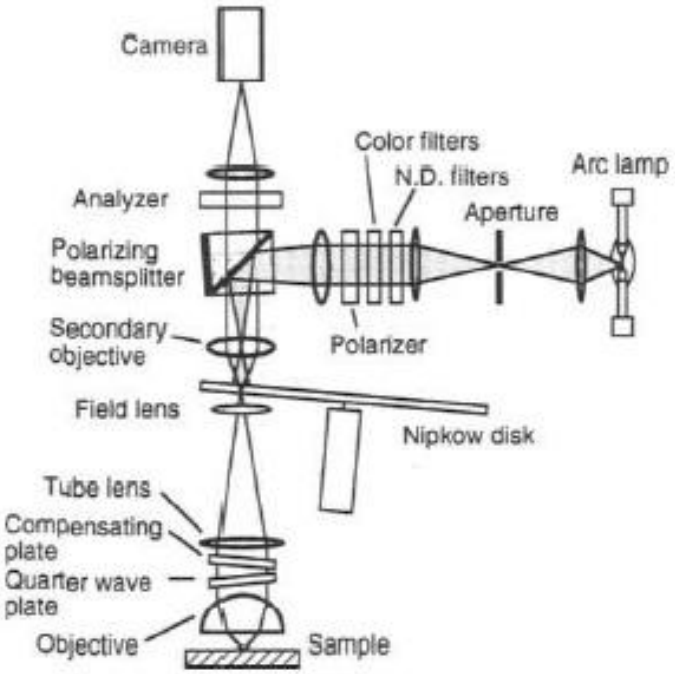

Figure 5- Schematic diagram of the one-sided Nipkow-disk Confocal Microscope [18].

Like the others, this type of microscope presented both advantages and disadvantages. It was less sensitive to vibration of the Nipkow disk than the TSM and it had a simpler optical design. However, because it had only one optical path for both illumination and reflecting light, it was difficult to correct for chromatic aberrations. It also had a low transmission disk which turned not to be a good choice for weakly reflecting specimens [10].

1.3.3 - SCANNING SLIT CONFOCAL MICROSCOPE

Other types of confocal microscopes, not based on the Nipkow disk, were developed and proposed. One example is the Scanning slit confocal microscope. A slit of illumination is used in an optical arrangement that allows the slit to be scanned over the back focal plane of the objective. This results in a lower scanning time because many points along the slit axis are scanned in parallel [10].

This type of microscope was developed along the years by several investigators. The simplest design was proposed by Baer, but Burns and Koester were responsible for the development of a scanning mirror microscope for ocular observation. Svishchev was another important investigator in whose designs are based some of the modern designs of real-time confocal microscopes with bilateral scanning. Thaer was responsible for developing the real-time scanning slit *in vivo* corneal confocal microscope. This microscope is based in two adjustable slits located in conjugate planes [10].

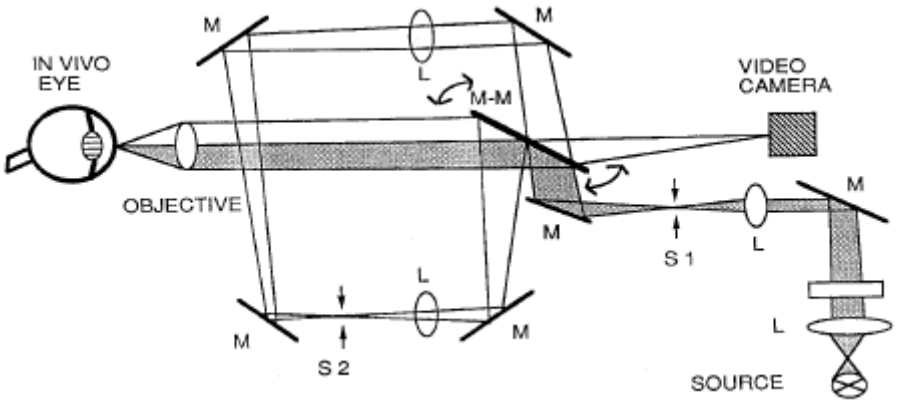

Figure 6 - Scheme of scanning slit confocal microscopy [10].

The design of the real-time scanning slit confocal microscope for *in vivo* corneal examination is presented in Figure 6. It is possible to see the light source, a halogen lamp. S1 and S2 are the confocal slits. The letter L indicates lenses. The objective is "split", with one half used for illumination, while the other half is for collecting the reflected light from the specimen. The grey paths represent the illumination path while the collection path is in white. The design also contains several front-surface mirrors (M) and an oscillating double-sided mirror M-M. This mirror is used for both scanning and descanning purposes [19].

The scanning slit confocal microscope brought several advantages to the world of corneal microscopy. This instrument can have its slit adjusted in width which allows the variation in the thickness of the optical section and the amount of light that reaches the specimen and the detector. It also has a much greater light throughput when compared to the Nipkow disk based microscopes. These advantages allow the instrument to capture images of specimens which are very transparent [10].

This microscope also has some disadvantages such as the lower transverse and axial resolution since it is only confocal in the axis perpendicular to the slit height [10].

1.3.4 - LASER SCANNING CONFOCAL MICROSCOPE

Laser-Scanning confocal microscopy (LSCM) was the most recent technique of confocal microscopy, with the first mechanical LSCM developed by Egger. It uses a coherent laser source and the beam is scanned over the back focal plane of the microscope by a set of galvanometer scanning mirrors. This type of microscopy uses pinhole apertures. The light, coming from the laser source, needs to pass two different pinholes before reaching the photomultiplier detector. The first pinhole is in a conjugate plane with the scanning point on the specimen, the second pinhole is positioned before the detector, as described in Figure 7. The second pinhole acts as a "filter", blocking the passage of out of focus light. The dichroic mirror has a double function. It reflects the laser beam onto the specimen, and allows the passage of the reflected light onto the second pinhole aperture [10, 20].

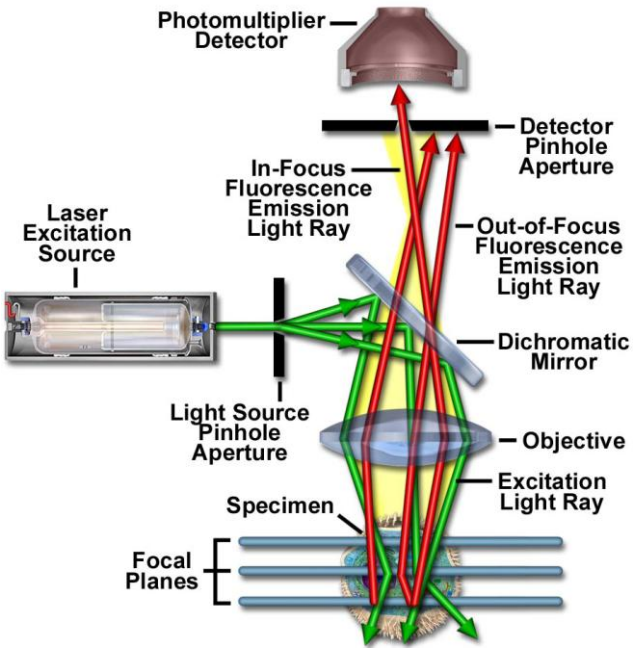

Figure 7 - Schematic representation of the optical path and the principal components in a laser scanning confocal microscope [20].

1.4 - LIMITATIONS

All the techniques described present disadvantages. It is impossible to say that one of these systems is perfect. There are limitations that are common to all of them. Some may be minimized, recurring to specific components; others are yet to be solved [10].

Confocal microscopy is very dependent on the wavelength used for illumination. Its value combined with NA has great influence on the resolution of the instrument. Therefore, the wavelength used should be short and the NA of the objective high in order to yield a great resolution. NA also plays an important role on contrast, magnification and image aberrations [10].

Since it is necessary to recur to a high NA objective to achieve a satisfactory level of resolution, the work distance of the instrument will be consequently short. The overall magnification will also be high due to the use of high NA., restricting the field of view and the area to be observed [10].

CHAPTER 2 - THE SLIT LAMP MICROSCOPE

The Slit Lamp Microscope can be defined as a long working distance microscope for observation of the eye. By using oblique illumination it provides oblique sectioned views of the cornea. Gullstrand developed its principle and Zeiss made the first instrument [10, 21].

This microscope was used for the first time for corneal endothelium examination by Vogt [10].

2.1 - WORKING PRINCIPLE

A lamp is attached to a standard stereomicroscope. The projected light (focused or diffuse) has high intensity and can illuminate the eye from different angles. This allows examination of all anterior structures of the eye [22].

In this type of microscope, the light is conveyed onto the specimen through an adjustable slit which limits the beam width. The microscope is built in a way that it always focuses the region that is being illuminated. To maximize the image contrast, the angle between the observation microscope and the viewing optical system can be changed [10].

The illumination lamp has freedom to rotate to accomplish the idea of different angles of observation. To obtain a focused image, the position of the lamp can be changed through both horizontal and vertical axis and through the rotational angle α (see Figure 8). The instrument position will affect the imaged area [22].

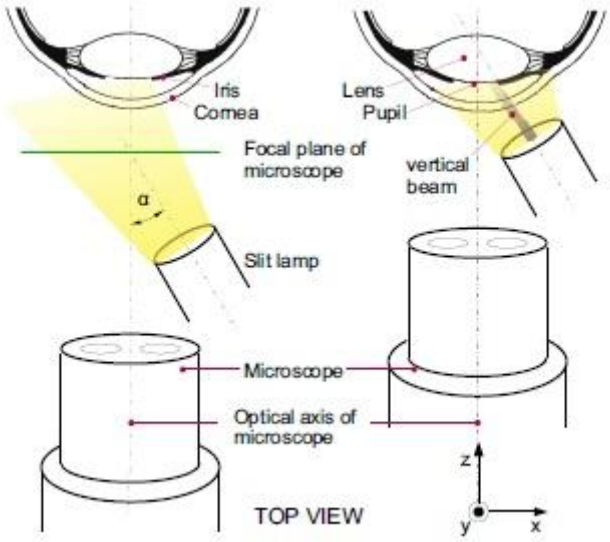

Figure 8 – Movement of slit lamp during focusing [22].

2.2 - OPTICAL COMPONENTS

In what concerns to optical design, the slit lamp microscope is comprised by the following components: a long working distance objective, a Galilean telescope, a relay lens and a binocular eyepiece [23].

2.2.1 - LITTMANN-GALILEAN TELESCOPE

The device invented by Galileo in the 16th century, the Galilean telescope, is used in the slit lamp microscope to control its magnification. This telescope uses two lenses: a positive and negative one. The combination of the different lens characteristics (curvature ray, thickness and distance between them) of each telescope gives different configurations and thereby different values of magnification [23].

The telescope works with both the object and the image at infinity - the rays entering the telescope positive lens are parallel and they leave the negative lens also parallel. This principle is presented in Figure 9 [23].

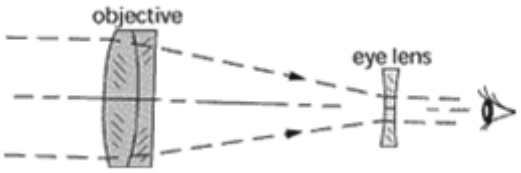

Figure 9 - The optical principle of Galilean telescope [9].

In the optical design of the slit lamp, the telescope is positioned between the objective and the relay lens. It has a system that comprises different pairs of lenses to achieve different magnifications. With this system, the different values of magnification are obtained only by changing the lenses features. The distance between lenses is the same for all magnifications. Figures 10 and 11 present the Galilean telescope in a slit lamp microscope [23].

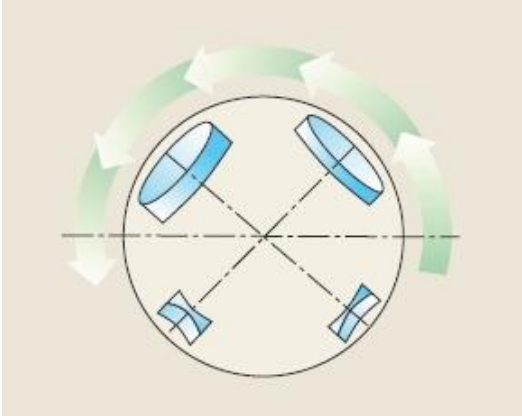

Figure 10 - Scheme representing the rotation movement of the different Galilean telescopes in the slit lamp microscope [24].

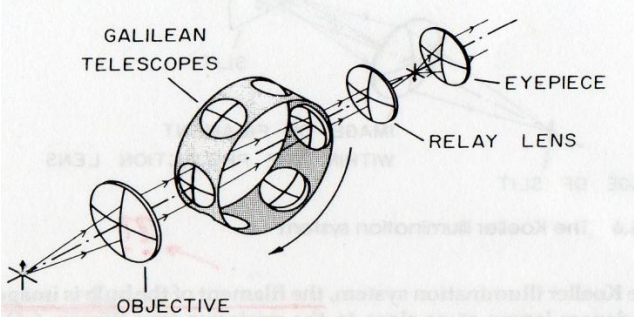

Figure 11 –System that allows the rotation of different Galilean telescopes [23].

2.2.2 - OBJECTIVE

The main characteristic of a slit lamp objective is the great value of focal length, which turns it into a long-distance objective. Currently, this value is typically 125 mm, but other close values are also found. The shape of this lens is convergent in order to transform the rays that diverge from the object into parallel at the exit [24].

In order to ensure that the light beam emerging from the objective is collimated, the object must be positioned at the exact focal point of this lens. If the focal length is 125mm, then the position of the object must be 125 mm before the lens first nodal point.

2.2.3 - RELAY LENS

A convergent lens is used to convert the collimated beam of parallel rays exiting from the Littmann-Galilean telescope into converging rays. The focal length is not fixed and its value is dependent on the eyepiece chosen as the microscope standard and the value of magnification power without Galilean telescope. The purpose of this relay lens is to produce an image in the object plane of the eyepiece [24].

2.2.4 - EYEPIECE

An eyepiece is an optical element which has the ability to magnify a near object (or an image originated on another element) to appear in a larger visual angle. It can be characterised by 5 different features: magnification, focal length, apparent field angle, object position and eye relief, being the magnification and the focal length directly related [25].

Since its first appearance, a wide range of different designs of eyepieces has been released and developed. However, for microscopy purposes, the most used designs are the Huygens and Kellner – Figure 12 and 13 [25].

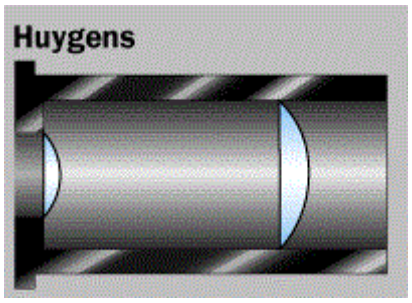

Figure 12 - Huygens Eyepiece design [9].

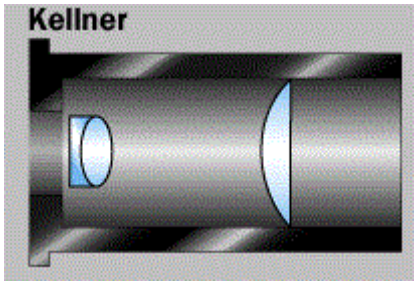

Figure 13 - Kellner Eyepiece design [9].

In slit lamp microscopy, it is common to use a binocular eyepiece for providing stereoscopic vision [26].

The binocular eyepiece is divided into two parts to work properly: the eyepiece lens assembly and the image orientation correction. Eyepiece lens assembly represents the optical needed to make the image visible to the observer. On the other hand, for image orientation correction, prisms are used mainly to correct the inverted and laterally reversed image. The most used prisms for microscope eyepieces are the Porro prisms

This type of prism configuration is made by recurring to two isosceles right-angled prisms mounted at a very specific place with their hypotenuses facing each other and their long axes exactly perpendicular as shown in Figure 14 [26].

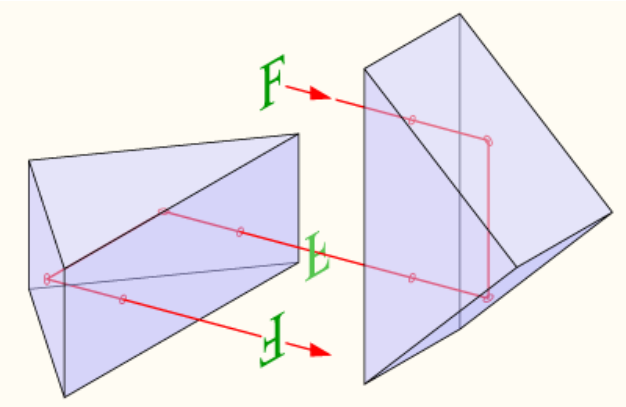

Figure 14 - Porro prism design [26].

As seen in Figure 15, four reflections are needed to present a non-inverted image to the observer [26].

The total angular magnification of the slit lamp microscope is related to the individual magnification of its optical components and is given by:

$$G = \frac{f_2}{f_1} \times g \times \frac{250\ mm}{f_3(mm)} \quad (4)$$

where f_1 is the focal length of the objective; f_2 corresponds to the focal length of the relay lens and f_3 is focal length of the eyepiece. The value 250 mm corresponds to the standard leas distance of distinct vision [24].

It is important to notice that the higher is the magnification, the shorter will be the field of view of the specimen. Therefore, the value chosen to magnify a specified object must be chosen carefully.

The slit lamp microscope needs an illumination system whose function is to provide the ideal light conditions for the best observation of the specimen.

In these microscopes, the most adopted technique is the Koeller illumination system. While providing a homogeneous slit image, it uses a variable aperture slit allowing to change the slit width and height [23, 24].

In Koeller system, the light comes from a lamp placed before the condensers. Behind the lamp, reflectors can be placed to increase the amount of light entering the condensers. The system is arranged so that the lamp position corresponds both to the mirrors curvature centre and the condenser first focus – Figure 15 [23].

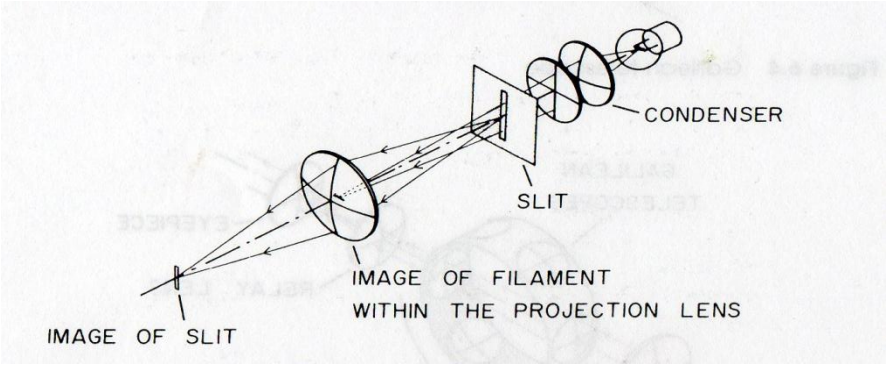

Figure 15 – The Koeller illumination system [23].

The condenser is responsible for imaging the filament of the lamp at the projector lens. On the other side, the projector lens is responsible for forming the image of the slit at the eye. To minimise the aberrations and to increase the depth of focus of the slit, the projection lens needs to have a very small diameter. Optical components used in the illumination system do not need to be as accurate as the optics used in the microscope part. However, its choice must be careful in order to avoid too much chromatic aberration that could cause fringes at the image. To keep up with this requirement, it is common to use two or more lenses at the condenser [23].

Prisms or mirrors are used in projection system to allow the passage of light from one side and to provide an upright image. The light is transmitted along a horizontal axis. For example, the Porro prisms described above could be used to accomplish this goal.

The illuminations and mechanical systems are coupled (i.e. they share a common axis which coincides with their focal planes) to ease the use of this microscope by the operator. The operator controls the movements of the microscope by two means: a joystick is responsible for controlling the x and y axis position and a screw to move around the z axis. The movements are common to both systems to ensure the coincidence between the two focal planes (detection and illumination) [23, 24].

2.4 - OTHER OPTICAL CHARACTERISTICS

The resolution, brightness and depth of field are important characteristics of the slit lamp microscope.

The resolution of a microscope is defined as the smallest distance between two points that can be separated. In this type of microscope it is directly associated with its numerical aperture. For a given numerical aperture, there are not significant changes in resolution by increasing magnification above a certain value. The same happens on the opposite way - increasing the numerical aperture beyond the value given by the system magnification is not recommended since the resolution is limited by the observer acuity and pupil size. Numerical aperture is also associated with the working distance of the microscope and the diameter of the objective. It is given by:

$$NA = n \times \sin(\alpha) \quad (5)$$

where α is the half angle subtended by the objective at the microscope's focal plane and n is the refractive index of the medium between the patient eye and the objective [23].

Depending on the magnification established for an instrument, the exit pupils size advisable for a good slit lamp microscope varies between 0.8 to 2.7 mm. Numerical aperture is defined to be between 0.04 and 0.08(values known for modern slit lamp models) [23, 24].

The microscope depth of field restrains the brightness of the instrument. It is not possible to have maximum brightness (not counting with the lamp brightness) and maximum depth of field. Higher brightness will result in lower depth of field [24].

2.5 - ILLUMINATION AND EXAMINATION METHODS

The slit lamp microscope is described as an instrument with the capability to observe different structures of the living eye. For that purpose, several configurations can be used in order to get the best image of each ocular structure.

The differences in these configurations result from the type of illumination, magnification power and slit width. Optical section, direct illumination, indirect illumination, scattering sclera-corneal illumination, fundus observation, fluorescence observation and assessment of lachrymal film are some examples of illumination techniques that can be executed on the slit lamp microscope [24].

2.5.1 - OPTICAL SECTION

Optical section technique, also known as direct focal illumination, is the most adopted technique in slit lamp examination. In this method, the illumination system and the viewing path should form a large angle, around 90º, as seen in Figure 16. Because the intersection between the illuminating and viewing path axes is in the anterior eye media, it allows the visualization of structures like the individual corneal layers [24].

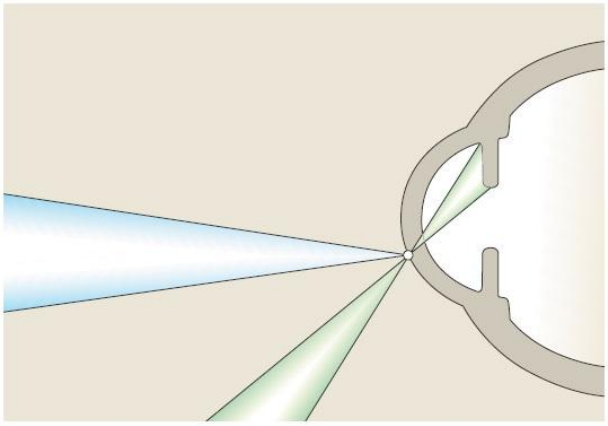

Figure 16 - Direct Focal Illumination [24].

It is the illuminating beam that defines the optical section in this observation method. When the slit is narrow (0,1 mm to 0,2 mm) and the angular aperture is small, the illuminating beam has the shape of two knife blades placed edge to edge [24].

The optical section provided by this examination method allows very detailed and precise information about the shape of transparent structures [24].

The magnification and slit width are two variables that can be changed during the examination. By changing them, different structures can be observed, ranging from the cornea to the posterior face of the crystalline lens [24].

In order to obtain good results with this method it is necessary that the background remains as dark as possible [24].

2.5.2 - DIRECT DIFFUSE ILLUMINATION

Another method to examine the different eye structures is the direct diffuse illumination. Here, the light source modified by placing a diffuser or ground glass screen in the illuminating path [24].

The recommended settings to perform this type o examination are well established, the slit must be fully opened, the angle between the illuminating and viewing paths should be around 30 º and the magnification can vary from 5x to 30x, depending on the structure to be observed (see Figure 17). Different structures can be assessed: general surveys of anterior eye segment, the surfaces of the crystalline lens and cornea, the lachrymal reflex or soft contact lenses (if applied) [24].

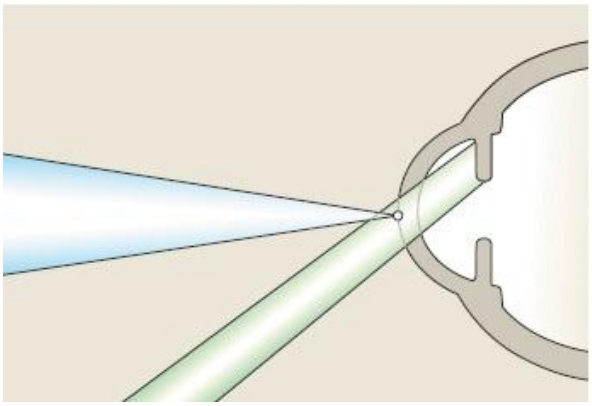

Figure 17- Direct Diffuse Illumination Method [24].

2.5.3 - INDIRECT ILLUMINATION

Indirect illumination (Figure 18Figure 18) is characterized by the non-intersection between the axis of the illumination and viewing paths at the focus. Instead, the slit lamp illuminating prism rotates around its vertical position and becomes decentred. This position will illuminate the area to be examined by a reflected indirect beam of light. The slit width varies from narrow to medium (2 to 4 mm) [24].

This method is mainly used to observe corneal features such as corneal scars, deposits, epithelial or stromal defects [24].

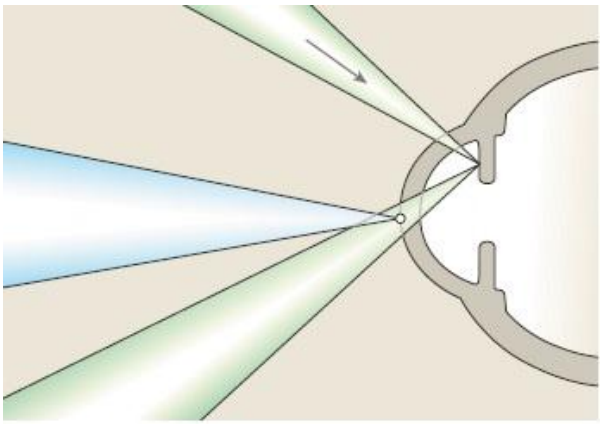

Figure 18 - Indirect Illumination Method [24].

2.5.4 - SCATTERING SCLERO-CORNEAL ILLUMINATION

As seen in Figure 19 19, the illumination path is directly pointed onto the limbal region of the cornea, using a decentred illuminating prism, with a very low angle of incidence. This method is based on the principle of total intern reflection – when a ray of light reaches a diopter, with an incidence angle higher than a critical value, all light is reflected. Something that happens only if the refractive index of the refraction medium is lower than that of the incidence medium. Total internal reflection allows the light to be transmitted through the corneal parenchymal layers. A normal cornea should appear completely clear as a bright shining ring around the entire limbus. This method uses a narrow slit and can locate irregularities in the corneal tissue like inclusions, scars, opacities and foreign bodies [24].

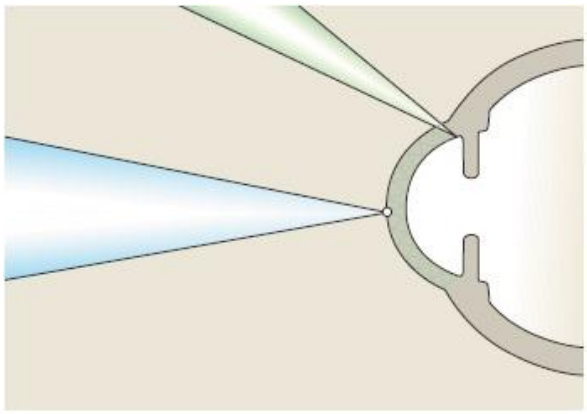

Figure 19 - Scattering Sclero-Corneal Illumination [24].

CHAPTER 3 – CONFOCAL AND SLIT-LAMP MICROSCOPY

The idea of transforming a slit lamp biomicroscope into a confocal scanning microscope is not new and, as far as we could find, two patents were already granted on the subject.

One of the devices patented [27] is based on a standard slit lamp coupled with an illumination system based on the Nipkow disk confocal microscope. The other one comprises a kit to convert a slit lamp microscope into a single aperture confocal scanning microscope.

The first device, depictured in Figure 2020, uses a rotation disk with multiple sets of pinholes (10) with its motion controlled by a small motor (10a). This disk is placed on the illumination side of the mechanism which is independent from the slit lamp microscope. As it can be seen in Figure 20, the confocal module (2) is independent from the slit lamp (1), make possible to restore easily to the slit lamp standard configuration. (27)

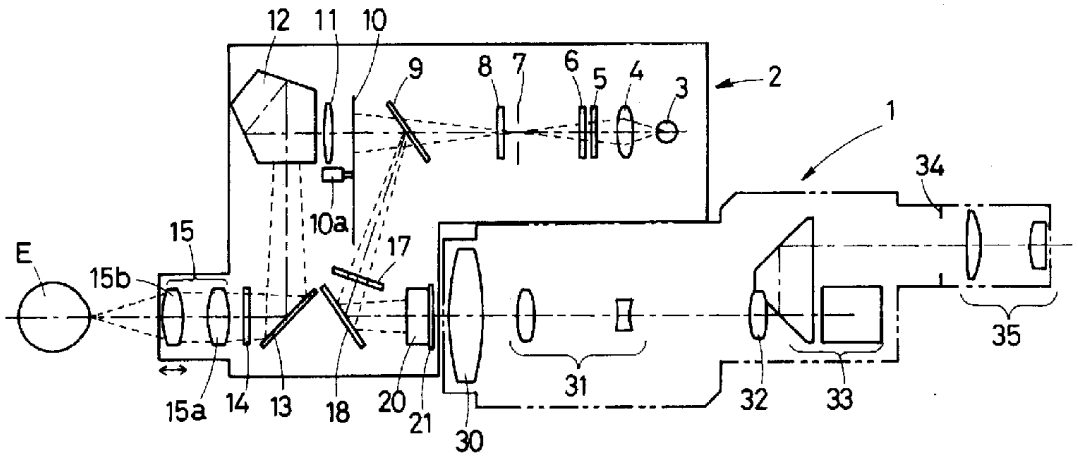

Figure 20 - Schematic diagram of the optical and illumination systems – Patent number 5701197 [27].

The confocal module includes its own illumination system. Light from this system illuminates the disk and is transmitted through its pinholes onto the specimen. The confocal module also contains a light delivery optical system to focus the reflected light from the specimen plane on the Nipkow disk and deliver it to the objective lens. All these systems are built in a single add-on module meant to be placed in front of the slit lamp microscope [27].

The illumination system (see Figure 20) comprises a light source (3), a condenser lens (4), a spectral filter (5), a linear polariser (8), an aperture (7), a dichroic mirror(9), the Nipkow disk (10), a field lens (11), a pentagonal prism (12), mirrors (13 and 18), another linear polariser that will operate as polarization analyser (17), a ʎ/4 waveplate, an objective lens (15) and light beam dividing mirrors (20 and 21). The light exits the light source (3) and passes through the linear polariser (8), leaving it linearised. Then, light passes is transmitted through the ʎ/4 waveplate (14) becoming circular polarised. After reflecting onto the specimen, light is again linear polarised by the ʎ/4 waveplate (14), but its direction is turned 90º from the illuminating light and can pass through the analyser (13) it is transmitted through the pinholes of the disc, illuminating the specimen. The reflected light is collected through the objective lens and crosses the path to the light beam deflecting mirrors, where the image will be formed to be collected by the slit lamp objective [27].

Before this system was published, another one, with a confocal system placed between the slit-lamp eyepiece and its objective, was invented. However it provided very low contrast and its usefulness was reduced [27].

The other patented granted concerns, as said before, a kit to convert a slit lamp into a single aperture confocal scanning microscope [28]. This patent presents two technical solutions: the first uses the standard illumination system of the slit lamp, with a few changes to its optical path such as addition of several lenses, an aperture and an oscillating aperture device. This aperture can comprise a set of multiple pinholes like a Nipkow disk or an oscillating multi –slit aperture. The mirror represented by number 28 of Figure 21 blocks a part of the light returning from image, leading to a decrease in resolution.

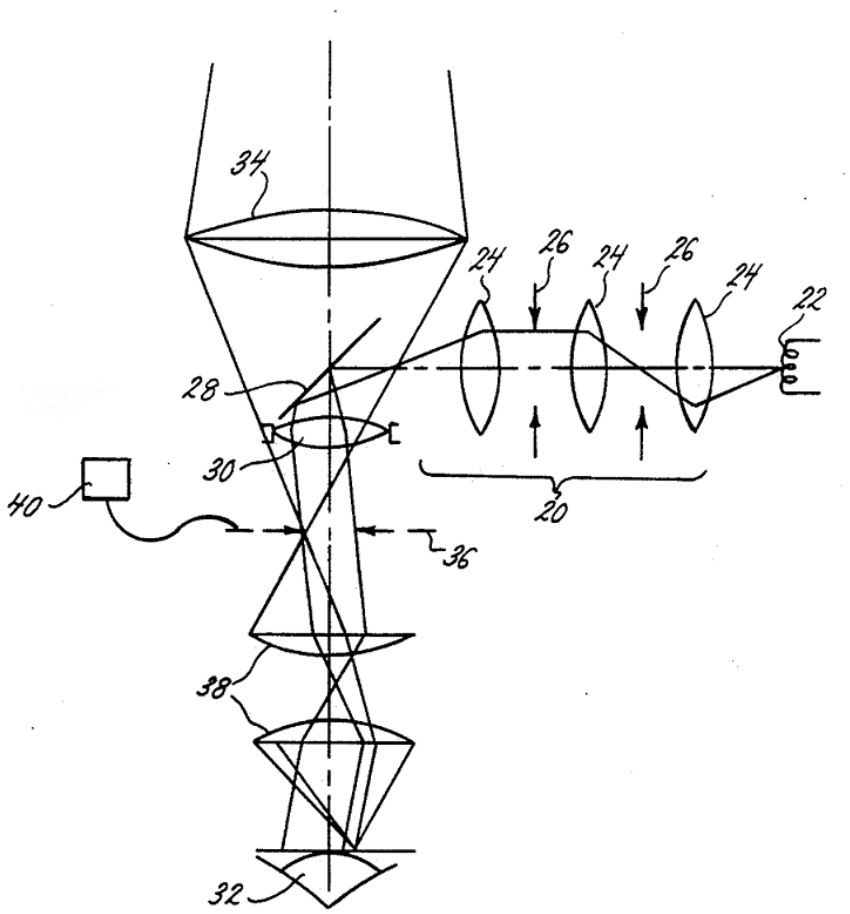

Figure 21 – First solution for the kit to convert a slit lamp microscope into a single aperture confocal scanning microscope. Patent number 5099354 [28].

The optical modifications to the slit lamp illumination system are shown in Figure 21 where are represented by the numbers 36, 38 and 40.

The other solution involves an independent illumination system. This illumination system can be used for direct and indirect illumination examination – Figure 22 [28].

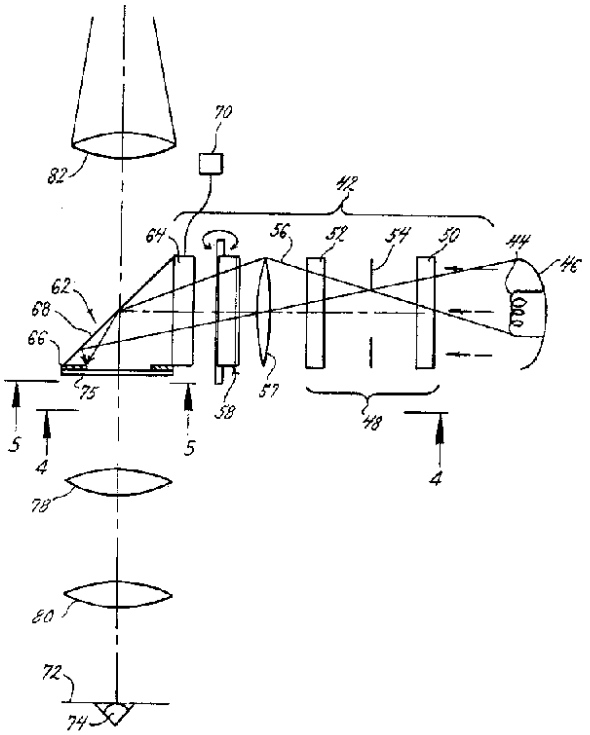

Figure 22 – Second solution to convert a slit lamp microscope into a single aperture confocal scanning microscope. Patent number 5701197 [28].

The illumination system is completely independent from the slit lamp standard illumination. Its light source is based on a standard lamp and includes a spherical reflector (44 and 46) and a set of cylindrical lenses and a rectangular aperture on a collimating arrangement. A defocused collimated light beam exits the light source and it is focused onto the rectangular aperture (54) by a spherical lens (50). After passing the aperture, light is defocused into a collimated incident light field light by another spherical lens (52). This arrangement allows the light to be highly collimated along both the width and length of the masking aperture (66).The focus on this masking aperture is guaranteed by the cylindrical lens (57). To block a variable part of the collimated light a V-shaped flap is incorporated on illuminator (58). The triangular aperture assembly comprises a cylindrical lens (62), a rectangular slit aperture (66) and beam splitter which joins the other two components at its edge. This assembly can be connected to an oscillator (70) and move in the plane of the aperture (62). The cylindrical lens is responsible for focusing the light in the plane of the masking aperture. This plane is

conjugate to the plane of the specimen. The entire system is free to move for examining different areas of the patients' eye, while the patient stays in rest as in a normal slit-lamp examination [28].

CHAPTER 4 – METHODS

As mentioned before, this project had as main purpose the development of an optical confocal module to be applied on slit lamp microscopes. During the year, the work was divided in different steps in order to achieve the main goal. The key steps are described in Figure 23.

OSLO (Lambda Research Corporation, USA) was the optical CAD (Computer-Aided Design) software used to simulate all the optical designs required by this project. Therefore, the first part of our work was to understand the physical principles behind optical CAD and how to use it.

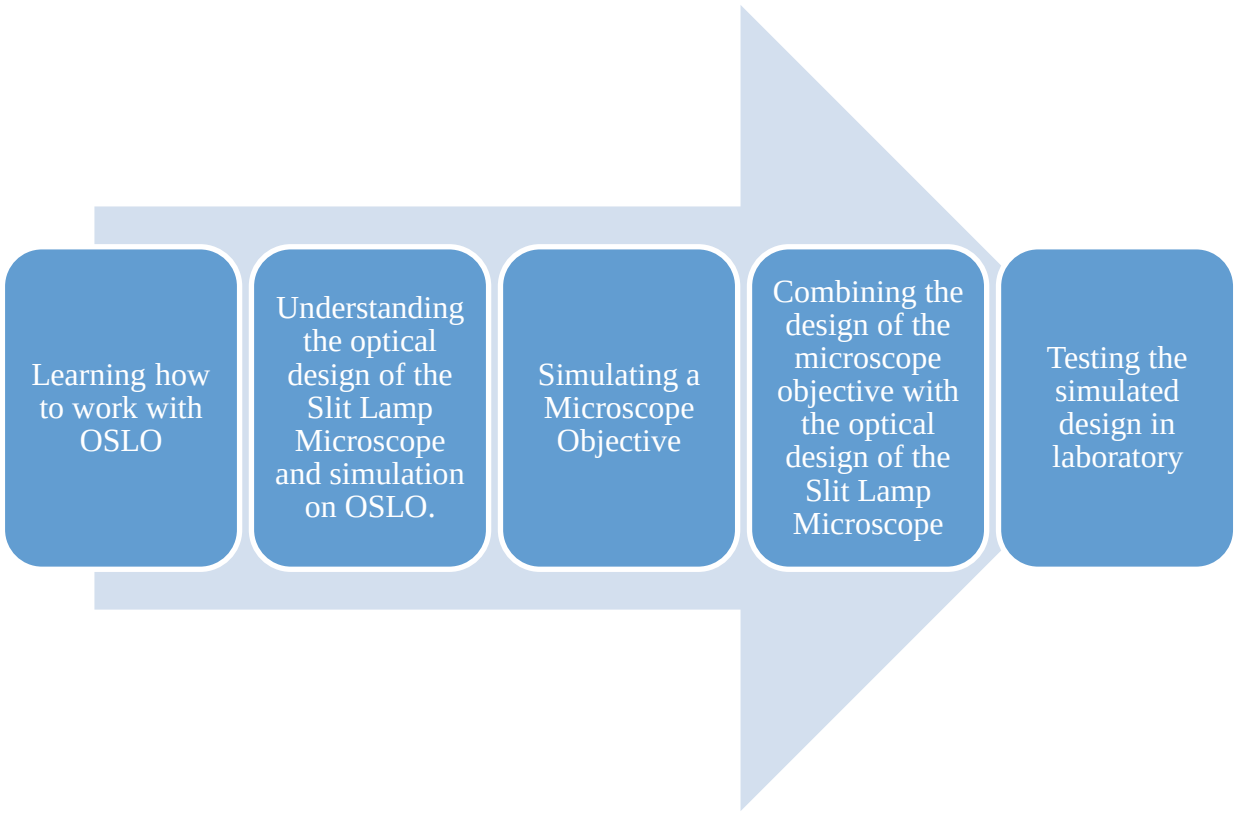

Figure 23 - Schematic Representation of the different stages of the Project.

4.1 - THE OPTICAL DESIGN OF THE SLIT LAMP MICROSCOPE SIMULATION

After learning how to use OSLO, it was necessary to understand the design of a slit lamp microscope and its optical characteristics. As said before, the slit lamp microscope is comprised by four main optical systems: eyepiece, relay lens, Galilean telescope and objective.

In Chapter 2, it is referred that the total magnification power of this instrument is given by the equation 5 [24]:

$$G = \frac{f_2}{f_1} \times g \times \frac{250\ mm}{f_3(mm)} \quad (5)$$

The information known about the optical characteristics of the components present in the slit lamp is scarce. Along with the information described above, only a few details are known and due to this, calculations had to be made in order to simulate the whole system with the OSLO software.

During the execution of this project, two different designs of slit lamp microscopes were made. One based on the Zeiss 30 SL-M model and other on a Nidek SL-1600 model.

4.1.1 - EYEPIECE

In order to begin a simulation project on OSLO it is essential to know the curvature radius of each lens to be added. Therefore, to simulate an eyepiece, it is necessary to have access to more information than just its magnification power.

One of the equations that rule the eyepieces establishes a relation between its magnification power (P_E), its focal length (f_E) and the standard least distance of distinct vision (D) - defined as 250 mm:

$$P_E = \frac{D}{f_E} \quad (6)$$

In Table 1 are presented the values of focal length determined for magnification power of 10 x, 12,5 x, 15x and 16x.

Table 1- Magnification Power and Respective focal length.

Magnification Power	Focal Length (mm)
10x	25
12,5x	20
15x	16,667
16x	15,625

Two eyepieces were chosen for the slit lamp simulations. Their choice was based on the specifications of each model considered. To simulate the Zeiss 30 SL-M model (Attachment B), the eyepiece designed had a magnification of 12,5x. For the other model, Nidek SL-1600 (Attachment C), the eyepiece chosen was the one with the magnification of 16x.

Since there was not any information about the type of eyepiece used in this instrument, it was decided to use a Huygens eyepiece design.

The Huygens eyepiece has a simple optical design with two plano-convex lenses. Therefore, to comply with this design it was essential to combine two plano-convex lenses to achieve an overall focal length of 20 mm for the first design and 15,625mm for the second one. These estimative were made recurring to the rules of Gaussian Optical Geometry (Attachment A). The eyepiece achieved for the first design had the characteristics described in Table 2. For the second design, the characteristics of the eyepiece are listed in Table 3.

Table 2 - Characteristics of 12,5x Huygens Eyepiece for Zeiss 30 SL-M model.

	R1(mm)	R2(mm)	D(mm)
Lens 1	15,65	1e20	4
Lens 2	0	1e20	4
Distance between lenses (mm)		30	

Table 3 - Characteristics of 16x Huygens Eyepiece for Nidek SL-1600 model.

	R1(mm)	R2(mm)	D(mm)
Lens 1	15,65	1e20	4
Lens 2	0	1e20	4
Distance between lenses (mm)		30	

4.1.2 - OBJECTIVE

The focal length of the slit lamp is usually given in the instrument data sheets. However, it is necessary to know other parameters before simulating the instrument. The magnification and distance between the objective and the eyepiece is essential. To calculate these values, two relations were used:

$$M_T = P_O \times P_E \quad (7)$$

$$P_O = \frac{D_{EO}}{f_O} \quad (8)$$

The first equation establishes a relation between the overall magnification power of a system (M_T) and the magnification power of both objective (P_O) and eyepiece (P_E). The second equation establishes that the magnification power of the objective is equal to the quotient between the tube length (D_{EO}) and the objective focal length (f_o). The distance, D_{EO}, was the value needed to start relating the eyepiece and the objective.

So, as the objectives and the eyepieces of the two slit-lamps have different values, the distances D_{EO} of the instrument also have to be different. These values are shown in Table 4.

Table 4 - Objective and tube length parameters for both slit lamp models.

	Original Eyepiece Magnification	Objective Focal Length (mm)	Objective Magnification (P_O)	Tube Length - D_{EO} (mm)
Zeiss 30 SL-M	12,5x	125	1,28x	160
Nidek SL-1600	16x	130	1x	130

Once the D_{EO} value is known, it is possible to estimate the real distance between the objective and the eyepiece. Again, these distances differ between the two instruments. The calculation is made by adding to D_{EO} the focal lengths of objective and eyepiece. For the Zeiss 30 SL-m the value is 305 mm while for Nidek SL-1600 is 235,625mm. The optical parameters to simulate these two lenses in OSLO software are presented in Table 5.

Table 5 - Specifications for objective lens of both slit lamps models considered.

	Curvature Radius 1 (R1)	Curvature Radius 2 (R2)	Thickness	Material
Zeiss 30 SL-M	128.7	-128.7	3.2	BK-7
Nidek SL-1600	134	-134	2.5	BK-7

4.1.3 - RELAY LENS

The last essential component to simulate a slit lamp microscope is the relay lens. The only parameter known about this lens is that it is positive. However, and since the parameters of the other components are already known, it is possible to obtain the focal length of this lens by using the equation 5.

The specifications of the relay lens, like the objective and the eyepiece, are not the same in every slit lamp model. Therefore, it was necessary to calculate two relay lenses, one for Nidek SL-1600 and another one for Zeiss 30 SL-M. For the first one the calculated focal length was 130 mm while for the second one was 160 mm. With this information, and recurring again to the Gaussian Optical Geometry, it was possible to simulate these two lenses in OSLO. Their optical parameters are presented in Table 6.

Table 6 – Lens Specifications for relay lens of both models considered.

	Curvature Radius 1 (R1) (mm)	Curvature Radius 2 (R2) (mm)	Thickness (mm)	Material
Zeiss 30 SL-M	164	-164	8.2	BK-7
Nidek SL-1600	134	-134	2.5	BK-7

4.1.4 - GALILEAN TELESCOPE

The Galilean Telescope was not, initially, considered in the design of the slit lamp since every slit lamp microscope has one position in which this device is absent. However, different combinations of lenses were designed to build 3 different Galilean telescopes that could be introduced in the final design.

The magnification introduced by each Galilean telescope is relative to the microscope model in use. Zeiss 30 SL-M model supports 4 different magnifications with Galilean telescope: 6x, 10x, 25x, and 40x. Since the other parameters of the equation 5 are known, it is possible to obtain the magnification given by the Galilean telescope. The values are specified in Table 7.

Table 7 - Galilean telescope magnifications for both slit lamp models.

Total Magnification	Galilean Telescope Magnification
40 x	2,5 x
25 x	1,56 x
10 x	0,625 x
6 x	0,375 x

The same calculations were made for the Nidek SL- 1600 model. Here, the total magnification available with the Galilean telescope were also 40x, 25x, 10x, and 6x. Although, the parameters of the other components are different, the magnification without Galilean telescope is the same. Therefore, the individual Galilean telescope magnification will be the same as the Zeiss model – see Table 7.

After obtaining the individual magnification given by each Galilean telescope, it was possible to determine the optical characteristics of the telescope. As said before, the Galilean telescope is built with two lenses, one positive and one negative. It is also known that the total magnification of the Galilean telescope is given by the equation 9:

$$M_T = \frac{f_E}{f_O} \quad (9)$$

The magnification power (M_T) is known and, the distance between the two lenses was fixed. The focal length of the telescope objective (f_O) and the focal length of the telescope eyepiece were calculated recurring to the equation 9 and to the OSLO software.

Once all the information concerning the slit lamp microscope optical components was collected and calculated, it was possible to simulate the slit lamp, using the OSLO

software. The optical design of the slit lamp is depicted in Figures 24 and 25, one for each model design.

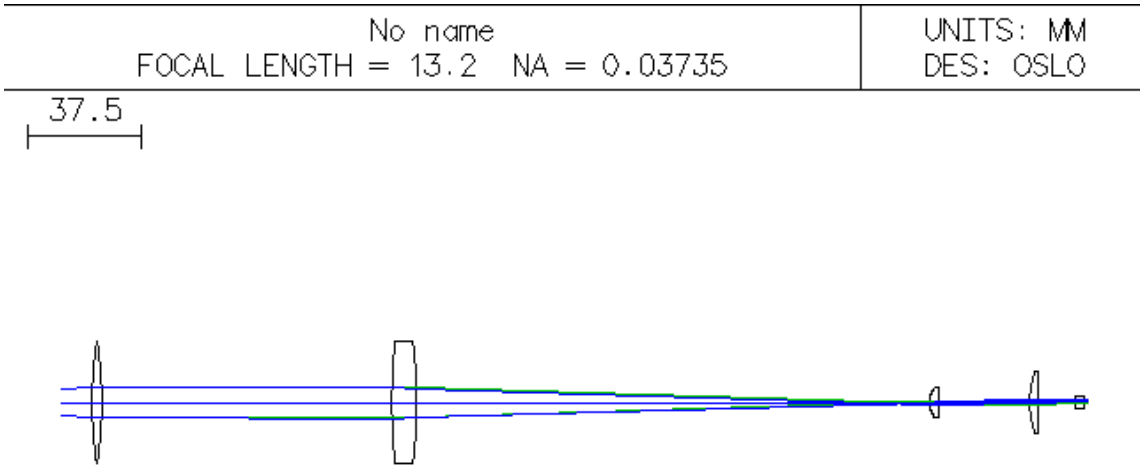

Figure 24 - Slit Lamp Simulation Design for Zeiss 30 SL-M model.

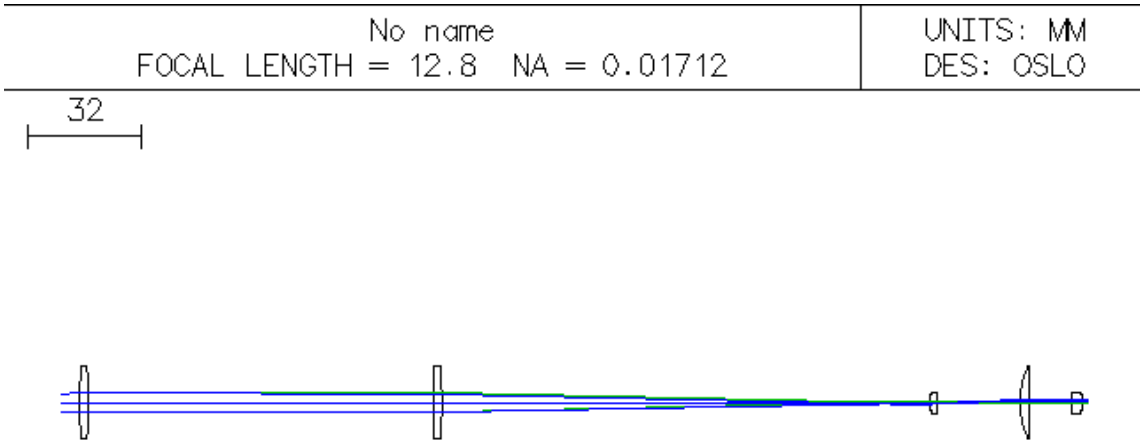

Figure 25 - Slit Lamp Simulation Design for Nidek SL-1600 model.

These simulations do not take in account the Galilean telescope since its introduction in this slit lamp microscope is not mandatory. Both designs have a 16mm positive lens to simulate the eye optics.

4.2 - SIMULATION OF A TYPICAL MICROSCOPE OBJECTIVE

Every confocal microscope includes a high quality microscope objective. Since the purpose of this project is to design a confocal module for the slit-lamp, the presence of a microscope objective in the optical design module is mandatory. Due to this, a microscope objective was designed and simulated for posterior coupling to the previous design of the slit lamp microscope.

The design of the microscope objective was based on a patent registered by Esswein. [29] This objective was designed to have a 40x magnification power and a numerical aperture of 0,65 with correction to infinity. Although the optical characteristics of this objective were described in the patent document, the diameters of the lenses were not compatible with the design of the slit lamp. Due to this, some changes in optical characteristics were made to fit with the slit-lamp design. The changes made did not affect the desired characteristics of the objective: magnification power, numerical aperture and correction to infinity

The optical specifications of the objective are listed in Table 8 and the simulation projected is depicted in Figure 26. The object was 2,4 mm distant from the objective (working distance).

Table 8- Lens Specifications for 40x, 0.65 NA objective.

Lens Number	Curvature Radius (R1) (mm)	Curvature Radius (R2) (mm)	Curvature Radius (R3) (mm)	Thickness	Distance from the previous surface	Material
1	-9.5	-6.45	----------	6.3	2,4	SK2
2	40	-16	----------	5	0.9	SK16
3	50	11	-23.6	2 (R1-R2) 5 (R2-R3)	8	SF56 (R1-R2) K7(R2-R3)

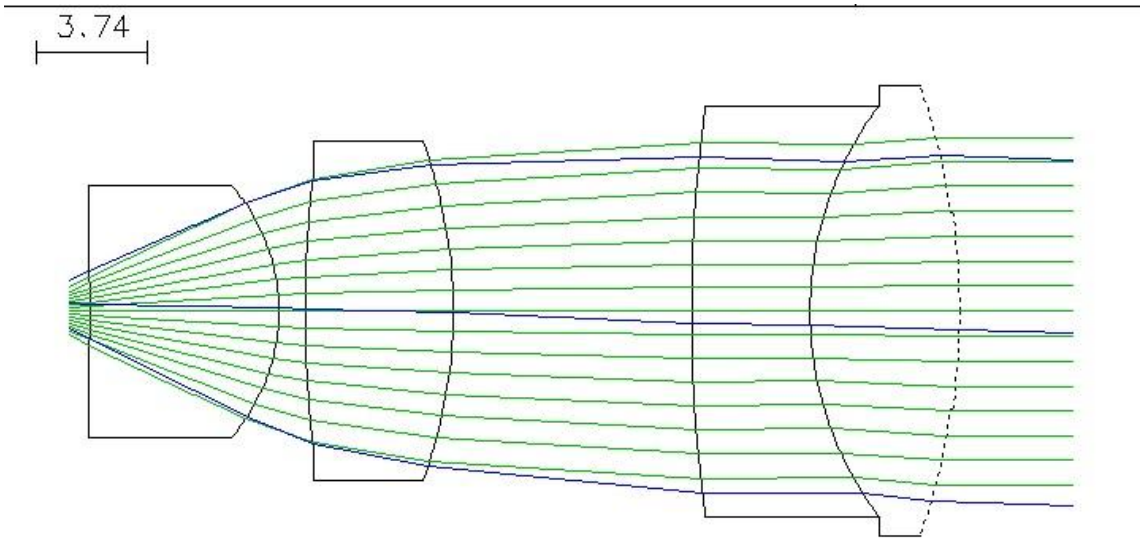

Figure 26 - 40X, 0,65 NA Microscope Simulation Design.

4.3 - COUPLING THE MICROSCOPE OBJECTIVE WITH THE SLIT LAMP MICROSCOPE

Having the simulation of both the objective and the silt lamp microscope, it was possible to start studying how to couple the two devices.

First, some changes on the design of the slit lamp microscope had to be made. Since it was intended to acquire the images provided by the microscope with a CCD camera, the use of an eyepiece became optional. Due to this, and to simplify the design, the lenses corresponding to the eyepiece were removed – Figure 27.

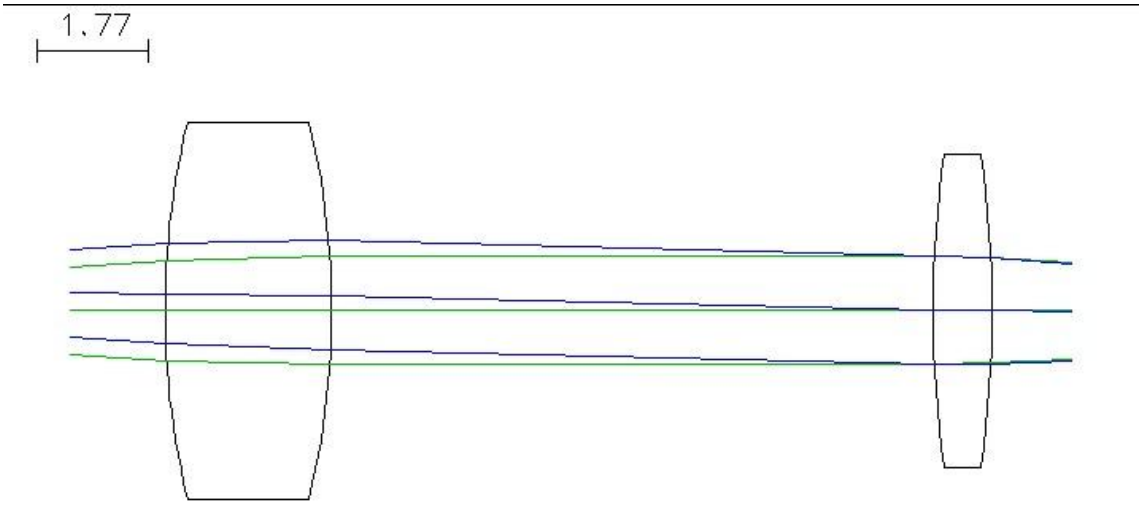

Figure 27 - Slit Lamp design without eyepiece and Galilean Telescope.

After observing a real slit lamp microscope, it was concluded that the relay lens was placed after the point where the optical path was intersected and diverted to the CCD camera. Though, the lens correspondent to the relay lens was also removed from the design. The whole design was reduced to one lens only, the slit lamp objective – Figure 28.

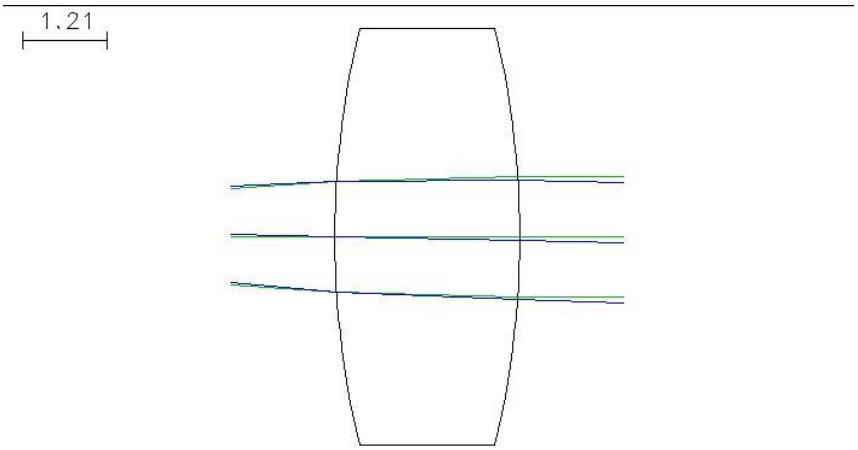

Figure 28 - Slit-Lamp Objective.

The first lens in the slit lamp microscope is the objective. This objective must be placed at a fixed distance from the object, depending on its focal length. This means, that the position of the object must coincide with the focal point of this lens. That way, the ray lights exiting from the objective lens will be collimated.

Placing a typical microscope objective before the slit lamp objective without any optical component between them will change the optical path of the instrument. To prevent this from happening, another lens must be used to form an image exactly on the focal point of the slit lamp objective. This lens had to be negative since the rays coming from the typical microscope objective are collimated. – Figure 29.

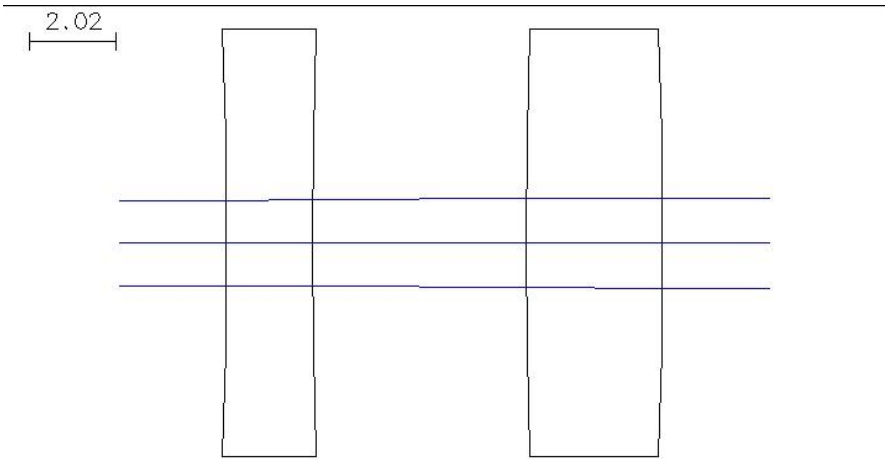

Figure 29 - The effect of a negative lens on the slit lamp objective.

The last change made to the design was the addition of a positive lens after the slit lamp objective to create an image on the CCD with the required overall magnification.

This design was based on the characteristics of 30 SL-M Zeiss model of slit lamp microscope. The optical characteristics used for the simulation are presented in Table 9. The optical design obtained is depicted in Figure 30.

Table 9 - Specifications for Zeiss 30 SL-M slit lamp simulation

Lens Number	Curvature Radius 1 – R1 (mm)	Curvature Radius 2 – R2 (mm)	Curvature Radius 3 – R3 (mm)	Thickness	Distance from the previous surface	Material
1	-9.5	-6.45	----------	6.3	2.15	SK2
2	40	-16.3	----------	5	0.9	SK16
3	50	11.5	-23.6	4(R1-R2) 5(R2-R3)	8	SF56 (R1-R2) K7 (R2-R3)
4	-103.7	103.7	----------	4	50	BK7
5	128.7	-128.7	----------	3.2	25	BK7
6	500	-500	----------	5.9	100	BK7

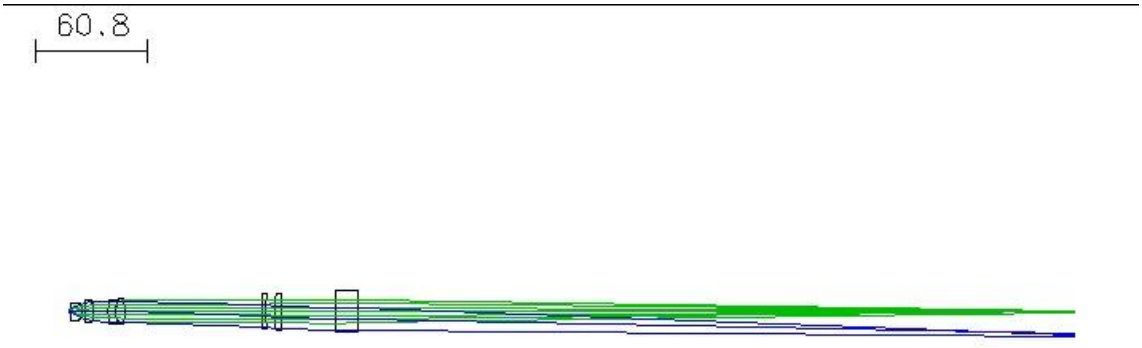

Figure 30 - Coupled system simulation.

After the laboratory tests started, another simulation designed was tested in OSLO software. This new simulation took into account all the optical components of the slit lamp microscope as well as the microscope objective and negative lens used in the previous described design.

The specifications of this system are present in Table 10 and its optical design on Figure 31. The simulation was based on Nidek SL-1600 slit lamp model.

Table 10 - Lens specifications for the second coupled system designed.

Lens Number	Curvature Radius 1	Curvature Radius 2	Curvature Radius 3	Thickness	Distance from the previous surface	Material
1	-9.5	-6.45	----------	6.3	2.15	SK2
2	40	-16.3	----------	5	0.9	SK16
3	50	11.5	-23.6	4(R1-R2) 5(R2-R3)	8	SF56 (R1-R2) K7 (R2-R3)
4	-103.7	103.7	----------	4	70	BK7
5	134	-134	----------	2.5	19	BK7
6	134	-134	----------	2.5	140	BK7
7	5.17	1e20	----------	2.5	140	BK7
8	22.05	1e20	----------	2.5	10	BK7
9	16	-16	----------	3	6	BK7

Figure 31- Second coupled system simulation.

4.4 - TESTING THE SIMULATED DESIGN IN LABORATORY

To test the simulated design in laboratory environment, optical components had to be purchased in order to mount a device which would include the lenses necessary to test the simulation made in OSLO. The list is present in Table 11. All the components were ordered from ThorLabs (ThorLabs Inc. New Jersey, USA):

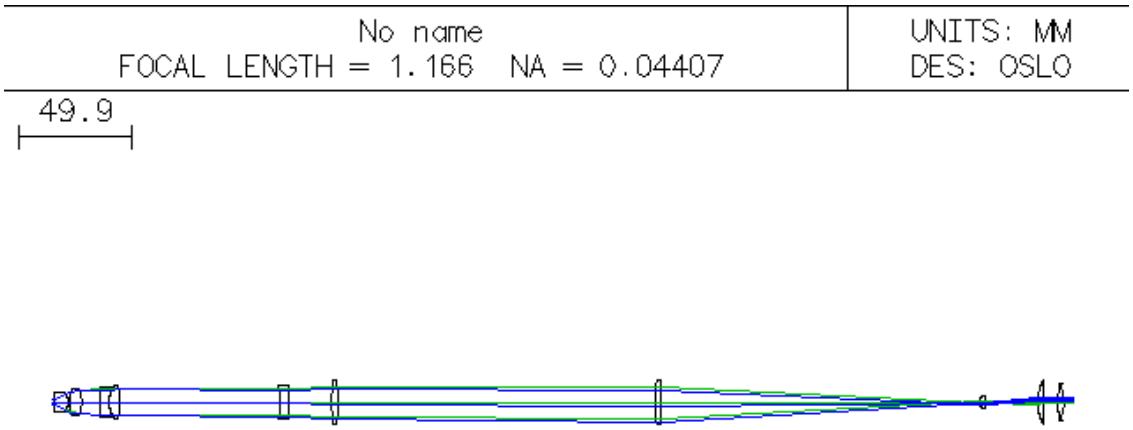

Table 11 - List of ordered optical components to evaluate the design in laboratory.

Products' Designation	Reference
Cage System Adapter to switch between 30 mm and 60 mm	LCP02
Rotating Adjustable Focusing Element 1/2''	SM1V05
Adapter with External SM1 Threads and Internal RMS Threads	SM1A3
Lens Tube, L=1'' with one retaining ring included	SM1L10
Lens Tube, L=2'' with one retaining ring included	SM1L20
Mini Series Cage Assembly, 2'' Long with 4mm of dimater	SR2
N- BK7 Bi-Concave Lens, 25,4 mm diameter, f=-100mm, uncoated	LD1613

After fixing the device containing the lenses, it was necessary to add a new illumination system and a camera to acquire images. The illumination system provided was temporary, with a blue led lamp coupled to a diffuser placed behind the target – retro-

illumination. As for the camera, the model used was the Cohu 1100 series RS-170 CCIR Monochrome camera. Its specifications are present in Attachment D.

In the laboratory, some of the components used were not exactly the same as the ones simulated. The objective was the main difference between the two projects. In the simulation project, the developed objective had 40x magnification power, a NA of 0,65 and was corrected to infinity. For the laboratory project, the objective used (Zeiss Achroplan water immersion 0.75) had the same magnification power, was also corrected to the infinity, but the NA was 0.75. Although the two objectives were very similar, the lens design of Zeiss Achroplan is unknown, since we could not find any information about it.

Another problem faced while mounting the device in the laboratory was the acquisition of images. Initially, the project determined that the camera intersected the optical path before the relay lens. However, experimentally, this was not possible. The solution provided was to mount the camera behind the 16x eyepiece with a lens with a focal length of 16mm between them. That way, it was possible to acquire images with a reasonable quality to proceed with the tests described in the next chapter. The simulation of this design is described in the section 4.3.

Two different test targets were used to test optical characteristics. A negative USAF 1951 test target (Melles-Griot USAF 1951 Chromium Negative 04 TRN 003) was used to measure lateral resolution, of magnification and to assess distortion. A sinusoidal target (Edmund Optics NT54-804) was used to test the contrast response of the system and its modular transfer function (MTF). Their pictures are presented in Figure 32 and in Figure 33.

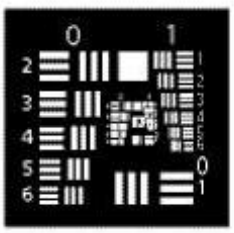

Figure 32 - USAF 1951 chromium negative resolution test target.

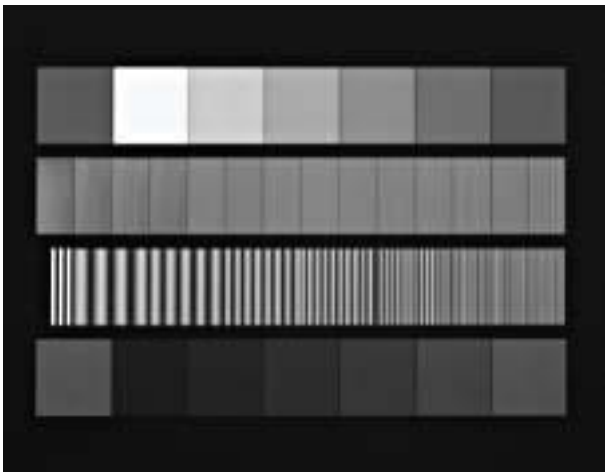

Figure 33 – Sinusoidal test target (Edmund Optics NT54-804).

The complete system mounted on the slit lamp microscope is depicted in Figures 34, 35 and 36.

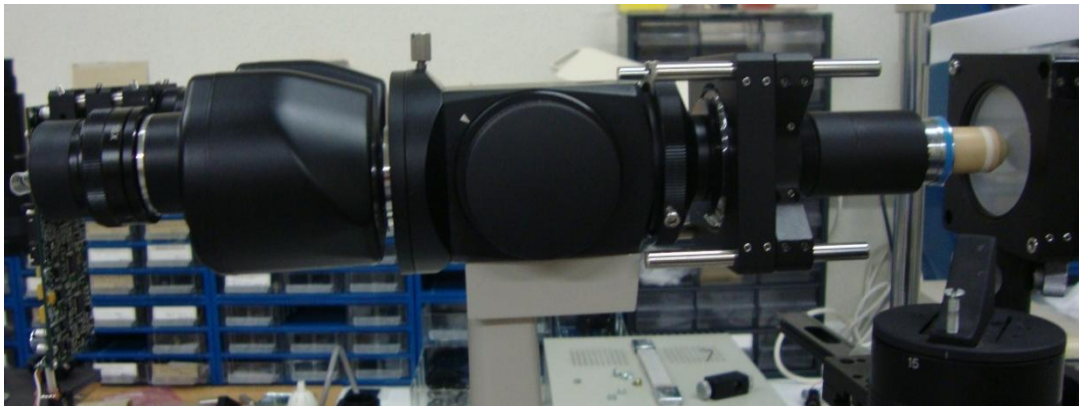

Figure 34 - Picture of the overall system.

Figure 35 - Picture of the CCD Camera mounted on the eyepiece.

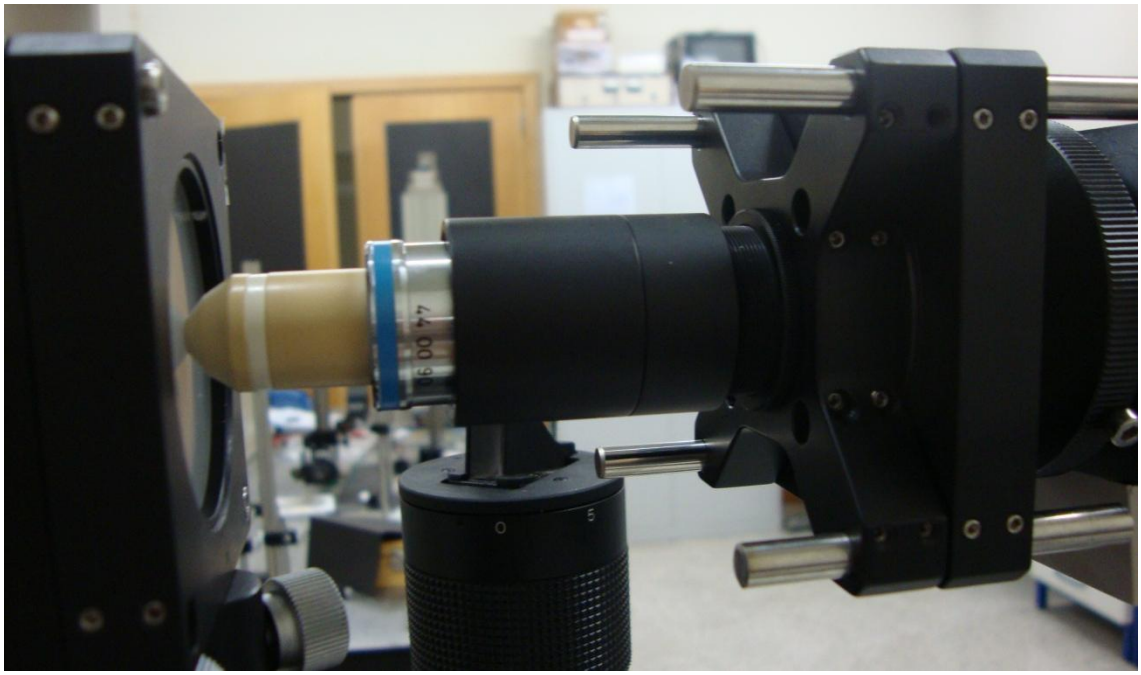

Figure 36 - Picture of the device containing the microscope objective and the negative lens

A 3D model of the slit lamp microscope and the coupled device was also designed. The results are depicted in Figures 37, 38 and 39.

Figure 37 – Slit Lamp with optical module – overall system.

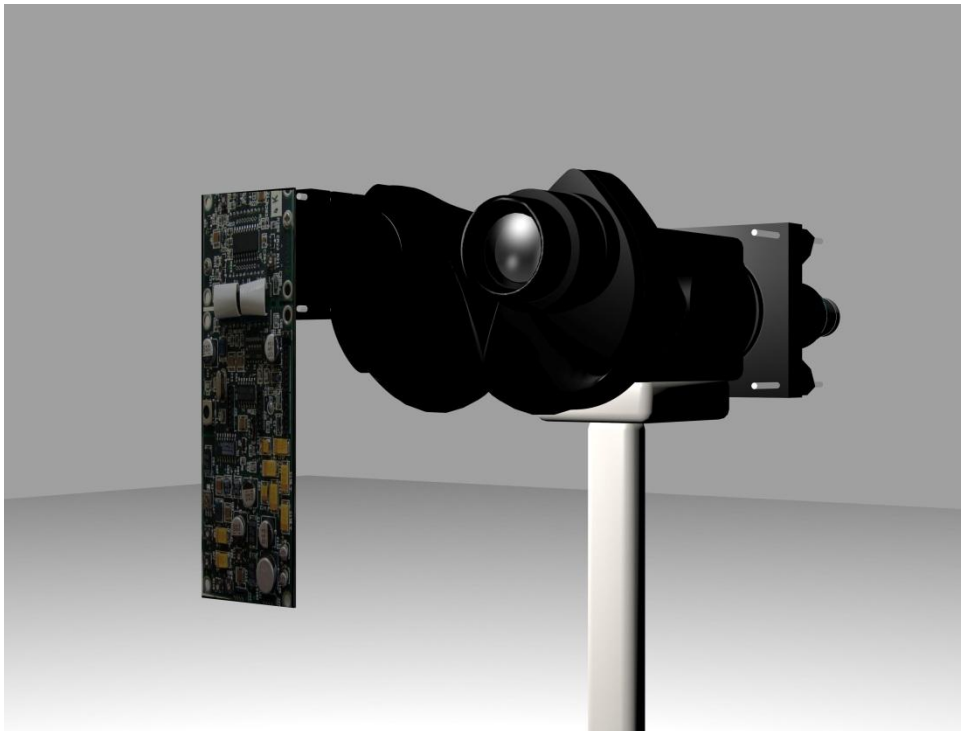

Figure 38 – Slit Lamp with optical module – eyepiece and CCD camera.

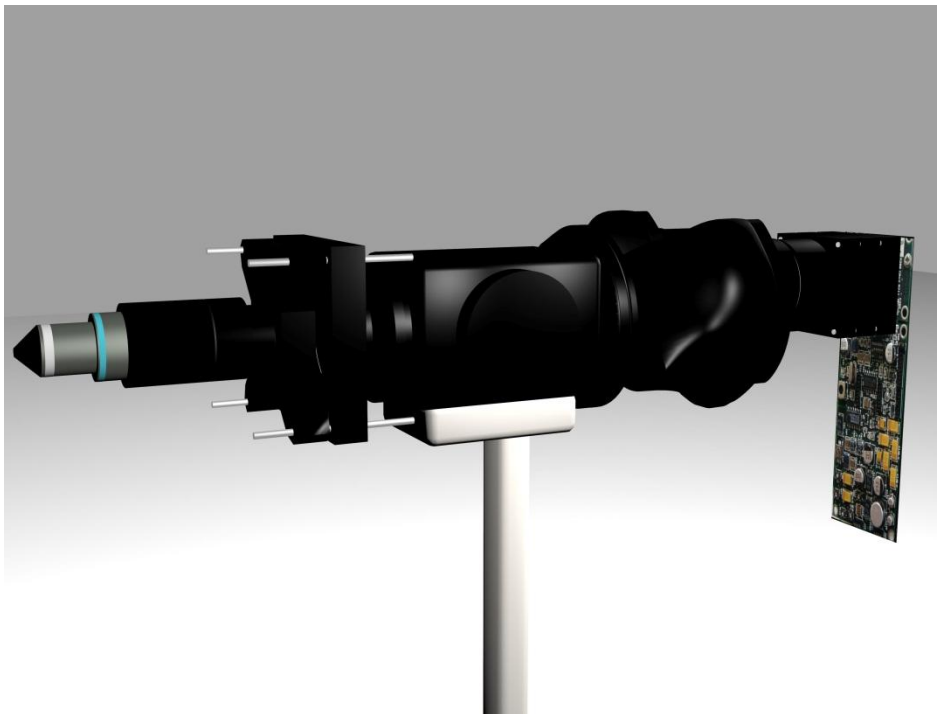

Figure 39 – Slit Lamp with optical module – optical components.

CHAPTER 5 – RESULTS AND PROJECT ANALYSIS

In this chapter two different types of results are present. Since the project had a simulation phase on OSLO and a laboratory test phase, the results for both will be presented separately.

5.1 - SIMULATION ON OSLO

5.1.1 - TESTS PERFORMED

OSLO can perform different optical tests to evaluate the quality of optical designs. In order to evaluate the designs described in the previous chapter, the tests chosen were: the image quality, ray analysis report, PSF (Point Spread Function) analysis, MTF analysis and energy analysis. These tests were performed for designs presented in Chapter 5: slit lamp designs and coupled system designs. With the help of OSLO software, it was also possible to determine the magnification of the system.

The image quality test is mainly a visual test. Recurring to the extended source tool *xsource /grid* it was possible to observe the simulated image of a grid-shaped object.

The ray analysis test outputs plots representing the level of the main Seidel aberration types.

The Point Spread Function (PSF) analysis produces three PSF plots for different positions of the field, on-axis, 70% of the field and full field. It outputs both 3D and 2D (linear spread function) plots. These plots demonstrate the energy distribution in an image for a point object source, often called the optical impulse response. A diffraction limited system shows a perfect Gaussian distribution in these plots.

The OSLO software also performs modular transfer function (MTF) analysis. This test is made by simulating a sinusoidal object, with black and white lines at a precise spatial frequency. The plot provided by the software presents the contrast modulation against the spatial frequency. MTF is correlated with the spatial resolution of the system. This limited spatial resolution is associated with the diffraction limit. According to Rayliegh's resolution criterion, the Rayleigh diffraction limit, line pairs per millimetre (lp/mm) is given by:

$$Rayleigh\ limit = \frac{1}{1.22f/\#\lambda} \quad (10)$$

where f/# is the f-number of the system and ʎ is the wavelength..

This limit in a MTF distribution graphic corresponds to 9% of MTF value. The frequency corresponding to this value is the diffraction limited spatial resolution of the system in study [30].

The energy analysis gives the designer a plot representing the image energy for a circle with a given radius. This is related with the Airy's diffraction pattern. The angular irradiance distribution for a circular slit is given by the following equation:

$$I = I_0\left[\frac{2\delta_1(u)}{u}\right] \quad (11)$$

where $u = \frac{\pi D}{\lambda}\sin(\theta)$, D is the circular aperture diameter, ʎ is the wavelength, I_0 is the maximum irradiance and δ_1 represents the first order Bessel function. The first zero of δ_1 defines the limits of the Airy disk, the central disk of high irradiance of the diffraction pattern, In this region, it is deposited 84% of the energy diffracted by the aperture. The circumference of the second black disc defines the region where 91% of the energy is deposited and the third black disc of the diffraction pattern sets the limits for the location where lies 93,8% of the energy.

The energy distribution of a lens system can be compared against to the ideal diffraction-limited distribution, given by the Airy pattern. The radial coordinates of Airy pattern are given by the following equations:

$$u = \frac{\pi D}{\lambda}\sin(\theta) = \frac{\pi D}{\lambda} \times \frac{r'}{R} \quad (12)$$

$$r' = \frac{uR\lambda}{\pi D} \approx \frac{uf/\#\lambda}{\pi D} \quad (13)$$

where *f/#* corresponds to the f number. As this value has a direct relation with NA, (f/#=1/2NA), the above equation becomes:

$$r' = \frac{u\lambda}{2\Pi NA} \quad (14)$$

The radius of the regions with 84% and 91 % are given by the following equations:

$$r'_{84\%} = \frac{0.61\lambda}{NA} \quad (15)$$

$$r'_{91\%} = \frac{1.115\lambda}{NA} \quad (16)$$

The values given by these equations can be compared to the values given by the energy distribution analysis provided by OSLO test [15].

All the simulations wre made with a wavelength of 587 nm.

5.1.2 - SLIT LAMPS MICROSCOPE SIMULATION DESIGNS

For the first model simulated, Zeiss 30 SL-M model, the design obtained did not include the Galilean telescope. For this design, the tests described above were implemented.

The first one, the ray curve intercept analysis, produced the results contained in Figure 40.

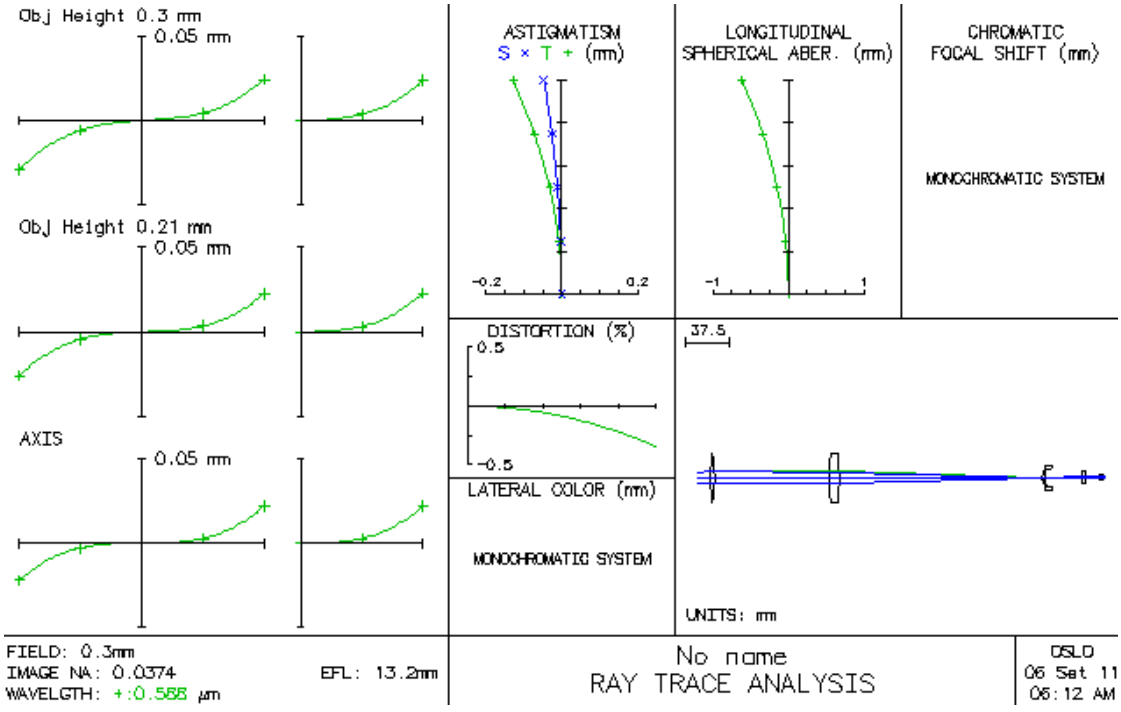

Figure 40 – Ray trace analysis results for Zeiss 30 SL-M slit lamp.

This test produces a series of plots where is possible to estimate the value of different aberrations. In all the plots the limit value is small, less than 1. This means that the level of aberrations is low.

The astigmatism plot shows a slight difference between the tangential rays (green –T) and sagittal rays (blue - S), being the aberration in tangential section slightly higher. As for spherical aberration, by observing the correspondent plot, it can be concluded that the variation with the pupil radii is very low which implies that the spherical aberration is also very low and do not affect the final image significantly.

The graphic for distortion shows the variation of this aberration with the field height. Observing the plot, it can be concluded that the level of the distortion is practically inexistent, since it is lower than 0,5%. This is confirmed by observing the Figure 41.

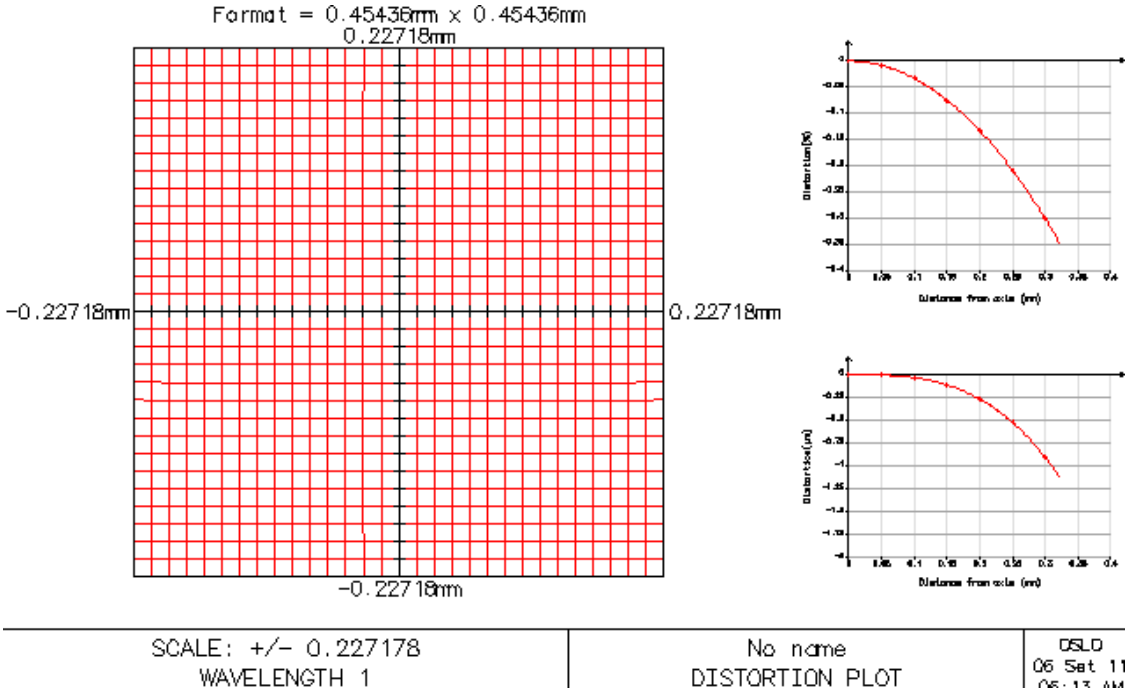

Figure 41 – Distortion test results.

In Figure 41, it is visible that the image does not appear distorted and that the deviation is very low in both graphics, measured in μm and in percentage (%).

The point spread function (PSF) was also tested. The results are presented in Figure 42.

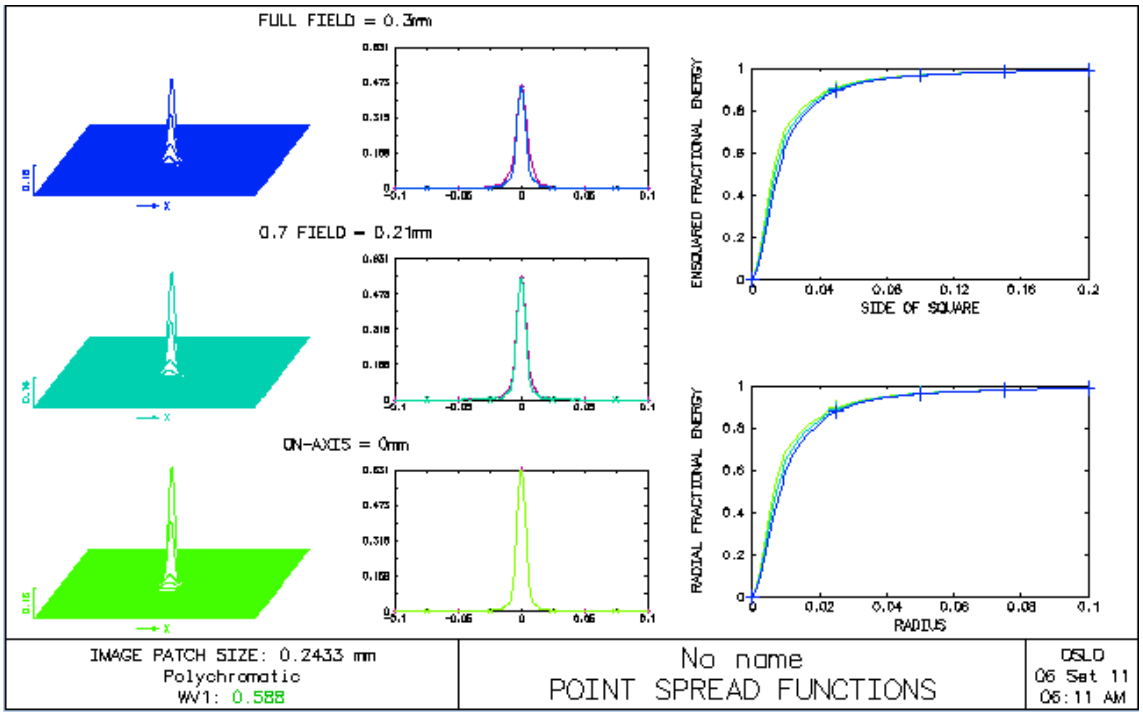

Figure 42 – Point Spread Function (PSF) test results for Zeiss 30 SL-M slit lamp model.

In all the plots, it is possible to see a well-centred and well defined peak. On-axis, 0% field, has a response very close to the ideal for an impulse input. When 70% and full field are considered, the peak height slightly decreases, but the shape continues to be similar to a Gaussian curve. This information allows two conclusions: the illumination spreading on the image is practically inexistent and the intensity of light decreases with the increasing of axis distance. These values point to a good quality of image.

In order to estimate the spatial resolution, the modular transfer function (MTF) was computed. The results are presented in Figure 43.

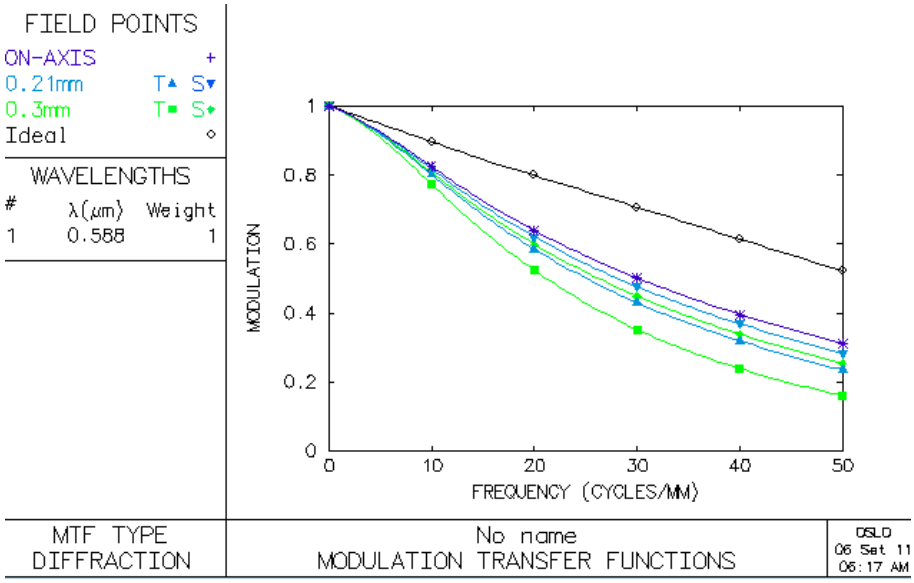

Figure 43 – Modular Transfer Function (MTF) results for Zeiss 30 SL-M slit lamp model.

In this plot, the lines corresponding to different field points have different responses. These curves are not coincident with the ideal response and the MTF performance decreases with the field size. However, the overall response can be considered as acceptable. For high frequencies (50 cycles/mm), the MTF value is above 0,2 which means that the system has good contrast response and a spatial resolution around 90 lp/mm – Figure 44.

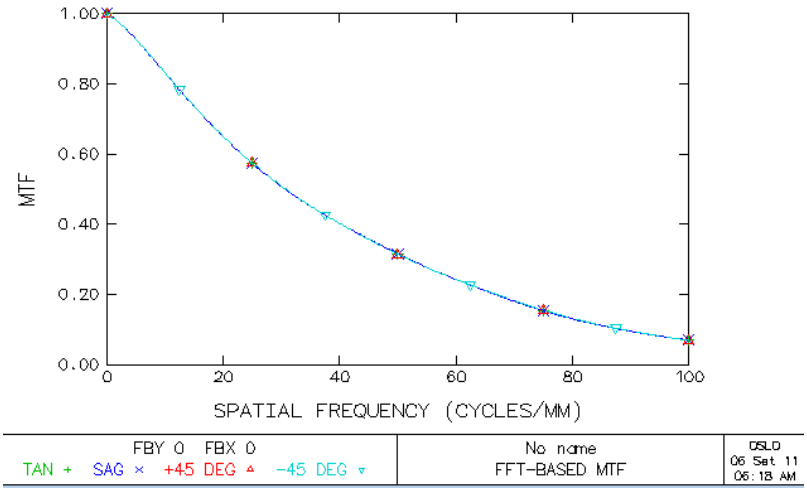

Figure 44 – MTF response results for Zeiss 30 SL-M slit lamp model.

In the last test to evaluate the design quality, energy analysis, the results, presented in Figure 45 show the energy response to the diffraction radius.

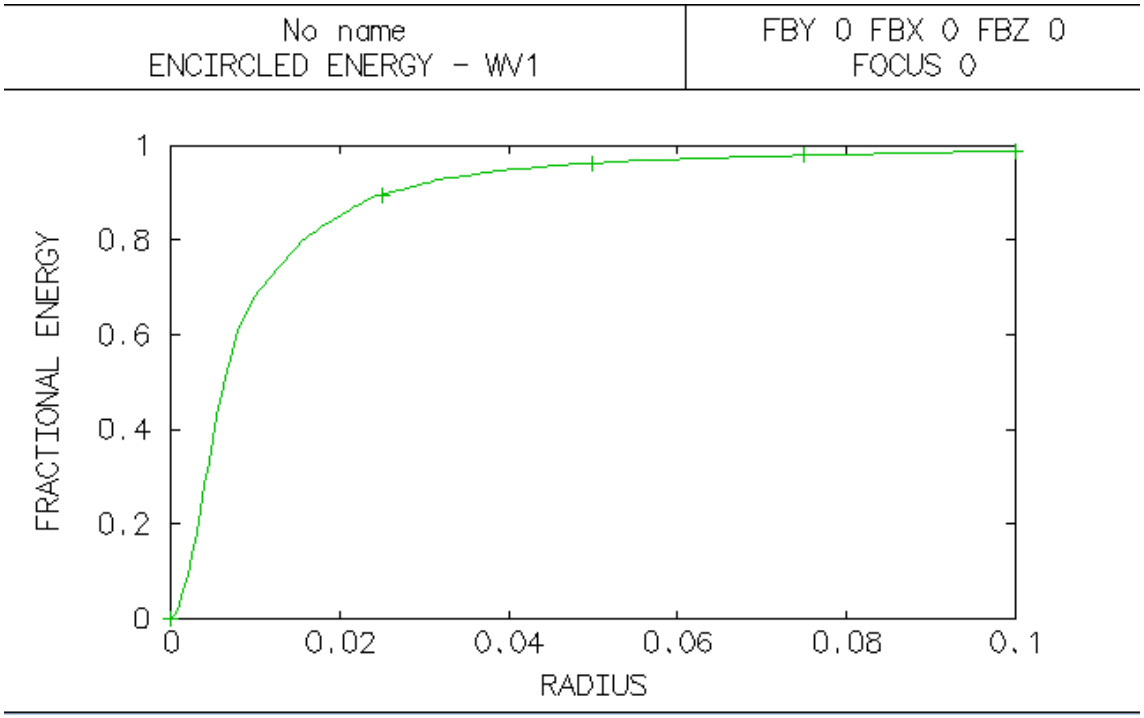

Figure 45 – Energy analysis results for Zeiss 30 SL-M slit lamp model.

Since the NA is 0.04 for this system, 84% of the energy should be within a radius of 0.009 mm. The energy plot demonstrates that 84% of energy is only reached for a radius above 0,02. This means, that the performance of the slit lamp is not diffraction limited, an expected result, though it is not far from the limit.

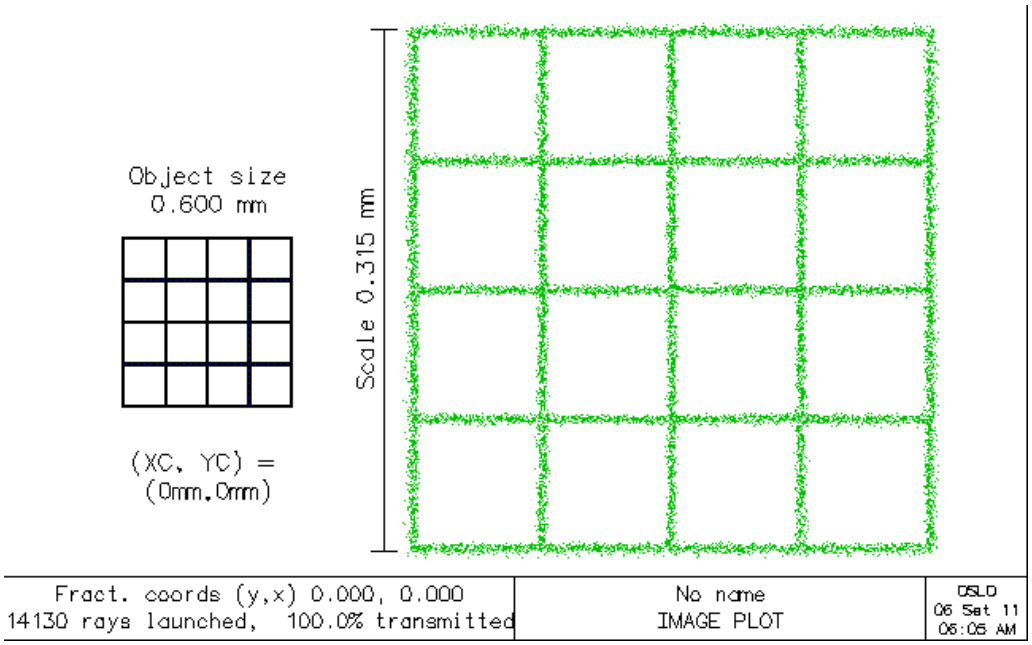

Figure 46 – Final image of a grid-shaped object with 0.3 mm height.

Figure 46 shows the image produced by the optical system for a grid shaped object. Visual inspection of the image allows us to state that the quality of the optical system is adequate for its purpose.

For the simulation design of the model Nidek Sl-1600, the same tests were performed. The figures in the following pages contain the results obtained for this design

Ray trace Analysis produced the results present in Figure 47:

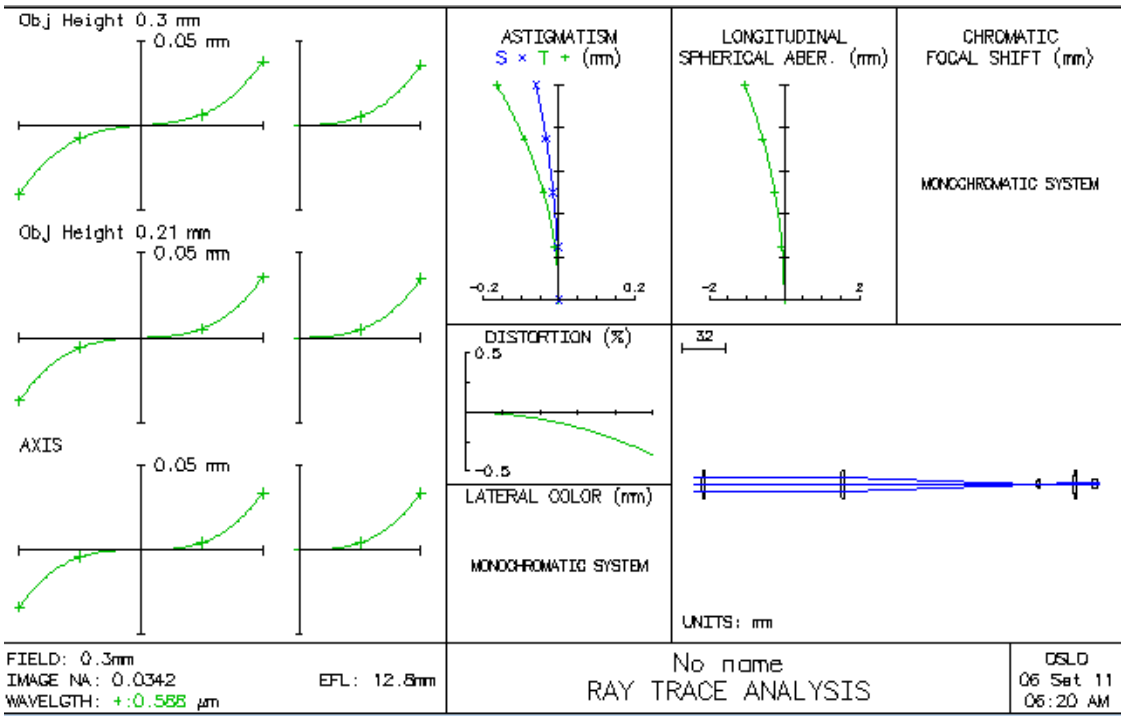

Figure 47 – Ray trace results for Nidek SL-1600 slit lamp model.

Like in the previous slit-lamp model, the limit values for different aberrations type are very low. Astigmatism is limited by 0.2 mm while longitudinal spherical aberration and distortion are limited by 0,5mm. In the astigmatism plot there is a difference between the sagittal and tangential rays. However since the limit value is low, this type of aberration should not affect the final image. The same happens with longitudinal spherical aberration, its variation with the pupil radii is also very low, which also means that its influence will not be visually percept in the final image.

The influence of distortion aberration can be confirmed by observation of Figure 48.

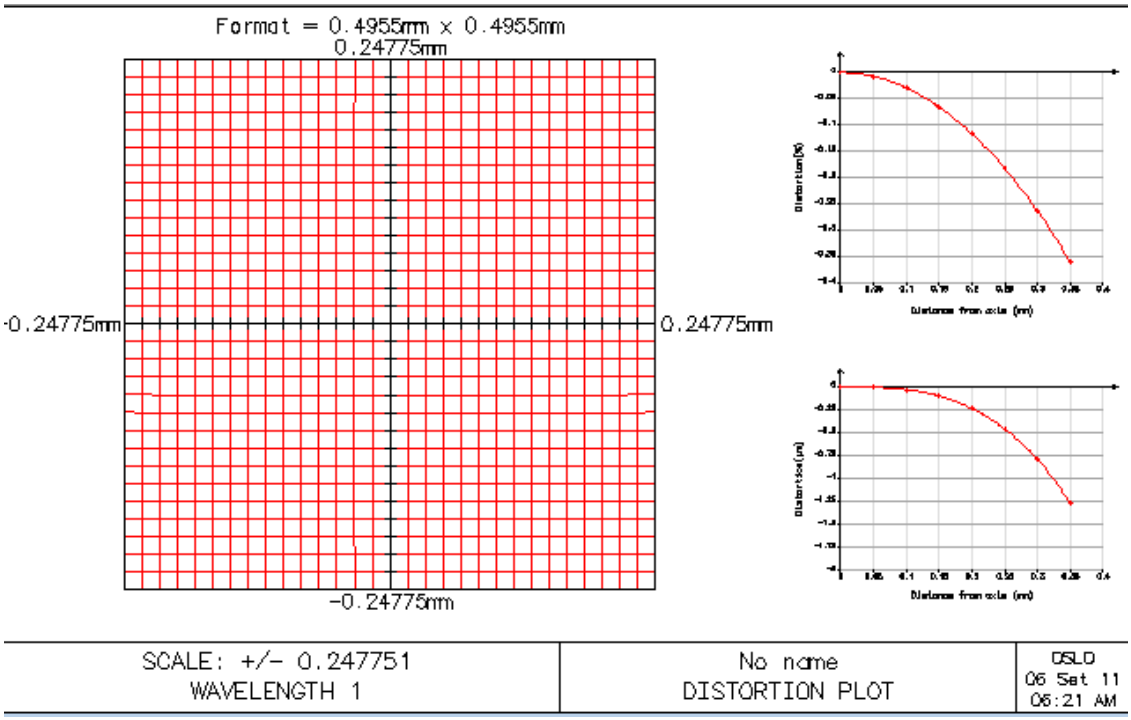

Figure 48 – Distortion results test for Nidek SL-1600 slit lamp model.

Observing the image and the plots, it is possible to understand that this type of aberration do not affect the image quality.

Figure 49 shows the PSF report for the respective test

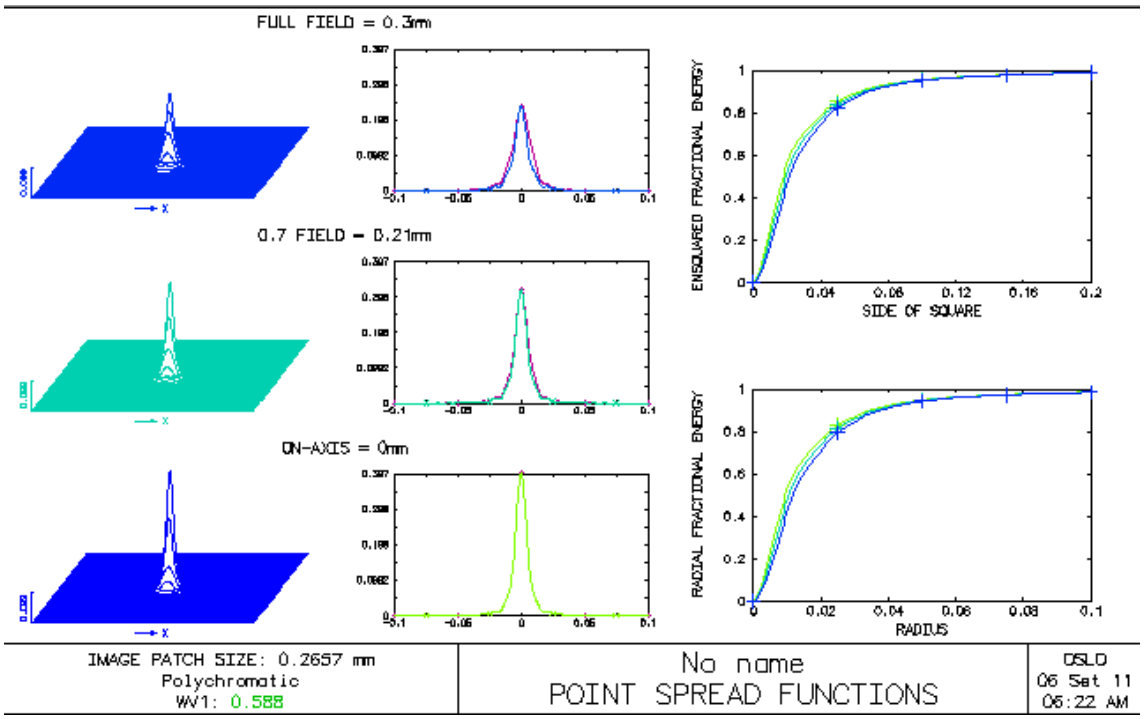

Figure 49 – Point Spread Function (PSF) test results for Nidek SL-1600 slit lamp model.

The PSF analysis shows a perfect Gaussian distribution in three positions of the field. However, the maximum value ate the peak decreases with the distance to the axis. This means that the intensity of light in the image is lower for objects off axis, but it also means that the spreading in the illumination is inexistent and that the image will appear as a single spot whatever is the distance from the axis.

Figure 50 depicts the results of the MTF test performed for Nidek design.

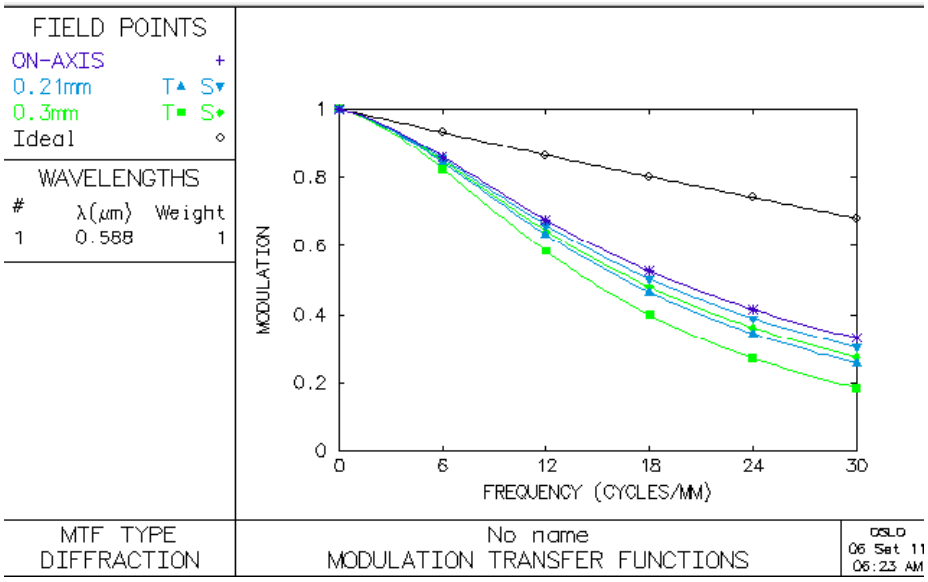

Figure 50 – Modular Transfer Function test results for Nidek SL-1600 slit lamp model.

By analyzing the MTF response, it can be concluded that none on the curves represented has an ideal MTF response, which means that the system is diffraction limited. However, the contrast response is considered good since for high frequencies (30 cycles/mm), the MTF value is above 0,20. From the plot, it can also be concluded that the MTF response decreases with the distance from axis.

The spatial resolution, associated to 9% of MTF value, is near 65 lp/mm – Figure 51.

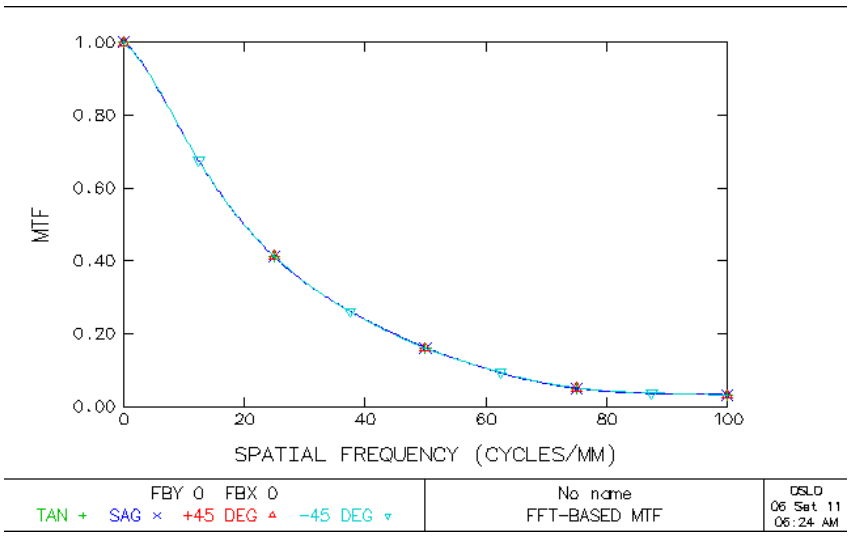

Figure 51 – MTF response results for Nidek Sl-1600.

The energy analysis response is presented in Figure 52

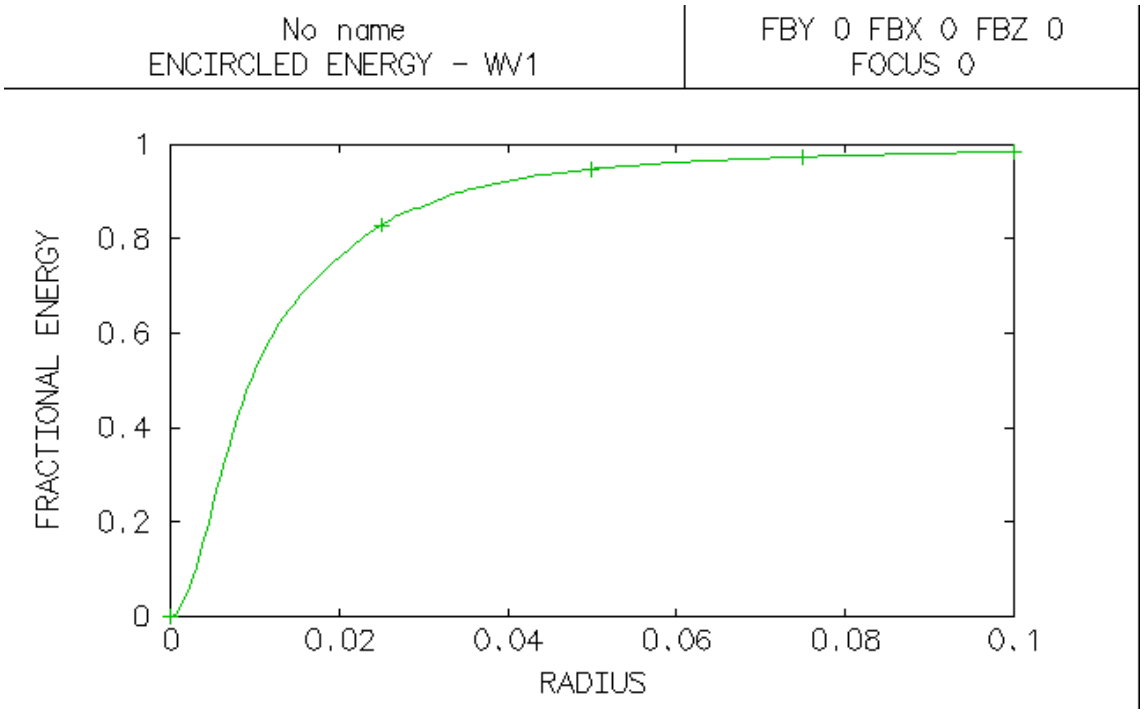

Figure 52 – Energy analysis results for Nidek SL-1600 slit lamp model.

As the NA is 0,04, according to equation 15, 84% of the energy should be deposited in the area limited by 0.009 mm radius circumference. From Figure 52, it can be concluded that this condition is not met. Instead, the radius value for 84% of energy is slightly higher than 0,02, not far from the diffraction limited value. This means that the system should have a good image quality.

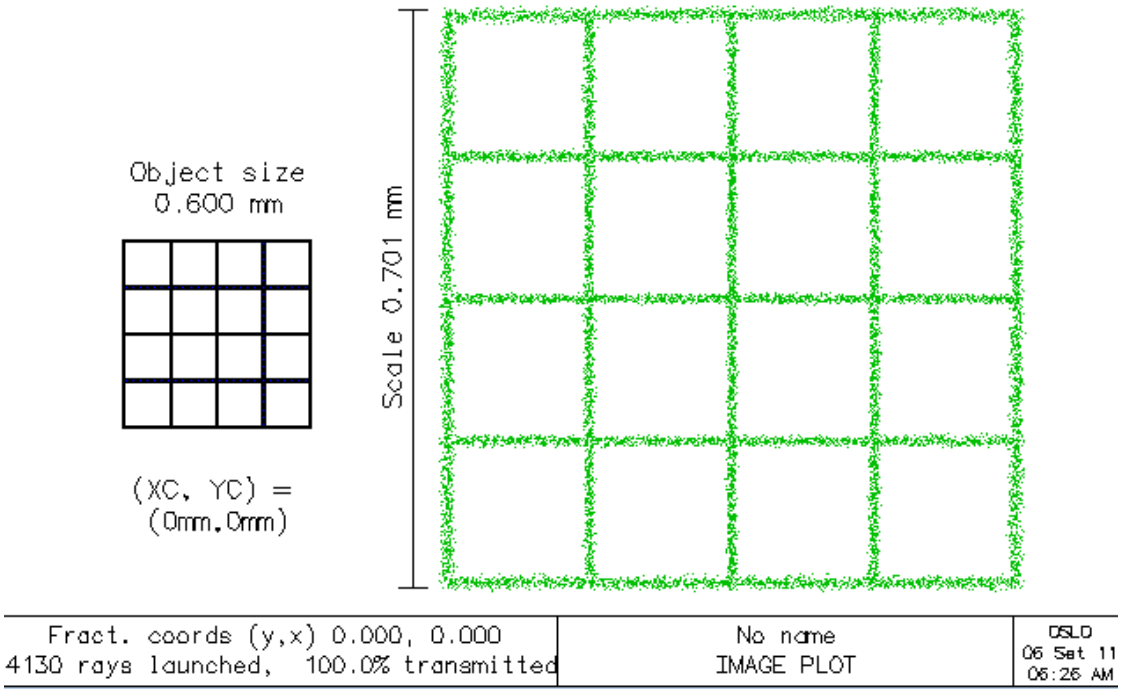

Figure 53 – Final image for a grid-shaped object for Nidek SL-1600.

Visually, the final image does not appear to be influenced by any type of aberration and it can be evaluated as having a good quality – Figure 53.

When comparing the performance of the two slit lamp microscopes designs, it can be concluded that the results for all tests are very similar between both models. The only relevant difference lies in the MTF values, where Zeiss 30 SL-M presents a better response than Nidek SL-1600. Even though, the two designs are considered to result in a good image quality. This means that modifications to these designs can be studied in only one of them, since the results should be similar, whatever is the chosen design.

5.1.3 - COUPLED SYSTEM DESIGNS

For the design based on the Zeiss 30 SL-M slit lamp model, the results are presented in the following pages. The optical path of this design includes a microscope objective, the long-working distance objective of the Zeiss slit-lamp, a negative lens and a positive lens to form an image with 40X magnification power.

Figure 54 presents the results for the ray intercept curves analysis test.

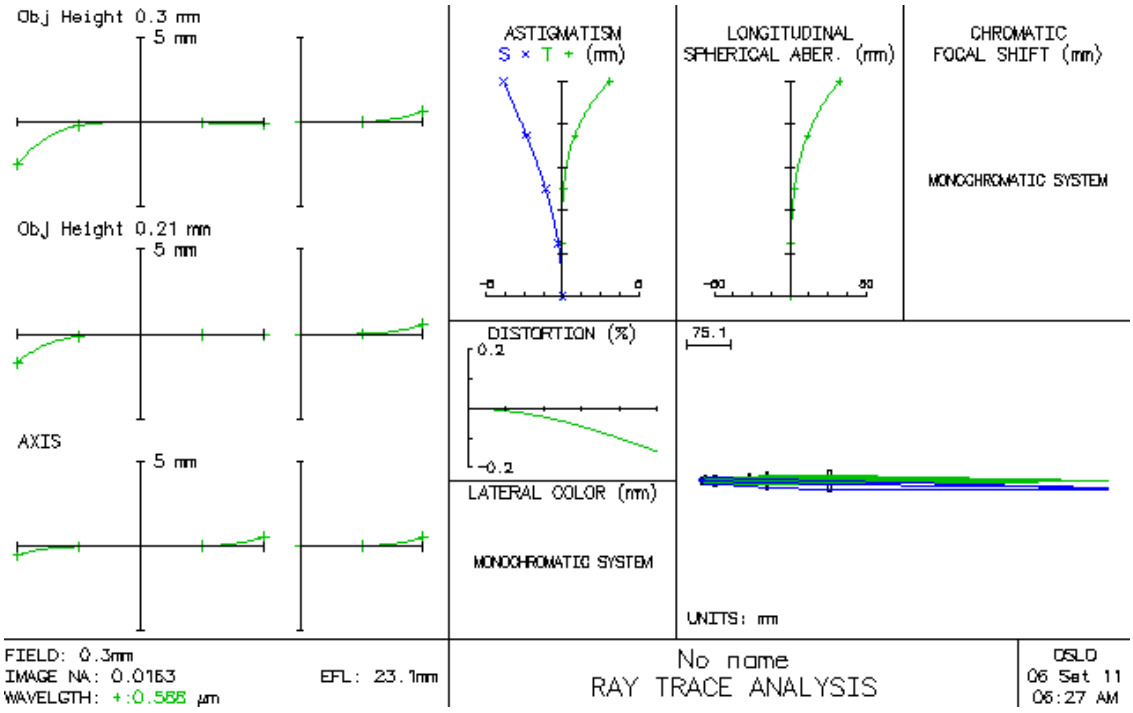

Figure 54 – Ray trace analysis results for the first coupled design simulated.

The observation of these plots demonstrates different levels of aberrations for the first coupled design.

The astigmatism graphic reports a slightly deviation limited by 5 mm. This means that, although the level of the astigmatism is not very high, it is not correct to consider the image as perfect. The difference between the sagittal and tangential rays is significant in this case, with tangential presenting a positive deviation while sagittal rays present a negative deviation. The resulting image may show imperfections, but, when visually evaluated, it is considered to have an acceptable quality for the design purpose.

The same happens with the spherical aberration. Here the limit value is a little high, but the resultant image does not appear to present a high level of imperfection. This can be visually confirmed with the extended source test described in the following pages.

As far as distortion is concerned, by observation of the distortion graphic reports present on Figure 54 and Figure 55, it can be concluded that the distortion level is low, without appearing any apparent deviation in the image.

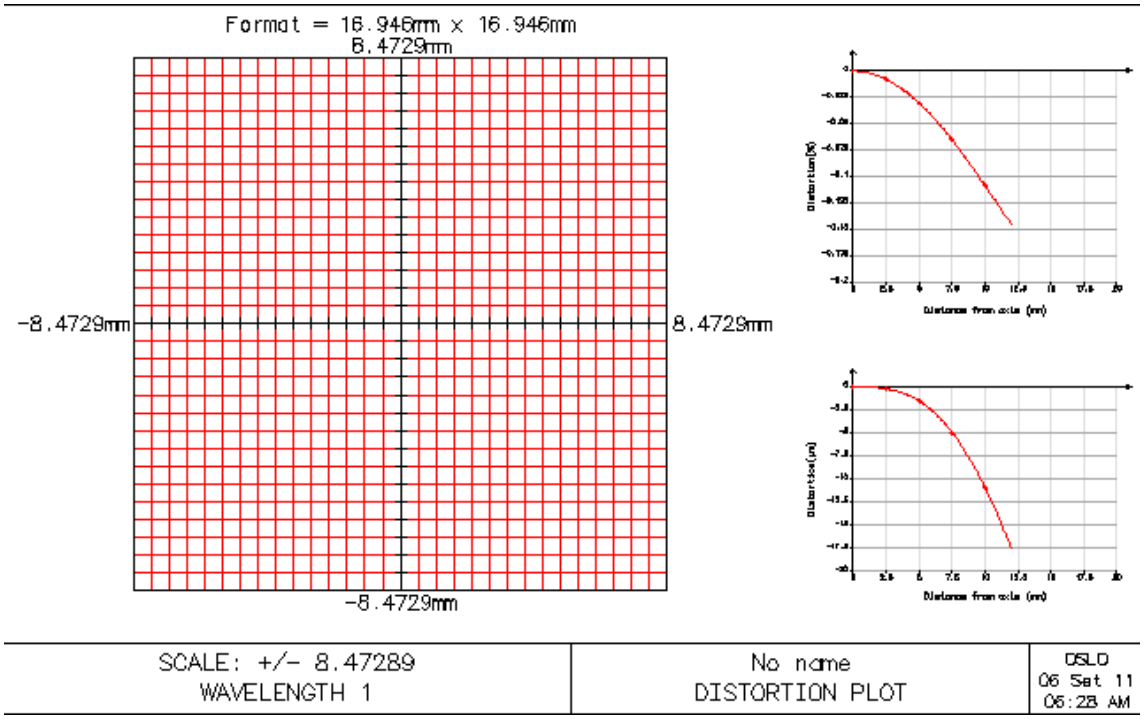

Figure 55 – Distortion test results for the first coupled system.

When compared to the slit lamp performance, in terms of aberration performance, the addition of the module slightly decreases the quality of the image. Nevertheless, the distortion levels decrease for this system. Distortion is not perceptible, an expected result, since the slit lamp image had already a very good quality.

The Point Spread Function (PSF) results are presented in Figure 56:

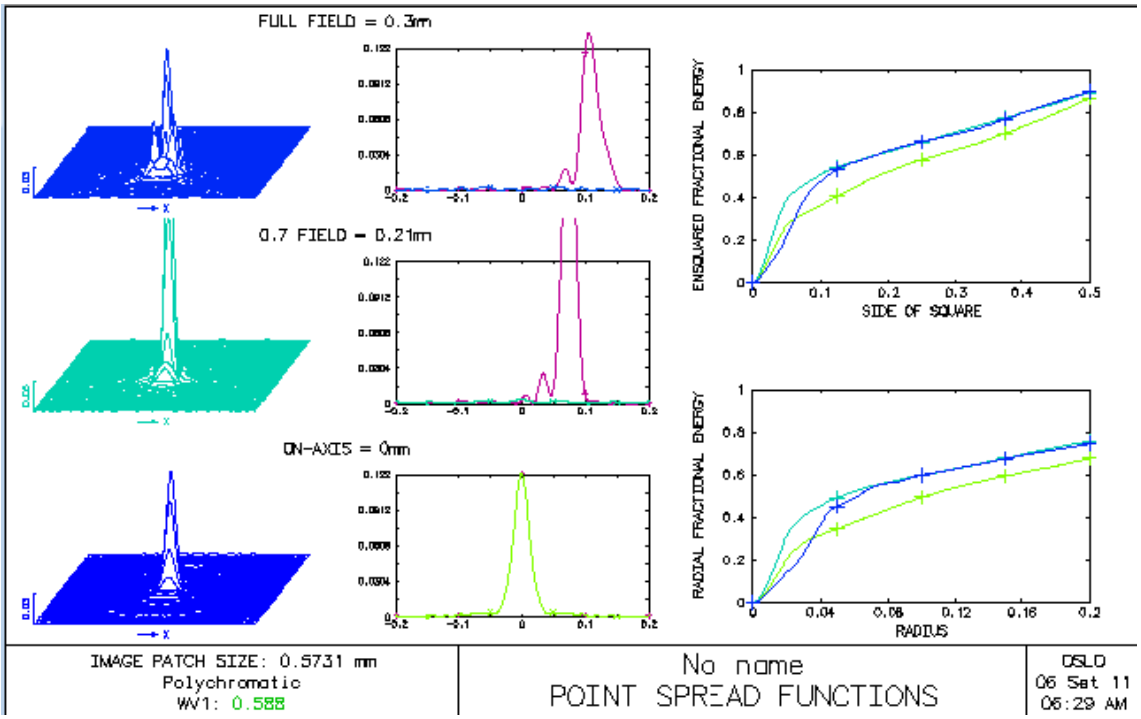

Figure 56 – Point Spread Function (PSF) test results for the first coupled design simulated.

In Figure 56, it can be seen that the response on axis is very similar to the ideal response. However, with 70% and full field, the response is not ideal, with a small deviation in the position of the peak and an illumination spreading around the main peak. This means that there is a loss in image quality as the distance from the optical axis increases.

When compared to the slit lamp performance, the optical module addition deteriorates PSF performance since the illumination spreading and peak deviations were not present on the slit-lamp simulation.

For the MTF, the results are described in Figure 57.

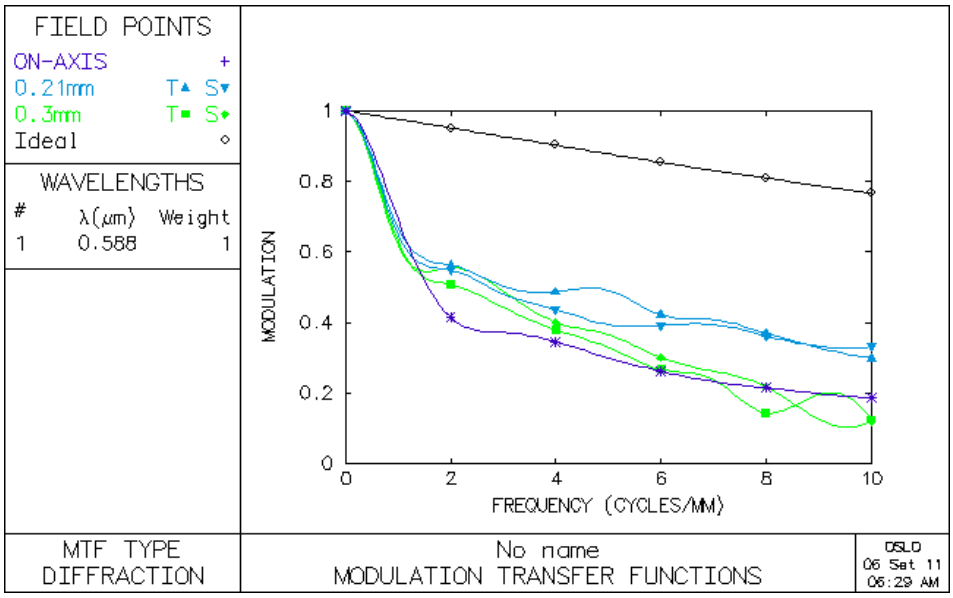

Figure 57 – Modular Transfer Function test results for first coupled design simulated.

The MTF response, presented in figure, is far from the ideal response. The system loses contrast very quickly with a very low response for higher frequencies (10 cycles/mm), beneath 0,2.

The spatial resolution at $MTF_{9\%}$ is near 20 lp/mm, a very low value when compared to the reference slit lamp, which means that this optical module worsens clearly the slit lamp performance – Figure 58.

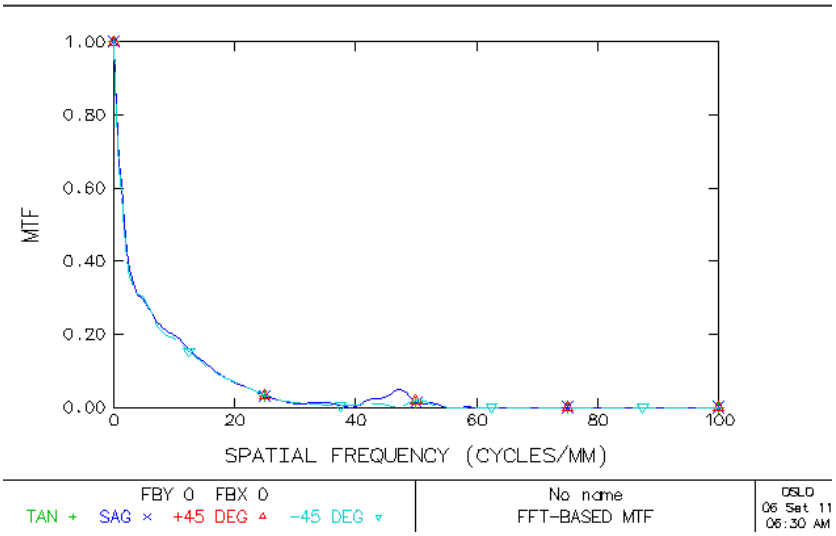

Figure 58 – MTF response results for first coupled design simulated.

The energy analysis test is presented in Figure 59.

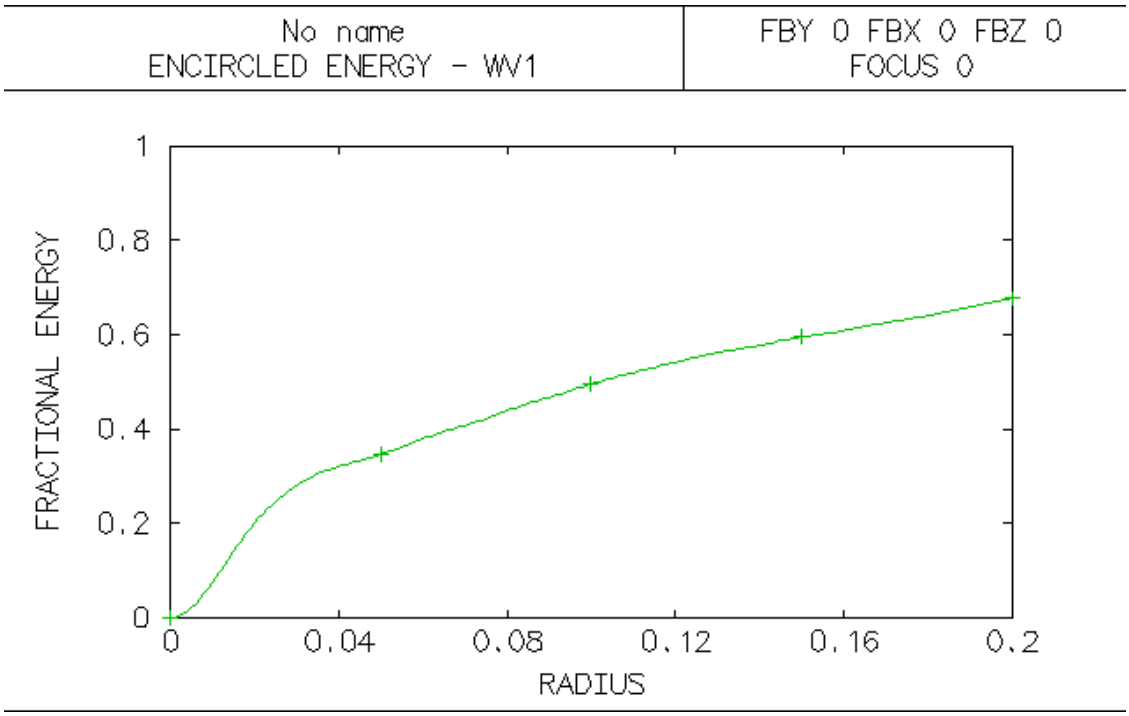

Figure 59 – Energy analysis results for first coupled design simulated.

According to the equation () with 0,65 NA, 84% of the energy should be included in a circle with 0,00055 radius. By observation of Figure 59, it is concluded that the system is not close to diffraction limited or even close to that. These results also demonstrate that the energy distribution is highly affected by the addition of the optical module.

Although the results do not point for a perfect system, when the image produced by this system is visually evaluated, it can be considered to have good quality. The results for a grid-shaped object are presented in Figure 60.

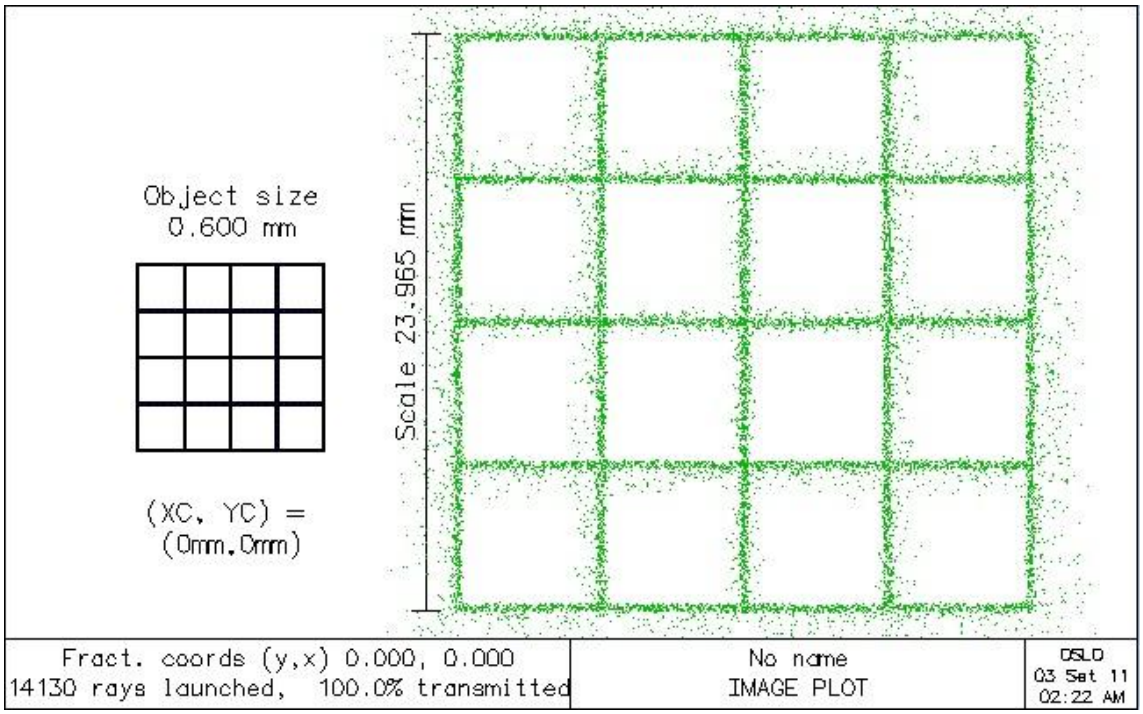

Figure 60 – Image produced by the first coupled system simulated by a grid-shaped object.

The following results are related to the second coupled design. This design was based on Nidek SL-1600 slit lamp model and it includes the microscope objective, all the optical components that constitute the slit lamp microscope and 16mm positive lens. The tests were the equal to those performed for the first coupled design.

Figure 61 shows the ray trace analysis for this system.

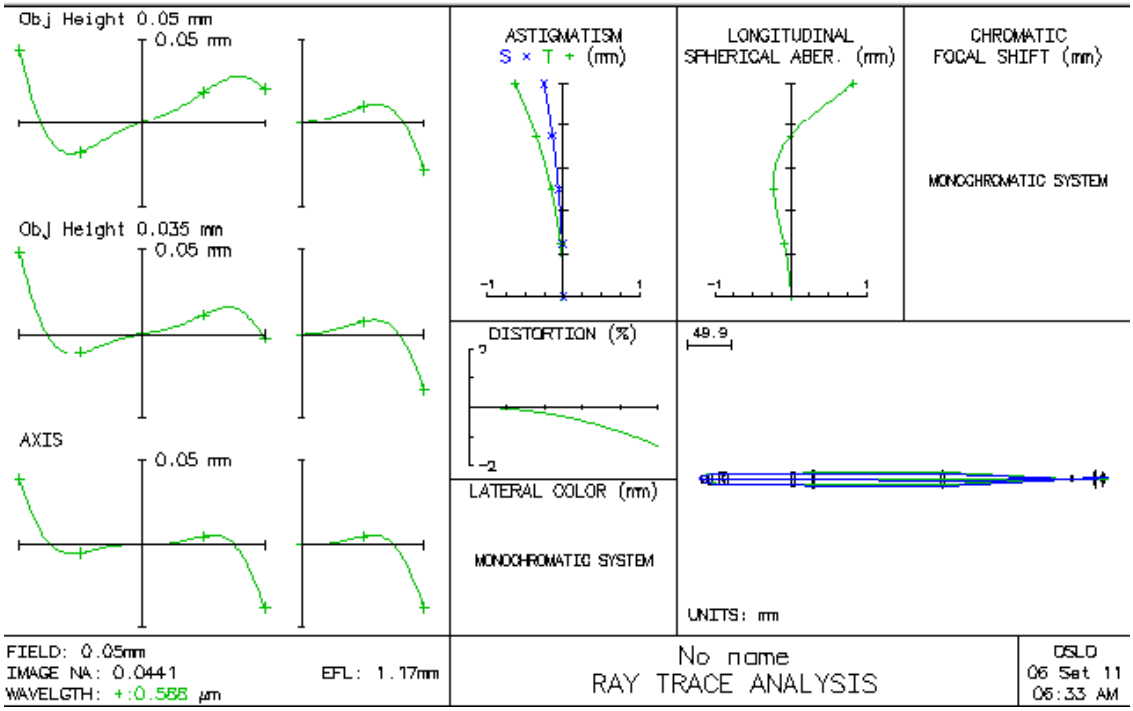

Figure 61 – Ray trace analysis test results for second coupled design.

Figure 61 reports a very low limit value (1 mm) for astigmatism aberration, which means that it will not have a high effect on the final image produced by this system. This value is not very far from the one obtained with Nidek SL-1600 slit lamp simulation design.

For the spherical aberration, the limit value (1 mm) is lower than the one obtained for the slit lamp (2 mm). This means that the image is not affected by this type of aberration and that the module helps correcting it.

The distortion is acceptable, with a deviation below 2% and with slight apparent imperfections on the image present in Figure 62.

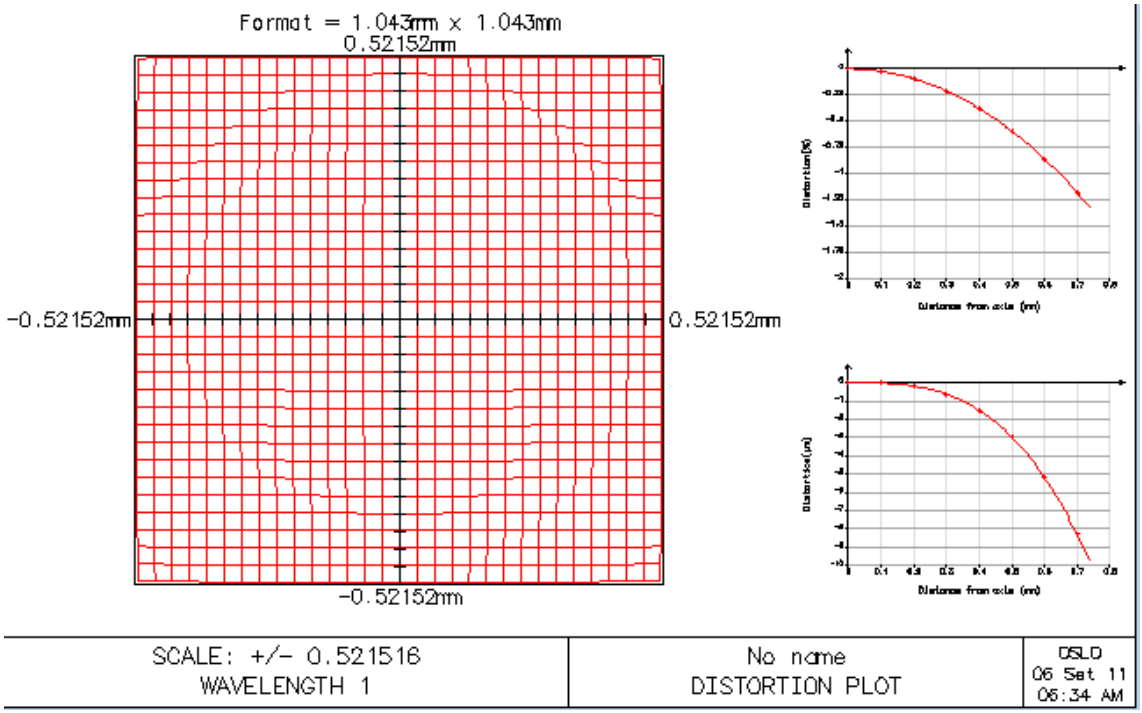

Figure 62 – Distortion test results for the second coupled design.

Although the limit value is higher than in the slit lamp microscope, meaning that the optical module degrades the image, this value is lower than the distortion measured (5%) in a commercial cornea confocal microscope, (Tomey Confoscan Model P4) used in our laboratory to image corneal nerves *in vivo*.. (6)

PSF test was also performed and the results are described in Figure 63.

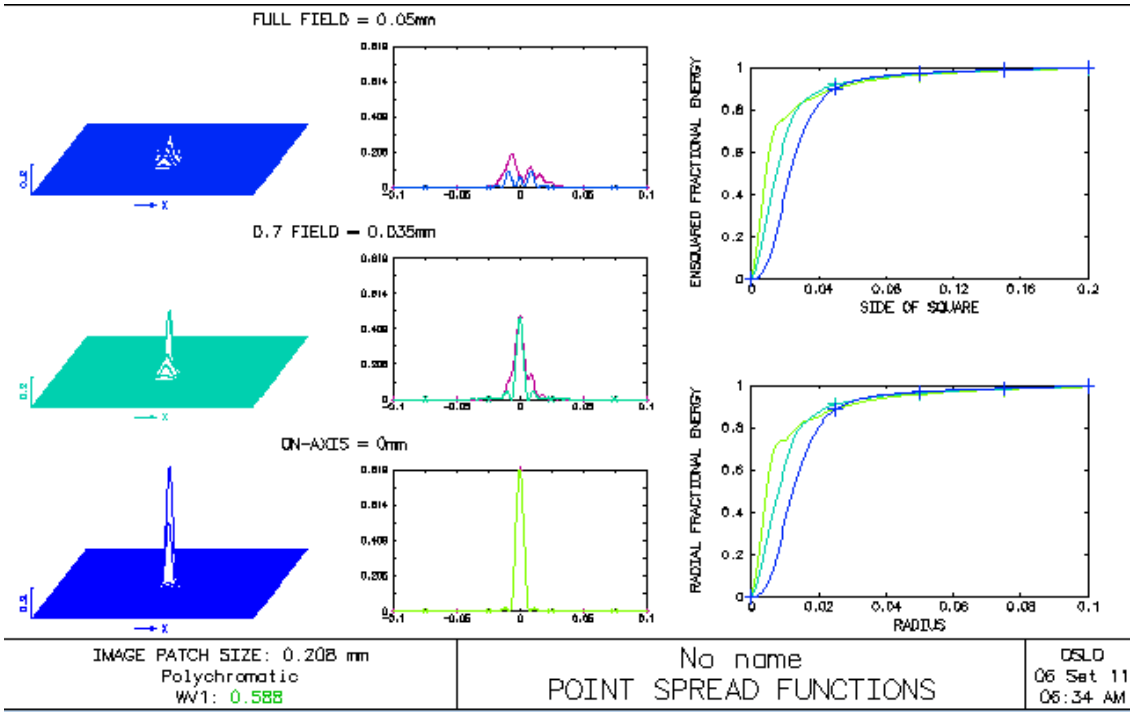

Figure 63 – Point Spread Function (PSF) test results for second coupled design simulated.

In Figure 63, it can be seen that the image on-axis has a response similar to the ideal response. When field increases, the peak value decreases, which means that there is a loss of illumination with the increasing distance from the axis. Out of axis objects also shows a slight spreading around the main peak.

When compared to the slit lamp PSF performance, it can be concluded that the addition of the optical module has a negative influence on the PSF curves.

MTF test produced the results presented in Figure 64.

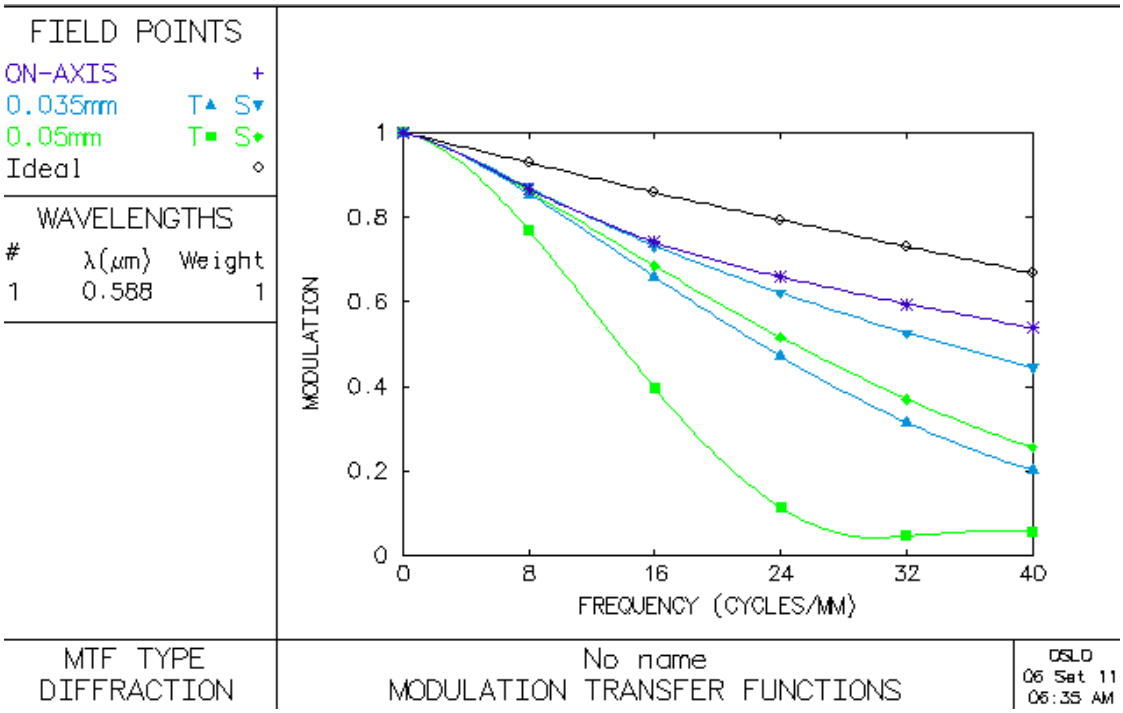

Figure 64 – Modular Transfer Function (MTF) test results for second coupled design.

Figure 64, like in the previous system, shows the MTF response obtained for this system. It is possible to conclude, that distance from the axis influences negatively the MTF response. For high frequencies (above 24 cycles/mm), the MTF values are lower than 0,2. On the other hand, on-axis response is considered to be good since it is very near to the ideal. For high frequencies the MTF response is above 0,5.

This MTF response is slightly worse than the slit lamp MTF response for objects off-axis. Therefore the optical module degrades the contrast and spatial resolution of the slit lamp microscope. However, on axis-objects present a better contrast response, with a 9% MTF value above 100 lp/mm – Figure 65. So for very small on-axis objects, the resolution of this new system is better than the one provided by the slit lamp microscope.

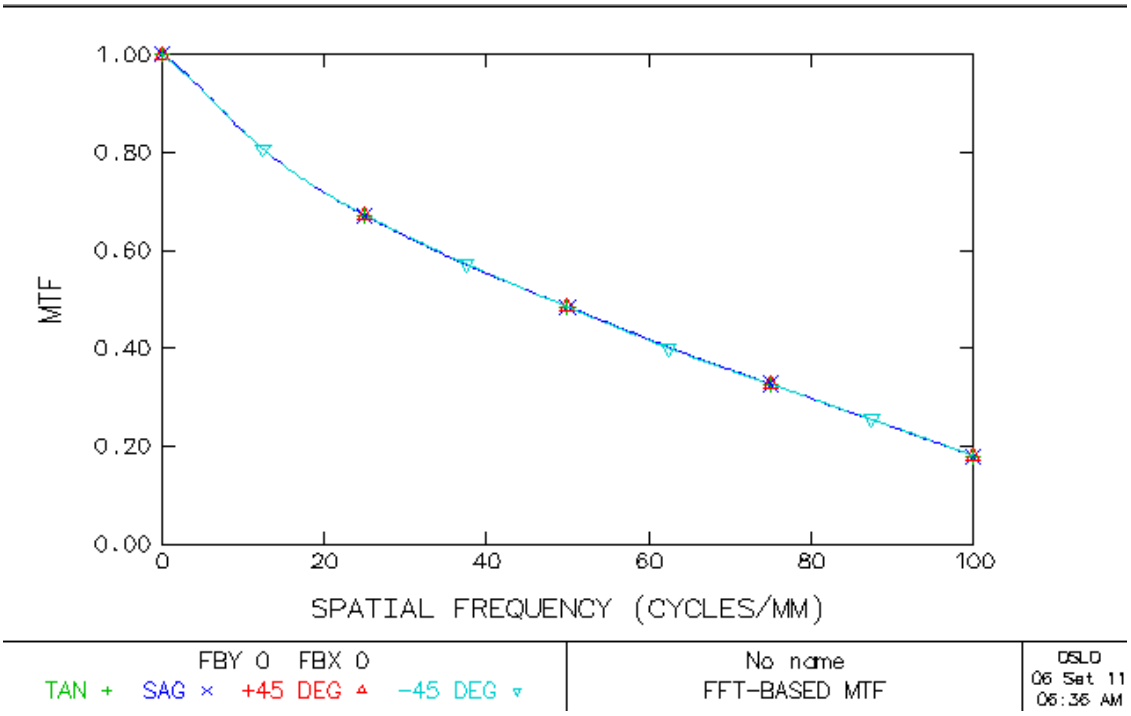

Figure 65 – MTF response results for second coupled design.

The energy analysis test is depicted in Figure 66.

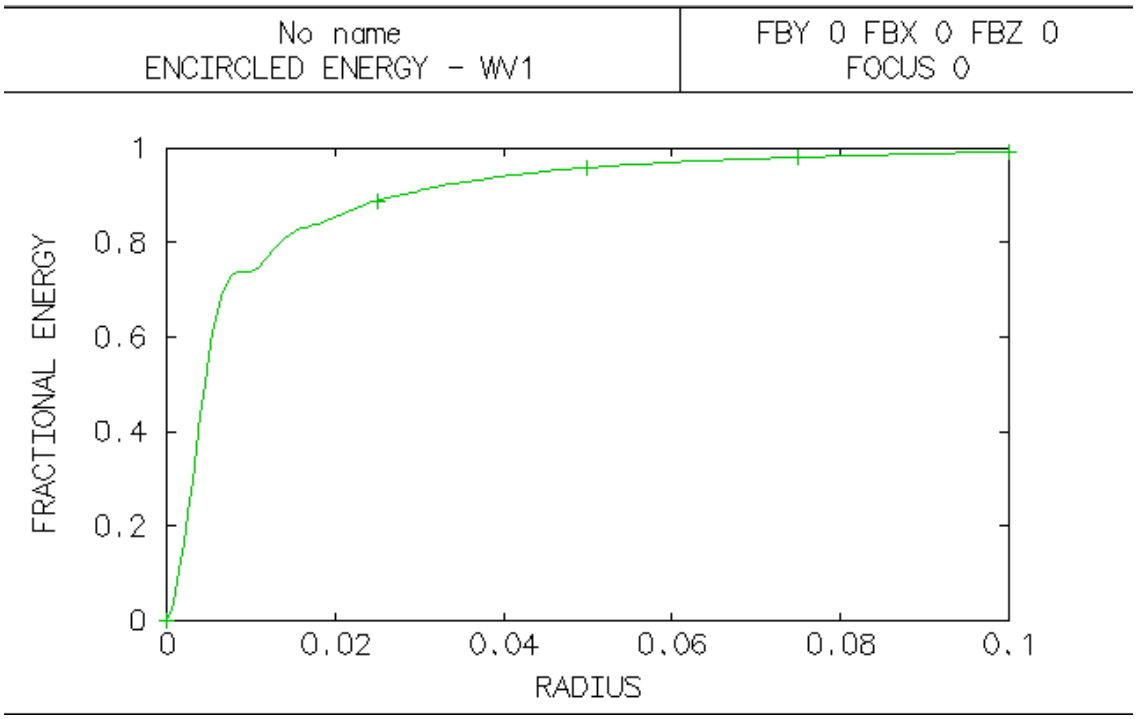

Figure 66 – Energy analysis test results for second coupled design simulated.

From equation 15, 84% of the energy should be deposited on a circle of 0,00055 mm radius. The plot present on Figure 66 does not present 84% at the value by equation 15, a value that is far from the diffraction limited.

The shape of the curve, when compared to the slit lamp, is very similar.

Although the system is not completely perfect, it presents better values than the first coupled system. The quality of the image produced can be considered as acceptable when visually evaluated. The final image of a grid-shaped object is depicted in Figure 67.

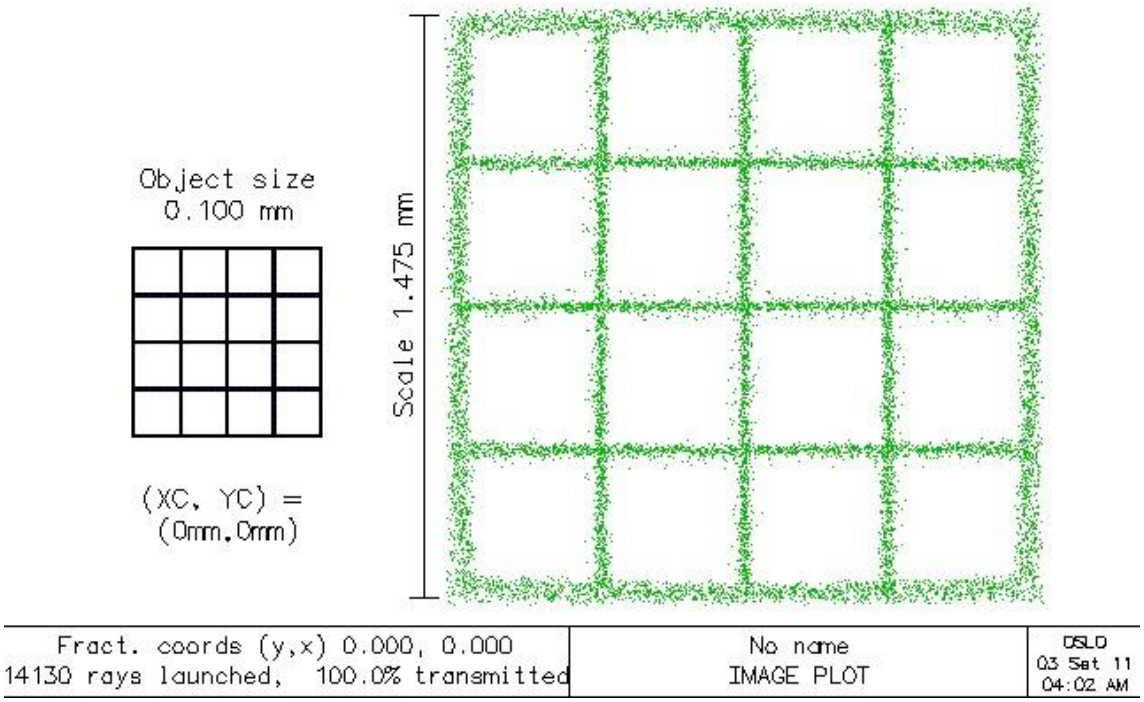

Figure 67 –Final image for a grid-shaped object produced by second coupled design simulated.

Comparing the performance of the two coupled designs, it can be concluded that the second one produces better results. However, this system is not perfect and modifications should be studied and made to optimise its performance.

The results produced by the second coupled design, in spite of not being perfect, were sufficient to proceed to laboratory tests. All the results showed on the following section were taken with an optical module mounted as described in this design.

5.2 - LABORATORY TEST

Due to the illuminations problems encountered during the laboratory test, it was only possible to test the system in terms of its magnification, field of view, distortion, spatial resolution, contrast and MTF.

To analyse the magnification provided by the system the target used was the USAF 1951. Since the size of each line or square present in the target is known and the size of the camera pixel also known, it is possible to calculate the overall magnification power of the new system.

The USAF 1951 resolution is divided in groups and elements. Each group has different elements, and each element is composed by 3 vertical and 3 horizontal lines of known length and width. These values are listed in Table 12 and 13.

Table 12 – Length (mm) of each line of USAF 1951

Element Group	1	2	3	4	5	6
-2	10	8,908987	7,937005	7,071068	6,299605	5,61231
-1	5	4,454494	3,968503	3,535534	3,149803	2,806155
0	2,5	2,227247	1,984251	1,767767	1,574901	1,403078
1	1,25	1,113623	0,992126	0,883883	0,787451	0,701539
2	0,625	0,556812	0,496063	0,441942	0,393725	0,350769
3	0,3125	0,278406	0,248031	0,220971	0,196863	0,175385
4	0,15625	0,139203	0,124016	0,110485	0,098431	0,087692
5	0,078125	0,069601	0,062008	0,055243	0,049216	0,043846
6	0,039063	0,034801	0,031004	0,027621	0,024608	0,021923
7	0,019531	0,015502	0,015502	0,013811	0,012304	0,010962

Table 13 - Width of each line of USAF 1951

Element Group	1	2	3	4	5	6
-2	2	1,781797	1,587401	1,414214	1,259921	1,122462
-1	1	0,890899	0,793701	0,707107	0,629961	0,561231
0	0,5	0,445449	0,39685	0,353553	0,31498	0,280616
1	0,25	0,222725	0,198425	0,176777	0,15749	0,140308
2	0,125	0,111362	0,099213	0,088388	0,078745	0,070154
3	0,0625	0,055681	0,049606	0,044194	0,039373	0,035077
4	0,03125	0,027841	0,024803	0,022097	0,019686	0,017538
5	0,015625	0,01392	0,012402	0,011049	0,009843	0,008769
6	0,007813	0,00696	0,006201	0,005524	0,004922	0,004385
7	0,003906	0,00348	0,0031	0,002762	0,002461	0,002192

Since in the laboratory test, the Galilean telescope magnification power was taken into account, the values of final magnification were measured for different positions of the Galilean telescope. The overall magnification calculated suffers the influence of the positive lens (f=16mm) used to acquire the images. Therefore, for the position of 16X in

the Galilean telescope, the magnification obtained for the slit lamp microscope combined with 16 mm lens, without any additional component, was 2X, eight times less than the slit-lamp magnification.

The images obtained for the different positions of the slit lamp microscope are presented in Figures 68, 69, 70 and 71.

Figure 68 - Image obtained with the Galilean telescope at the position 10X.

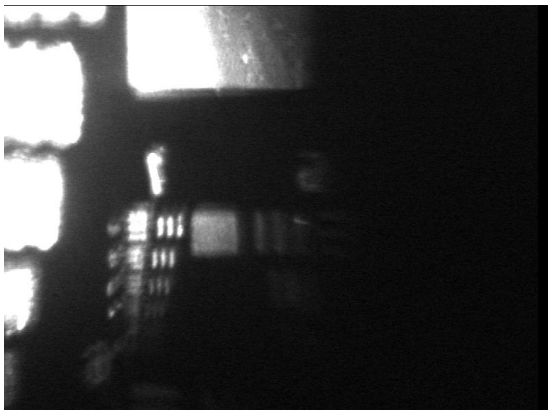

Figure 69 – Image obtained with the Galilean telescope at the position 16X.

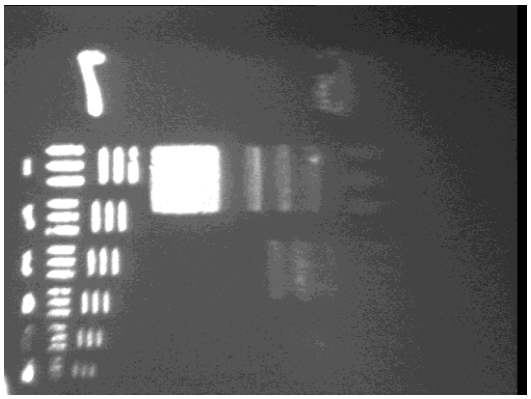

Figure 70 - Image obtained with the Galilean telescope at the position 25X

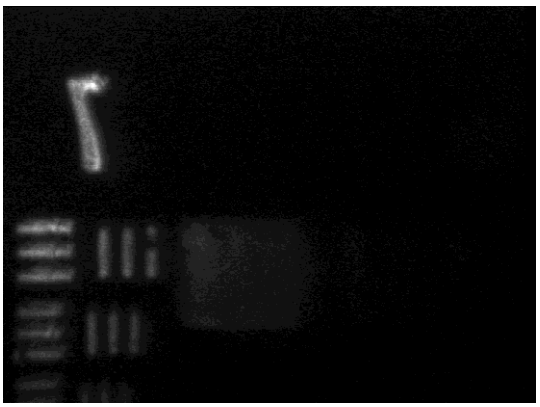

Figure 71- Image obtained with the Galilean telescope at the position 40X.

The overall magnification was calculated by analyzing the images with the ImageJ software (National Institutes of Health, USA).With the software, it was possible to choose the square placed at the middle of all figures and measure its size in pixels. The square chosen is the 1st element of group 6 and its size is . The size of the pixel for the used CC camera is 8,6 μm x 8,3 μm. The results are shown in the Table 14:

Table 14 – Magnification results for the coupled system.

Galilean Telescope Position	Magnification after f=16mm lens	Size of Square in Pixels	Overall Magnification
10x	1.25x	34x34	8,4x
16x	2x	60x60	14,83x
25x	3.125x	106x106	26,19x
40x	5x	149x149	36,82x

The previous results were taken from figures obtained without recurring to the use of an optical coupling gel between the microscope objective and the test target. To compare the magnification results with and without the use of gel, images of the same target for the Galilean positions of 16x and 25 were also taken – Figures 72 and 73. The results are in Table 15.

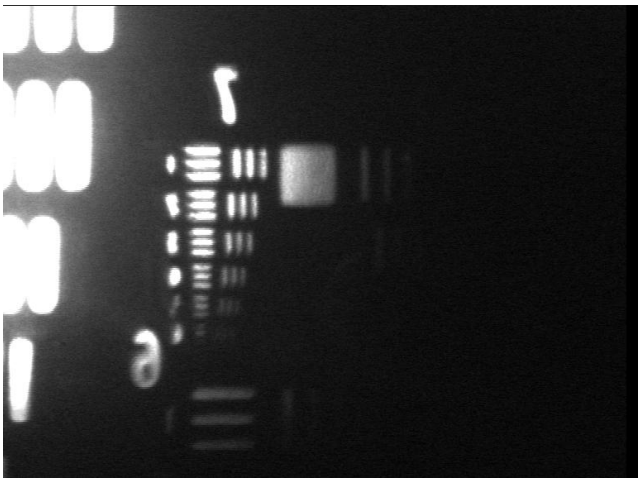

Figure 72 - Image obtained with the Galilean telescope at the position 16X with optical coupling gel.

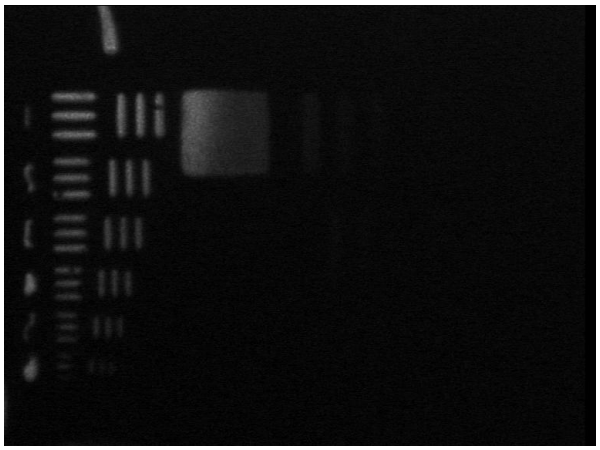

Figure 73 - Image obtained with the Galilean telescope at position 25X with optical coupling gel

Table 15 – Magnification results for the coupled system with optical coupling gel.

Galilean Telescope Position	Size of Square in Pixels
16x	65x65
25x	106x106

The field of view was evaluated based on information provided by Figures 68, 69, 70 and 71.

To estimate these values, the pixel size of each side of the 1st element of Group 6 (USAF 1951) was measured with ImageJ software and the size of each side of the image window was also measured. To estimate the amount of square that fitted the window, the number of pixels correspondent to the square was divided by the number of pixels of the window. This value was multiplied by the object size. The result corresponds to the field of view. The results are depicted in Table 16.

Table 16- Field of view results for different Galilean telescope positions.

Galilean telescope Position	Field of View(μm)
10x	563x656
16x	304,2x354
25x	190X220
40x	129x149

The results demonstrate that the 10x Galilean position the field of view is the most similar to the field of view specified for the system. However, at position 16x the field of view is also adequate.

Distortion was only measured for 16x and 25x positions of the Galilean telescope. Five types of images were acquired: square on centre of the window (reference image), on the upper left side, on the upper right side, on the left lower side and on the right lower side as depicted in Figures 74, 75, 76, 77 and 78.

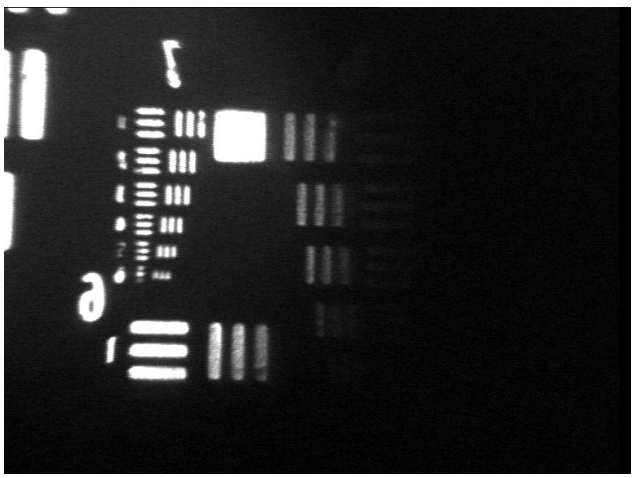

Figure 74 - 16X Galilean telescope centred square.

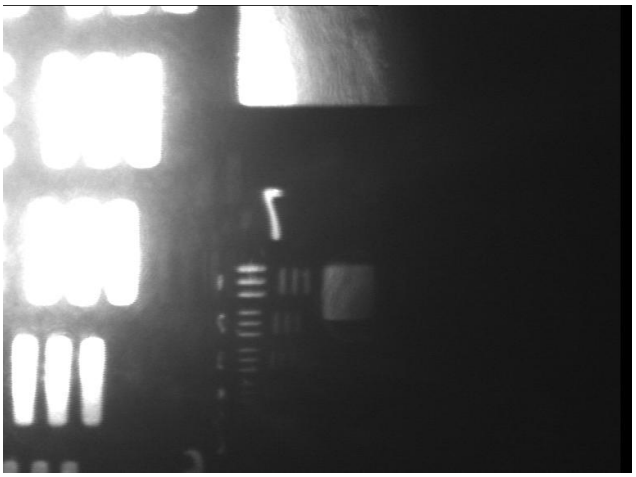

Figure 75 – 16X Galilean telescope down-right square.

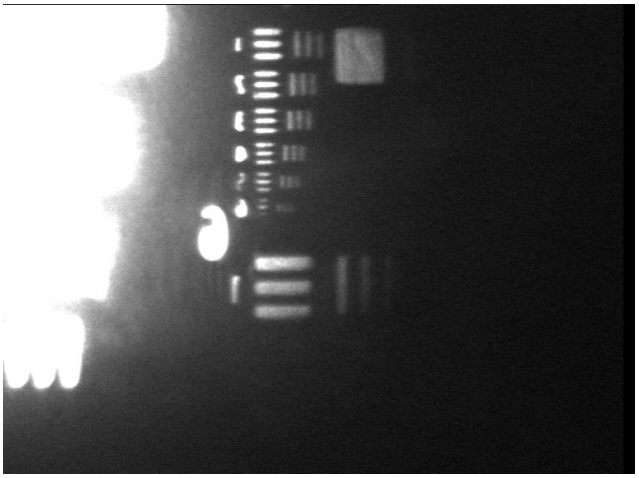

Figure 76 - 16X Galilean telescope upper-right square.

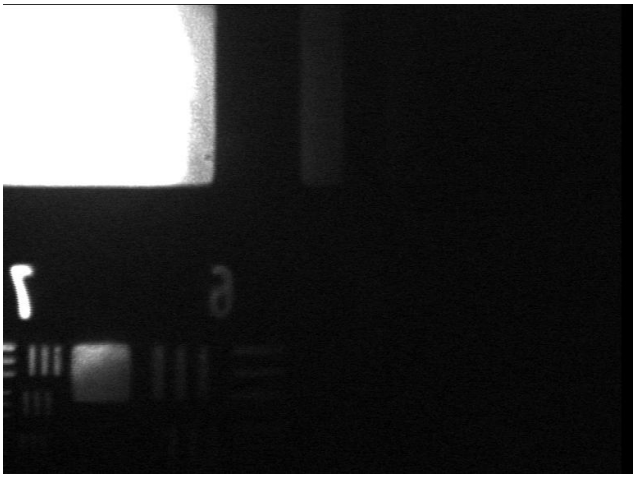

Figure 77 – 16X Galilean telescope down-left square.

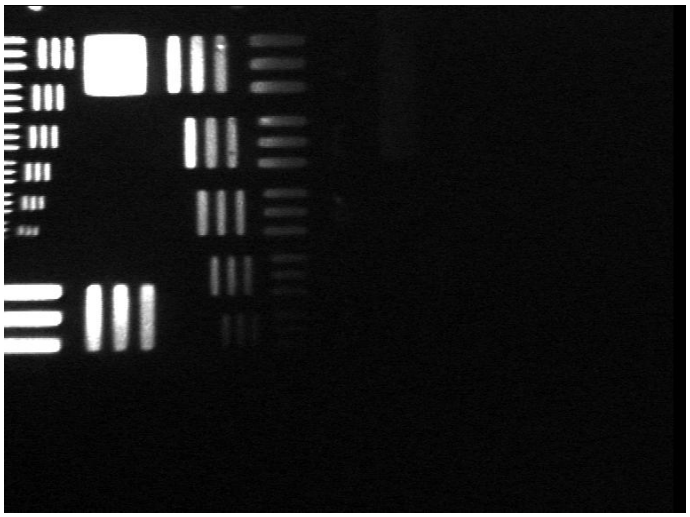

Figure 78 – 16X Galilean telescope upper-left square.

The value of the different squares diagonal was estimated and, based on equation 17 and Figure 79, the percentage of distortion was estimated. The PD value for 16x Galilean position was estimated to be 44,5 pixels and for 25 x Galilean position 70,7 pixels. The distortion values for both positions are presented on Table 17 and Table 18.

$$Distortion\ (\%) = \left(\frac{AD - PD}{PD}\right) x100 \quad (17)$$

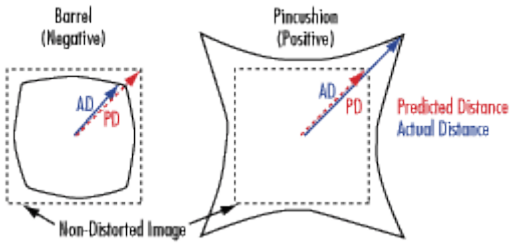

Figure 79 – Scheme demonstrating how the distortion is evaluated.

Table 17 – Distortion values for 16x Galilean telescope position.

Square Place	Distortion (%)
Upper Right	-6,3%
Upper-Left	9,5%
Down-Right	-9,5%
Down-Left	1,57%

Table 18 – Distortion values for 25 x Galilean telescope position.

Square Place	Distortion (%)
Upper Right	2,52%
Upper-Left	3,01%
Down-Right	5,06%
Down-Left	6,52%

The distortion levels estimated are not low and are quite far from the predicted distortion limit based on a commercial confocal microscope Tomey Confoscan Model P4. This means, that modifications on the optical module are required.

The USAF 951 target was also useful to estimate the spatial resolution of the system. Since all the elements present on the target were resolved by the system, from the specifications of the target, the resolution is better than 228 lp/mm, a value that corresponds to about 4μm.

It was also possible to evaluate the contrast response of the system. For that, the modular contrast of image (MCI) and the modular transfer function (MTF) were measured, using a sinusoidal target (Edmund Optics model NT54-804) – Figure 80.

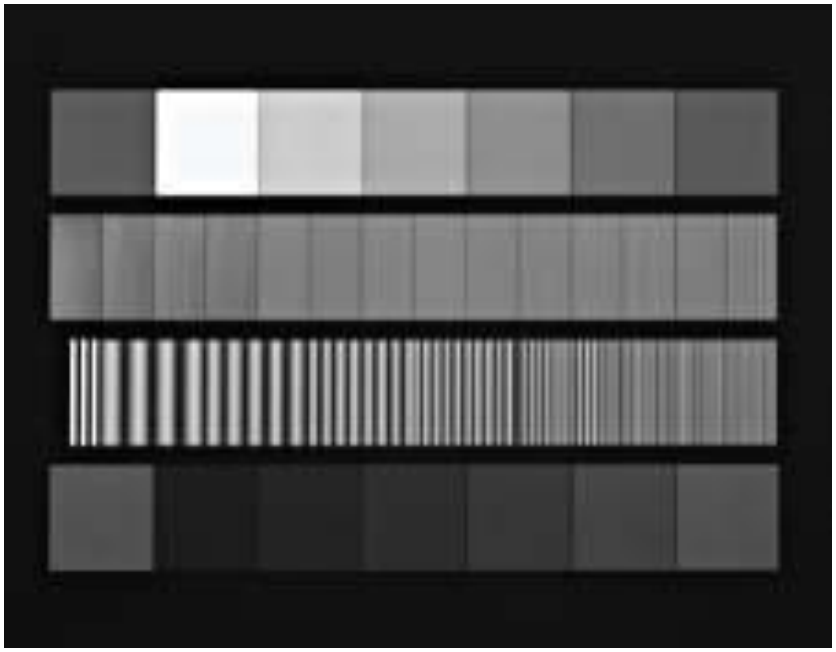

Figure 80 – Sinusoidal Target Edmund Optics model NT54-804

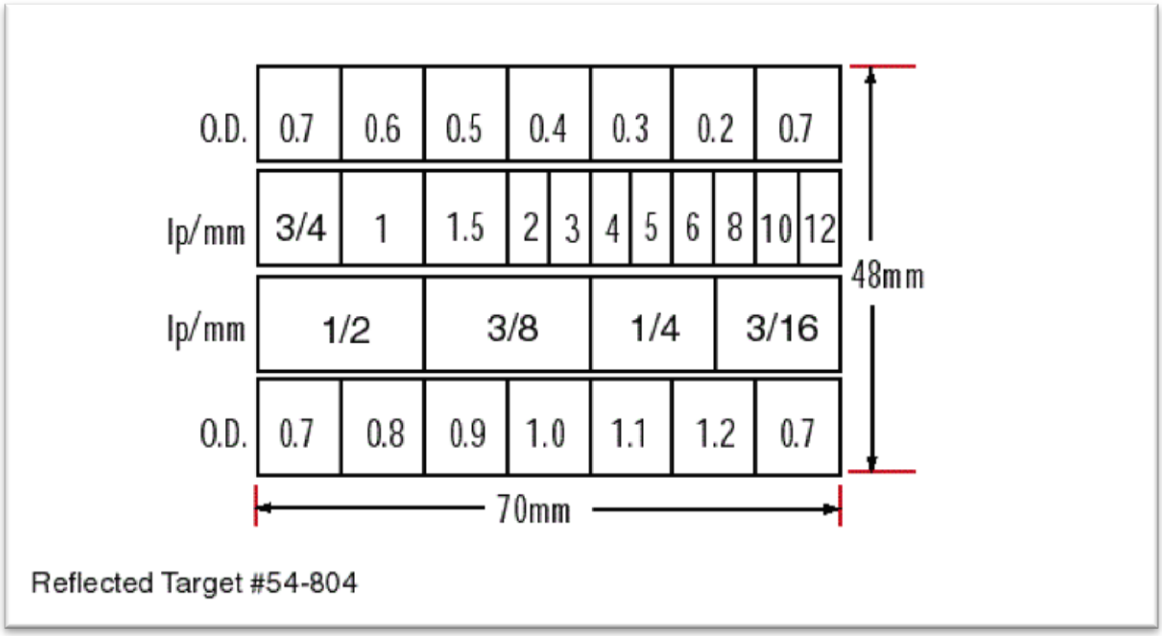

Figure 81- Sinusoidal target Edmund Optics NT54-804 model specifications

To estimate MCI, the values of the maximum (I_{max}) and the minimum (I_{min}) intensity of each image are obtained and the following relation is applied [31]:

$$MCI(\%) = \frac{I_{max} - I_{min}}{I_{max} + I_{min}} \times 100 \quad (18)$$

The MTF value is calculated based on the MCI and in the contrast of the object. From the target specification, the object contrast is 60%.

$$MTF = \frac{MCI}{MCO} \quad (19)$$

The following tables and plots contain the results obtained for both MCI and MTF with the Galilean telescope positioned at 16x:

Table 19 – MCI results for the Galilean telescope position 16X.

Frequency(lp/mm)	MCI (%)	STDV(MCI) (%)
4	52,095	2,924
5	44,971	1,295
6	40,094	1,559
8	32,260	1,863
10	29,606	2,165
12	27,505	4,642

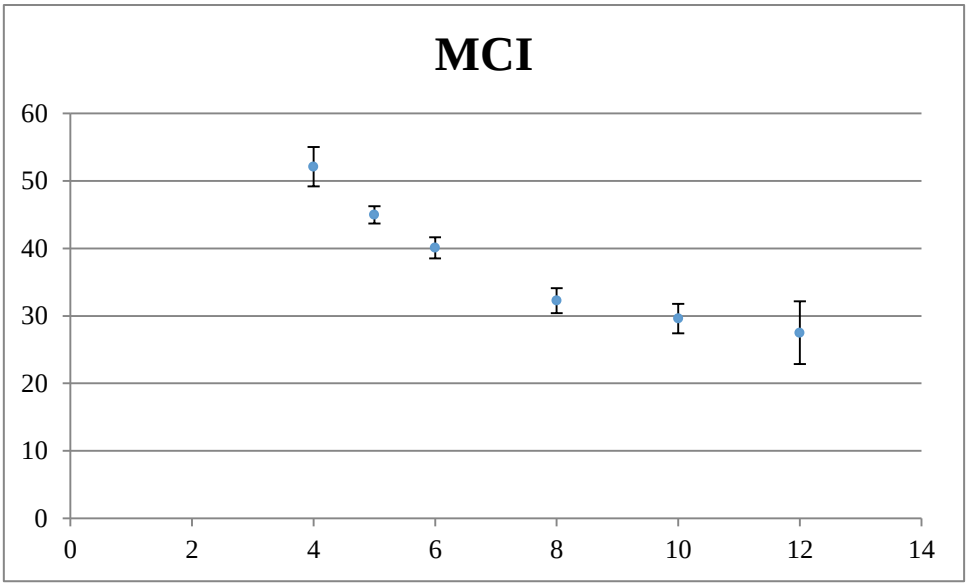

Figure 82 – Measured MCI response for the Galilean telescope position 16X.

Table 20 – MTF results for the Galilean position telescope 16X.

Frequency(lp/mm)	MTF	STDV(MTF)
4	0,868	0,049
5	0,750	0,022
6	0,668	0,026
8	0,538	0,031
10	0,493	0,036
12	0,458	0,077

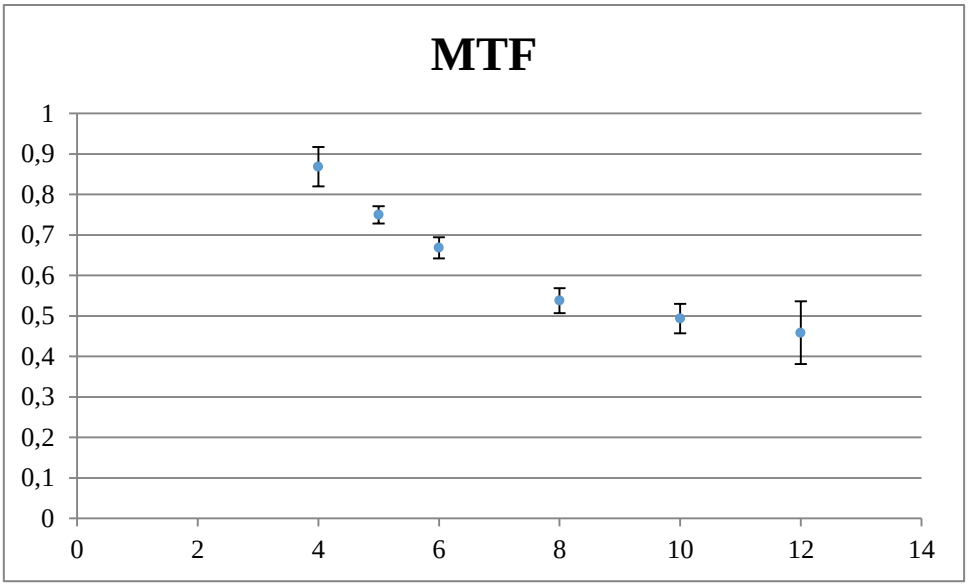

Figure 83 – Measured MTF for Galilean telescope position 16X.

From the MCI and MTF plots, it can be concluded that the system loses contrast when frequency increases. However, for the limit value of the target (12 cycles/mm), the MTF response is around 50%. This value is similar to the one obtained in the second coupled simulated design and far better than the one obtained with the first coupled design simulated.

From the spatial resolution limit value, it is predicted than MTF value at 10% should be near 228 lp/mm.

For the 25x position of the Galilean telescope, the MCI and MTF results are registered in tables 21 and 22 and Figures 84 and 85.

Table 21 – MCI results for the Galilean telescope position 25x.

Frequency (lp/mm)	MCI (%)	STDV (MCI) (%)
4	54,344	2,823
5	49,200	2,535
6	42,324	2,881
8	31,490	1,655
10	28,462	3,576
12	24,743	3,109

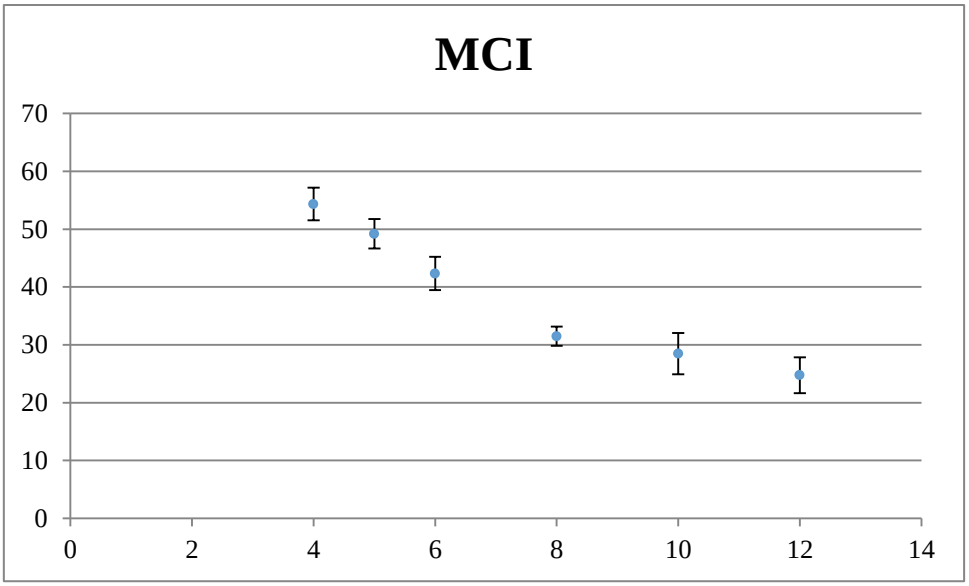

Figure 84 – Measured MCI for 25X Galilean telescope position.

Table 22 – MTF results for the Galilean telescope position 25X.

Frequency (lp/mm)	MTF	STDV (MTF)
4	0,906	0,047
5	0,820	0,042
6	0,705	0,048
8	0,525	0,0276
10	0,474	0,060
12	0,412	0,052

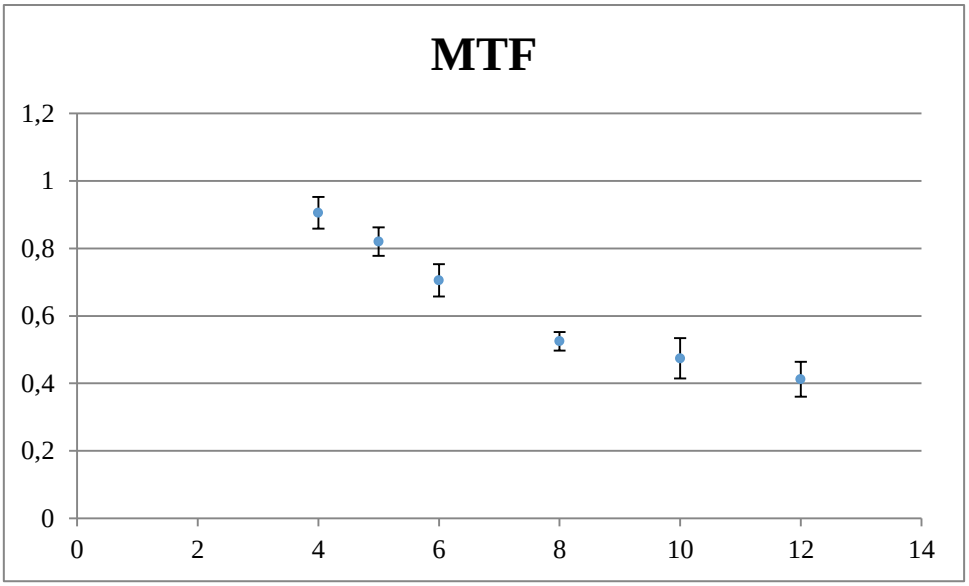

Figure 85- Measured MTF response at 25X Galilean telscope position.

When comparing the MCI and MTF results obtained with 25x and 16x magnification, it can be concluded that there is a loss on contrast when the magnification increases. At 12 cycles/mm, the MTF value for 16X is around 0,5, while for 25X is around 0,4.

CONCLUSION / FUTURE WORK

The addition of an optical module in the slit lamp microscope affects its performance and its optical specifications. As demonstrated in the analysis of the simulated designs, the most affected characteristics are the PSF, MTF and Energy distribution of the system. From the simulation studies, it can be concluded that the design based on the Nidek SL-1600 model presents a much better performance in terms of these parameters. The values obtained with this simulation are very similar to the specifications measured for a reference corneal confocal microscope, the Tomey Confoscan Model P4, which gives us confidence to state simulated design has a performance that complies with the goals of the project.

The device tested on laboratory and also produced good results, comparable to the Confoscan P4 specifications and proved to be an adequate basis for the final design. The lateral resolution is already according to the final specifications. The field of view, which varies with the Galilean telescope setting, was identical to Confoscan P4 on the 16X magnification. The distortion levels were similar to the ones measured on the Confoscan, when using the 25X setting on the Galilean telescope. However, for the 16X, the distortion was twice as high. It must be noted, that the correct calculation of the morphometric parameters of the corneal nerves network may require a very high performance in terms of distortion, better that the one presented by standard commercial confocal microscopes. There it is expected that improvements on the distortion performance provided by the optical module will be required.

The work done with the laboratory optical module also highlighted a number of technical difficulties that must be addressed and solved in the future. A major problem deals with sample illumination. As said before, an adequate illumination system is not yet developed since it was not straightforward to use the slit lamp lateral ports, (the slit lamp we used had a binocular beamsplitter module installed), usually reserved for photography purposes. This situation affected the quality of the acquired images and limited the system evaluation, namely preventing the measurement of the axial resolution. The placement of the CCD camera at the exit of the eyepiece was also an interim solution that could not be improved in due time. As the camera is acquiring the image from one ocular of a binocular system meant for stereoscopic viewing, the image is not centred on the CCD sensor.

Another problem lies in the mechanical system used by the slit-lamp for positioning and focusing. This system was not built for the fine movements required for observing individual corneal layers. This is an important issue that was not the object of this work.

Finally, it is important to stress that the optical module we developed is not confocal (although it showed a small depth of field, which we were unable to measure due to illumination problems). The inclusion of confocality is a step to be taken in the future.

BIBLIOGRAPHY

1. **Gooch, Clifton and Podwall, David.** The Diabetic Neuropathies. *The Neurologist.* 2004, Vol. 10.

2. **Rosenberg, M.E., et al.** Corneal structure and sensitivity in type 1 diabetes mellitus. *Invest Ophtalmol. Vis. Sci.* 10, September 2000, Vol. 41, pp. 2915-2921.

3. **Malik, R. A. , et al.** Corneal confocal microscopy: a non-invasive surrogate or nerve fibre damage and repair in diabetic patients. *Diabetologia*. 5, May 2003, Vol. 46, pp. 683-688.

4. **Kallinikos, P. , et al.** Corneal nerve tortuosity in diabetic patients with neuropathy. *Invest. Ophtalmol Vis. Sci.* 2, February 2004, Vol. 45, pp. 418-422.

5. **Ferreira, Ana, et al.** neuroCornea - Diabetic peripheral neuropathy early diagnosis and follow-up thorugh in vivo automatic analysis of corneal nerves morphology. *1st Portuguese Meeting in Bioengineering.* 2011.

6. **Morgado, António Miguel Lino Santos.** *Flurometria Ocular Não-Invasiva: técnicas e instrumentação.* Coimbra : s.n., 2002.

7. **Pocock, Gillian and Richards, Cristopher D.** *Human Physiology.* s.l. : Oxford Core Texts, 2006.

8. Washington University Physicians. [Online] [Cited: 24 April 2011.] http://wuphysicians.wustl.edu/dept.aspx?pageID=17&ID=6.

9. *Wikipedia - The Free Encyclopedia.* [Online] [Cited: 15th August 2011.] http://en.wikipedia.org/wiki/Eye.

10. **Böhnke, Matthias and Barry, Masters R.** Confocal Microscopy of the Cornea. *Progress in Retinal and Eye Research.* 1999, Vols. 18, No. 5, pp. 553 to 628.

11. **Müller, Linda J. , et al.** Corneal nerves: structure, contents and function. *Experimental Eye Research.* 2003, Vol. 76.

12. **Brightbill, Frederick S., McGhess, Charles N. J. and McDonnell, Peter J.** *Corneal surgery: theory, technique and tissue.* s.l. : Mosby Elsevier, 2009.

13. **Minsky, Marvin.** *Microscopy Apparatus. 3013467* United States of America, 7 November 1957.

14. **Wallace, Wes, Schaefer, H. Lutz and Swedlow, Jason R.** Microscopy Resource Center - OLYMPUS. *Resolution Criteria and Performance Issues.* [Online] [Cited: 17th August 2011.] http://www.olympusmicro.com/primer/digitalimaging/deconvolution/deconresolution.html.

15. **Hecht, Eugene.** *Óptica.* 2ª ed. . Lisboa : Fundação Calouste Gulbenkian, 2002. pp. 256, 265.

16. **Pawley, James B.** *Handbook of Biological Confocal Microscopy.* Madison, USA : Springer, 2006.

17. **Toomre, Derek K., Langhorst, Matthias F. and Davidson, Michael W.** Zeiss. *Education in Microscopy and Digital Imaging.* [Online] [Cited: 18 August 2011.] http://zeiss-campus.magnet.fsu.edu/articles/spinningdisk/introduction.html.

18. **Corle, Timothy R. and Kino, Gordon S.** *Confocal Sacnning Optical Microscopy and Related Imaging Systems.* San Diego, California, USA : Academic Press, Inc, 1996. pp. 68-95.

19. **Masters, Barry R. and Böhnke, Matthias.** Three-Dimensional Confocal Microscopy of Living Human Eye. *Annu. Rev. Biomed. Eng.* 2002.

20. **Claxton, Nathan S., Feleers, Thomas J. and Davidson, Micahel W.** Laser Scanning Confocal Microscopy.

21. **Fincham, E. F.** A New Form of Corneal Microscope with Combined Slit Lamp Illuminating Device. 1st February 1924, pp. 113-122.

22. **Gierl, C., et al.** Automatic Focusing of a Motorized Photo Slit Lamp Microscope. *Proceedings of the 29th Annual International, Conference of the IEEE EMBS.* 23-26 August 2007.

23. **Henson, David B.** *Optometric Instrumentation.* s.l. : Butterworths, 1983.

24. **Zeiss.** Eye Examination with the Slit Lamp.

25. **Gross, H., Blechinger, F. and Achtner, B.** *Handbook of Optical Systems.* s.l. : Wiley-VCH, 2008. pp. 89-110. Vol. 4.

26. **Thompson, Robert Bruce and Thompson, Barbara Fritchman.** *Astronomy Hacks - Tips & Tools for Observing the Night Sky.* s.l. : O'Reilly Media Inc. , 2005. pp. 28-32.

27. **Yano, Nobuyuki.** *Slit Lamp Microscope provided with a confocal scanning mechanism. 5701197* Okazaki, Japan, 23 December 1997.

28. **Lichtman, Jeffrey W., Pepose, Jay S. and Dave, Rakhal.** *Kit for Converting a Slit Lamp Biomicroscope into a Single Aperture Confocal Scanning Biomicroscope. 5099354* Washington Universusty, St Louis, Mo., 24 March 1992.

29. **Esswein, Karlheinz.** *Acrhomatic micrscope objective. 4362365* Germany, 9th March 1981.

30. **Clark, R. N.** R. N. Clark's Photography. [Online] 8 April 2001. [Cited: 28 August 2011.] http://www.users.qwest.net/~rnclark/scandetail.htm#diffraction.

31. **Spring, Kenneth R. and Davidson, Michael W.** Nikon - Microscopy U - The Source for Microscopy Education. [Online] [Cited: 27th August 2011.]

ATTACHMENT A – GEOMETRIC OPTICS

In order to estimate parameters for simulation, geometric optics relations for thick lenses were used.

Thick lenses obey the Gauss equation:

$$\frac{1}{s_0} + \frac{1}{s_i} = \frac{1}{f}$$

where s_0 is the object position, s_i is the image position and f the effective focal length of the lens.

Another relation to estimate the effective focal length of a lens, f, is given by:

$$\frac{1}{f} = (n_l - 1)\left[\frac{1}{R_1} - \frac{1}{R_2} + \frac{(n_l - 1)d_1}{n_l R_1 R_2}\right]$$

R_1 is the first curvature radius of the lens, R_2 the second curvature radius, n_l the refractive index of the lens and d_1 the lens thickness.

To estimate the place where the principal points of a lens are located, the following equations are used:

$$h_1 = -\frac{f(n_l - 1)d_l}{R_2 n_l}$$

$$h_2 = -\frac{f(n_l - 1)d_l}{R_1 n_l}$$

where R_1 is the first curvature radius of the lens, R_2 the second curvature radius, n_l the refractive index of the lens and d_1 the lens thickness.

The equation used to calculate the effective focal length, f, of system with two lenses is:

$$\frac{1}{f} = \frac{1}{f_1} + \frac{1}{f_2} - \frac{d}{f_1 f_2}$$

f_1 is the effective focal length of the first lens, f_2 the effective focal length of the second lens and d the distance between them.

The principal points of a system of two lenses are related by:

$$\overline{H_{11}H_1} = \frac{fd}{f_2}$$

$$\overline{H_{22}H_2} = \frac{fd}{f_1}$$

where f is the effective focal length, d distance between lenses, f_1 the effective focal length of the first lens and f_2 the effective focal length of the second lens.

Technische Daten

ZEISS

Carl Zeiss
D-7082 Oberkochen
West Germany

Spaltlampe 30 SL/M — Best.-Nr. 321745

Spaltleuchte	
Lichtquelle	12 V/30 W Halogenlampe, regelbar
Filter	blau, grün, grau (10, 20, 40% Transmission), diffus
Spalthöhe	in Stufen 0,3/1/3/5/7/9 mm
Spaltbreite	kontinuierlich progressiv 0 bis 9 mm
Spaltdrehung	kontinuierlich ± 90°
Spaltdezentrierung	± horizontal
Einstrahlwinkel	0° bis 20° bei horizontalem Spalt
Hornhautmikroskop	
Vergrößerung	durch Galileiwechsler 5, 8, 12, 20, 30x bei Okularen 12,5x und Tubus f = 125 mm
Gesichtsfeld	40–7 mm Durchmesser
Numerische Apertur	0,025–0,064
Stereowinkel	10°
Objektiv	Brennweite f = 125 mm
Tubus	gerade f = 125 mm mit Pupillendistanzverstellung 50–75 mm wahlweise Schrägtubus oder Tubus f = 160
Okulare	Brillenträgerokulare 12,5x mit Ametropieausgleich ± 8 dpt. wahlweise 16x, 20x Einbau von Strichplatten möglich
Instrumentenbasis	
Bewegungsbereich	x/y/z = 127/88/28 mm Steuerhebelbereich radial 18 mm
Fixierung	für x/y Bewegung, Mikroskopdrehung, Differenzwinkel
Kopfstütze	Kinnstütze mit Schraubverstellung

Änderungen in Ausführung und Lieferumfang im Rahmen der technischen Weiterentwicklung vorbehalten.

Zubehör

		Best.-Nr.
Ophthalmometer-Meßgerätezusatz		321736
Lichtquelle	2 x 6 V 10 W Halogenlampe	
Meßbereich Radius	r = 4,0 bis 11,2 mm Skalenintervall 0,01 mm	
Meßbereich Achse	0° bis 180° Tabowinkel, Skalenintervall 1°	
Fehlergrenze Radius	r = ± 2,0 · 10⁻² mm im gesamten Meßbereich, bei Anwendung einer Kalibrierkurve: r = ± 0,5 · 10⁻² mm	
Mikroskopzusatz 8x	für Endothelbetrachtungen	301332
Vergrößerung	100 160 240	
Gesichtsfeld	1,8 mm 1,3 mm 0,8 mm	
Wechslerstellung	12 20 30	
Meßokular zur Längen- und Winkelmessung	Brillenträgerokular 10x	305510
Skala, linear	15 mm, Intervall 0,2 mm	
Winkelskala	180°, Intervall 2°	
Hornhautdicken-meßeinrichtung	Meßbereich 1,1 mm	321737
Vorderkammertiefen-meßeinrichtung	Meßbereich 6 mm	321738
Zeiss-Applanations-Tonometer SL 10-30	Anzeigebereich 0–80 mm Hg (1 Skalenteil = 0,98 mN)	301750
Tonometerhalter		301745
Tonometerhalter	mit Objektiv f = 125 mm	301743
Hruby-Linse	mit Kulisse	301747
Gonioskop		321462
Mitbeobachtungs-einrichtung	für 1 Mitbeobachter, mit Teiler 50 und Brillenträgerokularen 12,5x mit Dioptrienfeststeller	325126
Photoeinrichtung	komplett mit optischem Teiler 50, Kameragehäuse Pentax K 1000, Okular mit Fokussierhilfe, Kleiner Elektronenblitz mit Halter	321577
Urban Stereo-Photoadapter		303726
Elektronenblitz-gerät 240	mit Aufsteckkappen für Fluoreszenz- und Übersichtsaufnahmen, Blitzhalter und Netzanschlußgerät	328160
Patientenstütz-einrichtung		301772
Zur Messung der Krümmungsradien von Kontaktlinsen:		
Klemmhalter		302086
Trägerprisma		302084
Kontaktlinsenhalter		302093
Küvette	für weiche Kontaktlinsen, mit sphärischer Eichfläche und Pinzette	302085

30-113-d Printed in West Germany AW V84 Uoo

ATTACHMENT C – NIDEK SL-1600 SPECIFICATIONS

MODEL	Slit Lamp SL-1600
RANGE OF MOTION	
Height shift, mm (RANGE OF MOTION)	30
Depth shift, mm (RANGE OF MOTION)	80
Fine movement by joystick,mm (RANGE OF MOTION)	±10
Side shift, mm (RANGE OF MOTION)	100
Chinrest height adjustment, mm (RANGE OF MOTION)	50
ADDITIONAL ATTACHMENTS	
Standard components (ADDITIONAL ATTACHMENTS)	Focusing rod, cap, hexagonal wrench, screwdriver, dust cover, spare illumination bulb, spare fixation bulb, 2 spare fuses, chinrest tissues, guide plate for Hruby lens and tonometer
Photographic capability (ADDITIONAL ATTACHMENTS)	CCD camera
Fixation light (ADDITIONAL ATTACHMENTS)	Yes
OPTIONS	Beam splitter, observation scope, TV camera set, Hruby lens and carrier, 10x eyepiece, 10x eyepiece with scale, 10x eyepiece with axis and scale
LIGHTING SYSTEM	
Slit length, mm (LIGHTING SYSTEM)	0.2, 1, 3, 5, 9, 14
Available filters	Blue, red-free, heat absorption

(LIGHTING SYSTEM)	
Slit width, mm (LIGHTING SYSTEM)	0-14, adjustable
Turning angle, deg. (LIGHTING SYSTEM)	±90
BULB USED	Halogen 12 V30 W
Tilt angle, deg. (LIGHTING SYSTEM)	0-15
Brightness (LIGHTING SYSTEM)	12 V
Alternative diaphragm sizes,mm (LIGHTING SYSTEM)	0.2, 1, 3, 5, 9, 14
POWER NEEDED, VAC (ENERGY)	100, 120, 220, 240; built-in voltage selector
UNIT SIZES	
Height, cm (in) (ACCESS)	46.8 (18.4)
Floor space cm (in) (UNIT SIZES)	45 x 41 x 46.8 (17.7 x 16.1 x 18.4)
WEIGHT, kg (lb) (DISPLAY)	20 (44)
MICROSCOPE	
Diopter adjustment range, diopters (MICROSCOPE)	-8 to +8
Objectives	130 mm focal length
Pupillary distance, mm (MICROSCOPE)	55-75
Microscope specifications (MICROSCOPE)	Stereo, binocular
Eyepieces (OCCULARS)	16x
Visual field,mm (MICROSCOPE)	6.5, 10, 16, 25, 39

Maximum magnification (MICROSCOPE)	6x, 10x, 16x, 25x, 40x
Magnification changing system (MICROSCOPE)	Mechanical discrete system5-magnification drum-changing system
FDA CLEARANCE (Interference compensation)	Yes
CE MARK (MDD) (Interference compensation)	Yes
MARKETING REGION (Interference compensation)	Worldwide, except USA

1100 Series — Board Level Monochrome CCD Camera

SPECIFICATIONS

ELECTRICAL

Sensor
1/2 inch or 1/3 inch interline transfer, microlens sensor

Active Picture Elements
RS-170: 768 (H) x 494 (V)
CCIR: 752 (H) x 582 (V)

Pixel Cell Size
RS-170: 1/2 inch: 8.4 µm (H) x 9.8 µm (V)
RS-170: 1/3 inch: 6.35 µm (H) x 7.4 µm (V)
CCIR: 1/2 inch: 8.6 µm (H) x 8.3 µm (V)
CCIR: 1/3 inch: 6.5 µm (H) x 6.25 µm (V)

Total Pixel Elements
RS-170: 811 (H) x 508 (V)
CCIR: 795 (H) x 596 (H)

Resolution
RS-170: 580 (H) x 350 (V) TVL
CCIR: 560 (H) x 450 (V) TVL

Synchronization
H&V, Crystal RS-170, Async

Shutter
1/60 to 1/10,000

Partial Scan/Region of Interest
Position adjustable in X and Y

AGC
20 dB range, auto or manual control

Signal To Noise
>55 dB (Gain 0, Gamma 1)
38 dB (Gain 20 dB, Gamma 1)

Gamma
.45 to 1.0, continually variable

Integration
2-16 fields

Lens Mount
C or CS (not included)

Auto Lens Output
Reference video provided to control auto iris lens

Sensitivity - 1/2 inch
Full video, No AGC: .04 fc, .43 lux
80% video, AGC on: .003 fc, .032 lux
30% video, AGC on: .001 fc, .010 lux

Sensitivity - 1/3 inch
Full video, No AGC: .05 fc, .53 lux
80% video, AGC on: .003 fc, .032 lux
30% video, AGC on: .002 fc, .021 lux

Power consumption
12 VDC, 3.6 W max. standard; 115/230 VAC adapter, optional

MECHANICAL

Dimensions
See illustration

Weight
1.50 oz (44 g) without lens

Ambient Temperature Limits
–20 to 60°C (4 – 140°F)

Relative Humidity
To 95% non condensing

Shock
15 g any axis, non operating condition, per MIL-E-5400T

ORDERING INFORMATION

11 X 2 X X X X / XXXX

Format
2 - 1/2" RS-170
5 - 1/2" CCIR
3 - 1/3" RS-170
6 - 1/3" CCIR

Power
2 - 12 Vdc, Standard

Sync Options
1 - Crystal/H&V Derive/Async Reset (Standard)
2 - Genlock (revert to crystal)
4 - Special Reset

Optical Filters
0 - None

Lens Mounts
0 - None
1 - CS
2 - C/CS

Options
0 - None
3 - Electronic Iris - RS-170*
4 - DC Lens Drive
5 - Electronic Iris - CCIR*

Lens Options
/XXXX - Please consult factory for lens selections.

** For manual lens only. Do not use with fluorescent lighting.*

DIMENSIONS

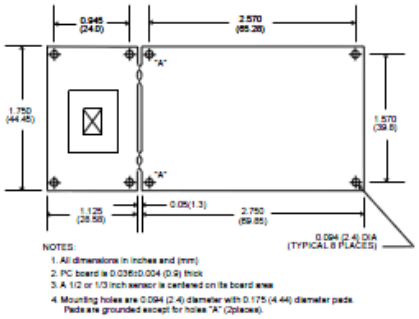

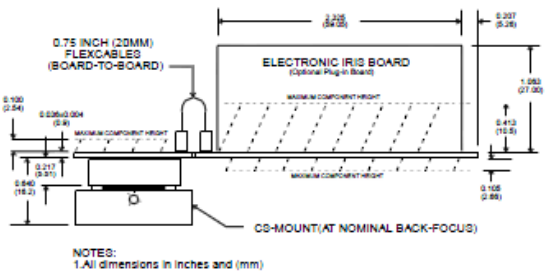

COHU
Cohu, Inc. / Electronics Division
ISO 9001 Certified

Cohu, Inc., Electronics Division
P.O. Box 85623
San Diego, CA 92186-5623
Phone: (858) 277-6700
FAX: (858) 277-0221
www.cohu-cameras.com
info@cohu.com

ADVANCED VIDEO TECHNOLOGY Made in the U.S.A.

1100 04-03
Printed in USA